SKOGSINDUSTRIELLA PROGRAMMET 1158

Development of a three-dimensional CFD model for rotary lime kilns

Lixin Tao, Daniel Nordgren & Roger Blom

värmeforsk
VÄRMETEKNISK FORSKNING OCH UTVECKLING

Development of a three-dimensional CFD model for rotary lime kilns

Lixin Tao, FS Dynamics Sweden AB
Daniel Nordgren, Innventia
Roger Blom, FS Dynamics Sweden AB

S09-207

VÄRMEFORSK Service AB
101 53 STOCKHOLM · Tel 08-677 25 80
November 2010
ISSN 1653-1248

Abstract

A general purpose three-dimensional CFD model for rotary lime kilns has been developed in this project. To simulate a rotary lime kiln the developed CFD model integrates three essential sub-models, i.e. the freeboard hot flow model, the lime bed model and the rotating refractory wall model. The numerical simulations using the developed CFD model have been performed for three selected kiln operations fired with three different fuel mixtures. The target is the lime kiln at the Södra Cell Mönsterås mill. To validate the CFD model in-plant measurements were carried out in the Mönsterås lime kiln.

The results from the CFD modelling and the measurement campaign show that the developed model predicts trends and absolute values in a good manner. Furthermore, an unexpected response in flame and wall temperatures near the burner was identified for the co-firing of oil and relatively wet sawdust, where the co-firing generated the higher temperatures compared to firing 100% oil.

Sammanfattning

I pappers- och massaindustrin ingår den så kallade kalciumcykeln där mesa, $CaCO_3$, konverteras till bränd kalk, CaO, i en roterande mesaugn. På så sätt kan kalciumet i ett senare steg återvinnas i kausticeringsprocessen. Mesaugnarna står för en stor del av energikonsumtionen i pappers och massaindustrin. På grund av stigande oljepriser och nya emisissionskrav har massabruken behövt utvärdera alternativa bränslen till mesaugnarna. Speciellt i Sverige är det önskvärt att öka andelen biobränsle Ett intressant alternativ till olja, som ofta är lättillgängligt på massabruk, är biobränsle i form av sågspån eller bark. Det föreligger dock vissa osäkerheter avseende hur biobränslet påverkar mesaugnens prestanda. En djupare förståelse av flammans karakteristik är nödvändig för att kunna skifta från olja till biobränslen på ett kontrollerat sätt. De senare årens framsteg inom CFD, Computational Fluid Dynamics, innebär dock att det är möjligt att studera och prediktera hur flammans karakteristik påverkar mesaugnens prestanda.

En tre dimensionell CFD modell för en roterande mesaugn har utvecklats i detta projekt. CFD modellen tar hänsyn till de tre huvudsakliga mekanismerna i tre sammankopplade submodeller; gas- och luftflödet i ugnen**,** mesabäddmodellen och den roterande, reflekterande, vägg modellen. Modellen är implementerad i det kommersiellt tillgängliga CFD verktyget FLUENT

Simuleringsmodellen för mesaugnen har använts för att studera tre olika lastfall och för tre olika bränsleblandningar. Modellen utgår från mesaugnen vid Södra Cells bruk i Mönsterås. Resultaten från CFD beräkningarna presenteras och diskuteras i syfte att skapa en förståelse för hur de olika bränsleförhållandena påverkar mesaugnens prestanda. Mätningar på mesaugnen i Mönsterås ufördes under en experimentperiod för att validera CFD modellen. Mätresultaten samt en diskussion och jämförelse med beräkningarna ingår i rapporten.

Utvärderingen av CFD simuleringarnas resultat jämfört med mätningarna påvisar en i överlag god överensstämmelse. Detta innebär att den utvecklade CFD modellen för roterande mesaugnar är ett kraftfullt verktyg för att studera den detaljerade flamkarakteristiken och brännarparametrar för roterande mesaugnar. Modellen är således också mycket användbar för att studera hur ugnens prestanda påverkas av olika driftsparametrar och brännarförhållanden. Mätsonden som användes för att mäta temperatur och rökgaskomposition visade sig fungerade bra trots den relativt dammrika miljön som råder i en en mesaugn.

Såväl mätningarna som CFD-simuleringar visar en oväntad respons avseende temperaturer i flam-regionen för fallen där brännaren eldas med både sågspån och olja. Dessa fall visar, trots en ca 2 ggr längre flamma, en högre lokal temperatur jämfört med fallet där endast olja bränns. Detta kan förklaras av den relativt höga fukthalten som uppmätts i sågspånet (4,2% H_20), vilket stöds av en utförd känslighetsanalys.

Nyckelord: mesaugn, CFD, modellering, simulering, beräkning, biobränsle

Summary

In the calcium loop of the recovery cycle in a Kraft process of pulp and paper production, rotary lime kilns are used to convert the lime mud, mainly $CaCO_3$, back to quick lime, CaO, for re-use in the causticizing process. The lime kilns are one of the major energy consumption devices for paper and pulp industry. Because of the rising oil price and new emission limits, the pulp mills have been forced to look for alternative fuels for their lime kilns. One interesting alternative to oil, often easily available at pulp mills, is biofuels such as sawdust and bark. However the practical kiln operation often encounters some difficulties because of the uncertainties around the biofuel impact on the lime kiln performance. A deeper understanding of the flame characteristics is required when shifting from oil to biofuels. Fortunately recent advances in modern Computational Fluid Dynamics, CFD, have provided the possibility to study and predict the detailed flame characteristics regarding the lime kiln performance.

In this project a three-dimensional CFD model for rotary lime kilns has been developed. To simulate a rotary lime kiln the developed CFD model integrates the three essential sub-models, i.e. the freeboard hot flow model, the lime bed model and the rotating refractory wall model and it is developed based on the modern CFD package: FLUENT which is commercially available on the market.

The numerical simulations using the developed CFD model have been performed for three selected kiln operations fired with three different fuel mixtures. The predicted results from the CFD modelling are presented and discussed in order to compare the impacts on the kiln performance due to the different firing conditions. During the development, the lime kiln at the Södra Cell Mönsterås mill has been used as reference kiln. To validate the CFD model, in-plant measurements were carried out in the Mönsterås lime kiln during an experiment campaign. The results obtained from the measurements are presented and discussed in this report.

Evaluation of the predicted results obtained from the CFD modelling against the in-plant measurements shows reasonable agreement. This demonstrates that the developed CFD model for rotary lime kilns can be used as a powerful tool to study the detailed flame characteristics and burner design parameters for a rotary lime kiln and to examine the impacts on the kiln performance due to varied kiln operation parameters and firing conditions. The additional probe measurement techniques that were used to acquire temperature and flue gas data did perform well in the dusty environment in the lime kiln.

Both in-plant measurements and CFD-simulations show an unexpected response, where despite an approximately 2 times longer flame, the temperatures is higher in the flame region when co-firing sawdust and oil compared to solely firing oil. This may be explained by the relatively high moisture content in the sawdust (4,2% H_20), as the results from a sensitivity analysis indicates.

Keywords: lime kiln, CFD, modelling, simulation, biofuel

Table of contents

1 INTRODUCTION 1

1.1 BACKGROUND 1
1.2 DESCRIPTION OF THE RESEARCH AREA 1
1.3 THE PURPOSE OF THE RESEARCH ASSIGNMENT AND ITS ROLE WITHIN THE RESEARCH AREA 2
1.4 GOAL OF PROJECT AND REFERENCE GROUP 3

2 LIME KILN #2 AT THE SÖDRA CELL MÖNSTERÅS MILL 4

3 METHODS 7

3.1 CFD MODELING OF ROTARY LIME KILNS 7
3.2 OPERATIONAL DATA AND ADDITIONAL FURNACE MEASUREMENTS 16

4 RESULTS 26

4.1 CFD MODELLING RESULTS 26
4.2 RESULTS FROM THE MEASUREMENT CAMPAIGN 49
4.3 EVALUATION OF THE SIMULATIONS AGAINST THE IN-PLANT MEASUREMENT DATA 56

5 ANALYSIS OF THE RESULTS 60

5.1 CFD MODELLING 60
5.2 KILN OPERATION AND MEASUREMENT CAMPAIGN 62
5.3 EVALUATION OF SIMULATION DATA AGAINST IN-PLANT MEASUREMENT DATA 65

6 CONCLUSIONS 71

7 RECOMMENDATIONS AND APPLICATIONS 73

8 SUGGESTIONS FOR CONTINUED RESEARCH 74

9 LITERATURE REFERENCES 76

1 Introduction

1.1 Background

In the calcium loop of the recovery cycle in a Kraft process of pulp and paper production, rotary lime kilns are used to convert lime mud, mainly $CaCO_3$, back to quick lime, CaO, for re-use in the causticizing process. The rotary lime kiln is a long cylinder typically 2-4 m in diameter and 80 – 100 m in length. It rotates about its axis at roughly 1-2 rpm and is sloped at 1-4 degree. Lime mud is fed from the elevated cold end and moves down the kiln due to rotation and gravity. The residence time for the lime mud in the kiln is typically two to three hours. At the hot end, in which the burner operates, the hot gases are produced and maintained at about 1200°C by burning fuel (natural gas, oil or solid fuels). Today there are about 300 lime kilns in operation at Kraft pulp mills around the world with a designed capacity of between 200-500 tones of quick lime per day.

The rotary lime kiln is actually a direct-contact counter-flow heat exchanger. The endothermic reaction that takes place in the lime calcination absorbs energy from the hot burnt gases flow above the mud. The lime kilns are one of the major energy consumption devices for paper and pulp industry. Because of the rising oil price and new emission limits, the pulp mills have been forced to look for alternative fuels for their lime kilns. Sweden is in the front line when it comes to alternative fuels for lime kilns and the practical experience is in some cases over 20 years. Today approximately 50% of the supplied energy to Swedish lime kilns comes from biofuels. In practice this means that still more than 150,000m^3 of oil is fired every year in Swedish pulp mills. Thus it is desired for industry to increase further the portion of biofuels fired in the lime kilns. However the practical kiln operation often encounters difficulties because of the uncertainties around the biofuel impact on lime kiln performance. A deeper understanding of the flame characteristics in relation to the burner design and kiln operation is required when shifting from oil to biofuels. Fortunately recent advances in modern Computational Fluid Dynamics, CFD, have provided the possibility and modelling tools to study and predict the detailed flame characteristics regarding the lime kiln performance. Furthermore, with an accurate prediction of changes to the flame shape and temperature, as well as the thermal balance between flame, bed and walls, possible negative effects from a fuel change on the refractory walls by an increased thermal load can be addressed.

1.2 Description of the research area

The modelling of rotary kilns has been developed over the years [4, 5, 6, 7, and 8]. Many of the developed models are so-called one-dimensional models in which the dimension of interest is the kiln longitudinal axis. A set of equations representing conservation of mass, energy and species, averaged over the kiln cross-section, are solved using appropriate numerical methods. This type of models can be efficient tools

for the optimization and operation of the kiln by studying the effects of key control parameters. However these models cannot provide a detailed understanding of the phenomena associated with kiln operation such as the combustion process and burner design. In the one-dimensional models, combustion aerodynamics is typically ignored by assuming a flame length. Another critical assumption that must be made in any one-dimensional model is that uniform conditions exist across the cross-section of the lime kiln. This assumption is obviously not true for rotary lime kilns in which the large gradients of temperature and species exist at the kiln cross-sections, especially in the freeboard gas flow.

The effort to develop a three-dimensional CFD model for rotary lime kilns has been carried out by Georgallis et al at University of British Columbia, Canada [3]. The model is based on a global solution of three sub-models for the hot flow, the lime bed and the rotating wall/refractories using a finite-volume CFD program developed by them at the university. The overall model has been validated against the UBS's pilot kiln trials (5.5 m laboratory kiln).

The recent research activities, financed by Värmeforsk, concerning the lime kiln modelling in Sweden have been reported by Kristoffer Svedin et al [2]. In reference to this project, the geometrical description has been reused, however, all other aspects of the modelling has been improved or re-implemented to relevantly address the physical aspects of the combustion and calcination process.

1.3 The purpose of the research assignment and its role within the research area

The project is research oriented and is divided into two parts:

- Development of a three-dimensional CFD model for rotary lime kilns
- Experimental validation and in-kiln measurements in a utility rotary lime kiln.

There has been great interest in Swedish industry for some years to develop a validated three-dimensional CFD model for the simulation of rotary lime kilns. For instance, a lime kiln simulation program (MesaSim) for evaluation of kiln operation impact when a new fuel is fired or there is a change in some process parameter, has been used for many years. However this program is based on one-dimensional approach and makes many simplifications on the flame aerodynamics and heat transfer around it. Thus it cannot provide the necessary information concerning the flame characteristics that is certainly the most important parameter when predicting the lime kiln performance. Some works on the CFD modelling of rotary lime kilns have been done during recent years in Sweden. However the achievement in this field has so far been limited and the lime bed has been treated in a simplified manner, as adiabatic or by assuming a fixed temperature profile along the furnace, ignoring the coupled interaction between flame and bed. In addition it is generally lacking of available experimental data in literature which can be used to validate the results from CFD simulations. The experimental validation study

related to the CFD modelling and in-kiln measurements in a utility rotary lime kiln have not been done so far.

1.4 Goal of project and reference group

The general objective of this project is to develop a general-purpose, three-dimensional CFD model for the simulation of rotary lime kilns. The CFD model integrates the all necessary modelling components: the freeboard hot flow, the lime bed and the rotating refractory wall and is developed based on the modern CFD package: FLUENT which is commercially available on the market.

The project has been carried out in two stages. At the first stage, the work focus on the formulation and programming of the individual sub-models for the FLUENT based lime kiln model at FS Dynamics Sweden AB. At the second stage, comparison and validation of the developed CFD model is performed together with the research group at Innventia. For the validations three different operating conditions for the rotary lime kiln at Södra Cell's pulp mill in Mönsterås are selected. During the experimental campaign, in-kiln measurements are made by the research group at Innventia. Afterwards the numerical simulations using the developed CFD model are carried out based on the selected kiln operations. Finally the overall model predictions are validated against the measurements at Mönsterås lime kiln.

The reference group from Värmeforsk consist of the following persons:
Niklas Ahnmark (SCA Packaging Obbola AB) – Chairman
Sten Valeur (Holmen AB)
Niklas Berglin (Innventia)
Per Olowson (Södra Cell FoU)
Daniel Solberg (SCA Östrand Massafabrik)

2 Lime kiln #2 at the Södra Cell Mönsterås mill

The target lime kiln in this project is the lime kiln at the Södra Cell Mönsterås mill. The kiln is designed to have a production capacity of 275 metric Tons Per Day (TPD). The kiln initially fired 100% heavy oil and now co-fires heavy oil and biofuel (bark powder, sawdust etc.). The kiln barrel has an outer diameter of 3.376 m and an inner diameter of 2.82 m and a length of 73.674 m. The kiln axis is inclined at an upward angle of 1.4° from the hot end and rotates at a speed of 1.6 rpm. Nine satellite coolers provide cooling of the lime product and heating of the combustion air. Just below the burner tip there is a 0.5 m high dam to increase the lime retention time in order to achieve good lime quality. The inner side of the kiln barrel is lined with two layers of refractory. Different materials are used at different locations to match the requirements for different temperatures. For simplicity, it has been taken in this work that the refractories have the thicknesses of 0.15 m and 0.05 m with the thermal conductivities of 1.7 W/m-K and 0.3W/m-K for the inner layer and the outer layer respectively. Figure 1 shows the layout of the MU2 furnace at Södra Cell in Mönsterås, as well as the general layout of the refractory layers.

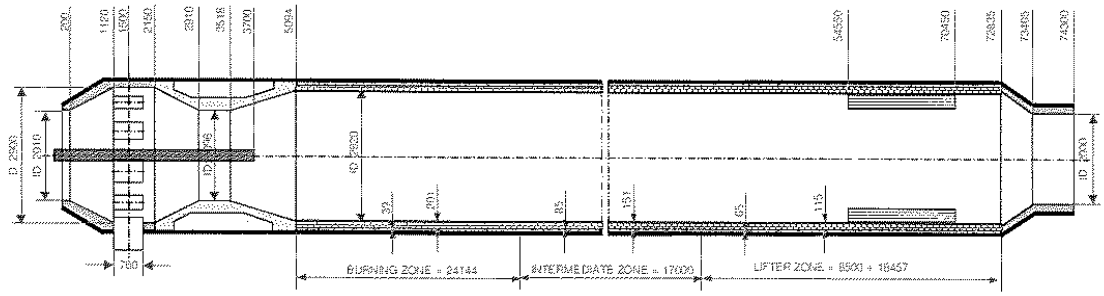

Figur 1. Layout och Eldfasta sektorer för Mönsterås mesaugn

Figure 1. Layout and refractory lining of Mönsterås lime kiln

The Mönsterås lime kiln uses a multi-fuel burner to co-fire heavy oil and biofuel. Figure 2 shows the conceptual design of the burner. The swirl angle for the swirl air is 40°. Primary air is supplied through central air, swirl air, and axial air, while the fuel transport air is supplied separately. Table 1 presents the burner design parameters.

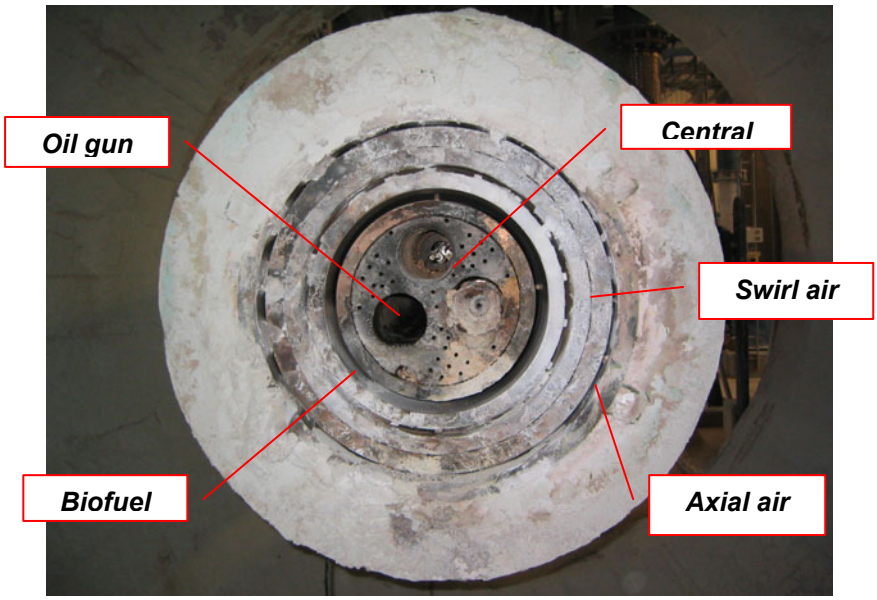

Figur 2. Principiell brännardesign

Figure 2. Burner design

Tabell 1. Brännarens mått och parametrar

Table 1. Burner design parameters

	Inner diameter(mm)	Outer diameter(mm)	Swirl angle (°)
Central air	0	216	0
Transport air (fuel)	251.4	284.6	0
Swirl air	387.2	391.2	40
Axial air	440.6	446.2	0

In this project a three-dimensional CFD model is developed to simulate the rotary lime kiln at the Södra Cell Mönsterås mill. Figure 3 presents the computational domain used for the kiln simulations. To capture the details of the burner geometry and the kiln/burner interactions, the numerical grid consists of approximately one and half million cells. The numerical grid is illustrated in Figure 4.

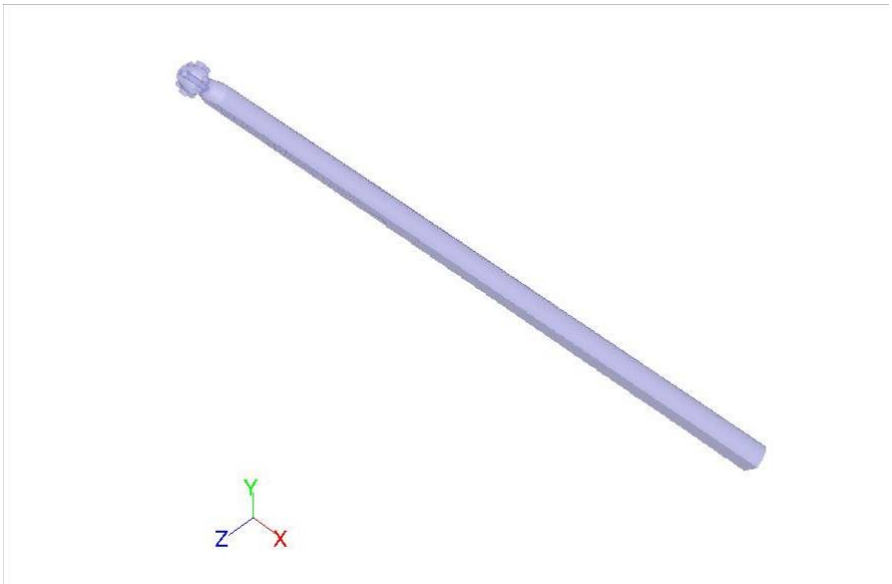

Figur 3. Simuleringsdomän för mesaugnen i Mönsterås (MU2)

Figure 3. Computational domain for Mönsterås lime kiln

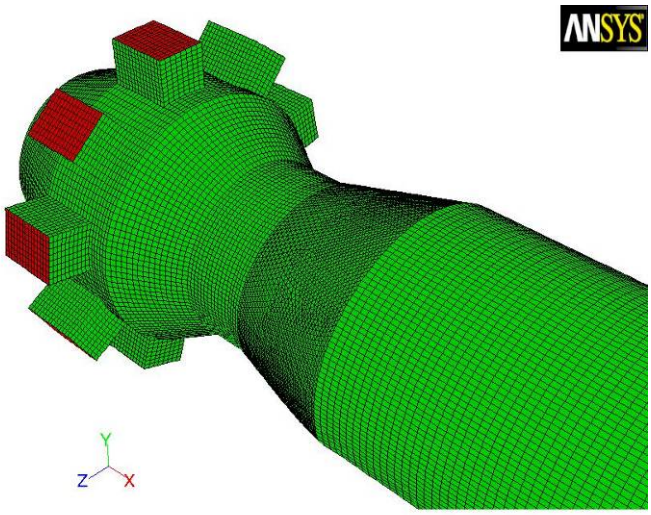

Figur 4. Tredimensionellt beräkningsnät för mesaugnen

Figure 4. Three-dimensional kiln model grid

3 Methods

3.1 CFD modeling of rotary lime kilns

In general the lime kiln process can be divided into four zones – drying, preheating, calcination and sintering. The following figure explains the temperature profile along a rotary lime kiln.

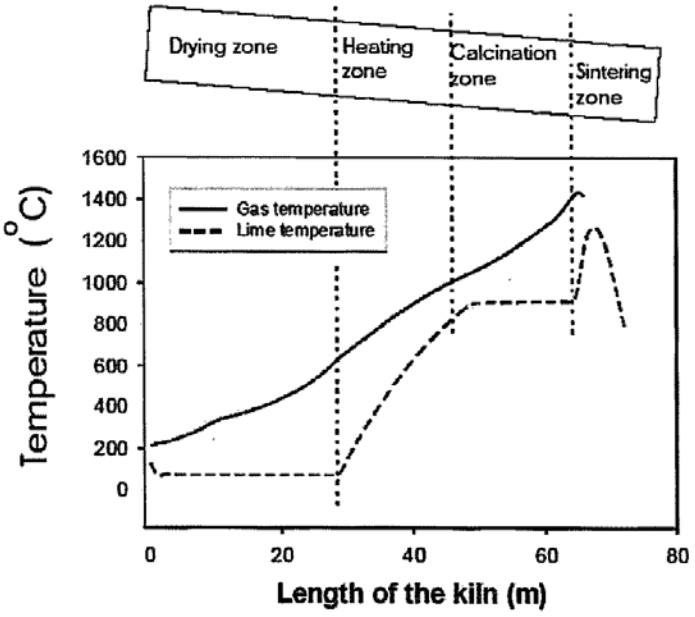

Figur 5. Temperarurprofil och reaktionszoner i roterande mesaugn

Figure 5. Temperature profile and reaction zones in a rotary lime kiln [2]

To enhance the heat transfer from the hot flue gas to the lime mud, the drying zone is traditionally equipped with a chain system. The chains also prevent the lime mud from forming large agglomerates. Modern lime kilns are often equipped with an external lime mud dryer instead of the chain system. The LMD-system feeds the kiln with nearly 100% dry lime at a temperature of approximately 250°C. This is exactly the case for the rotary lime kiln operated at the Mönsterås pulp mill. The preheating zone follows up the drying zone. In this zone the temperature of the lime mud is gradually heated up to around 850°C and the calcination is initiated. In the calcination zone, the temperature of the lime is more or less constant. The endothermic calcination reaction absorbs the energy from the freeboard hot flow to form as much burned CaO as possible. Finally the burned CaO is further heated up to a temperature between 1000°C and 1300°C when it sinters. Sintering is an operation during which the lime is heated just below its melting point and the lime particles adhere and form agglomerates.

A general three-dimensional CFD model for the rotary lime kiln must include modelling of the freeboard hot flow (with kiln and burner interactions), the lime bed process (with calcination chemistry) and the rotating wall (with heat loss to the surroundings). These three sub-models (freeboard hot flow, lime bed and wall) are integrated together through the heat and mass exchanges between them. Figure 6 shows the heat and mass transfer between the sub-models.

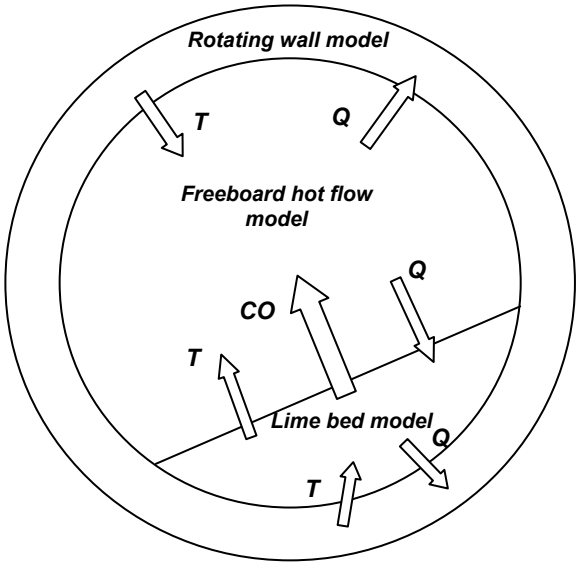

Figur 6. Värme- och massöverföring mellan submodeller

Figure 6. Heat and mass transfer between sub-models

3.1.1 Freeboard hot flow model

The freeboard hot flow model in this work utilizes the built-in models in FLUENT [10]. The approach for the hot flow solution in FLUENT is based on the finite volume method and unstructured grid. This allows simulating the flows in any complex three-dimensional geometry and is capable to capture details of the burner geometry and the kiln/burner interactions. The general flow model includes buoyancy effects, turbulence, transport and combustion of gaseous species, and thermal radiation.

In this project, the fuel fired in the Mönsterås lime kiln is oil and biofuel (sawdust) in the ranges from 100% oil to a combination of 50% oil and 50% sawdust. The particular combustion models used in the modelling of co-firing oil and sawdust are based on the discrete phase model available in FLUENT. The discrete-phase model in FLUENT follows the Euler-Lagrange approach. The gas phase is treated as a continuum by solving the time averaged transport equations such as momentum, energy and gas species while the discrete second phase (oil droplets and sawdust particles) is solved by tracking a large number of droplets/particles through the calculated flow field. FLUENT computes the trajectories of these droplets/particles as well as the heat and mass

transfers to/from them. The coupling between the gas phase and the discrete phase is achieved through appropriate sink/source terms in the gas-phase transport equations.

The burning process of an oil droplet is considered as two steps:

- Heating up the droplet to the evaporation/boiling temperature,
- Droplet evaporation/boiling.

In a similar way, the burning process of a sawdust particle is considered as three steps:

- Heating and drying of the particle,
- Evolution of volatiles (devolatilization),
- Heterogeneous surface reaction (char combustion).

The gas-phase combustion of the oil vapour and volatiles released from the discrete-phase is calculated by the combined eddy dissipation/chemical kinetics model using a two-step reaction scheme that is

- Oil vapour + oxygen => carbon-monoxide + water,
- Volatiles + oxygen => carbon-monoxide + water,
- Carbon-monoxide + oxygen => carbon-dioxide.

The turbulence is handled by the two equation realizable k-epsilon turbulence model with the standard wall function. The thermal radiation heat transfer is calculated using the P1 radiation model.

3.1.2 Lime bed model

Development of a proper sub-model for the lime bed, the main objective for the work presented in this report, is necessary. The lime bed process absorbs approximately half of the energy supplied by the burner and contributes as much as 20% additional mass flow (CO_2) to the freeboard gas flow field. Thus the lime bed process will significantly and interactively affect the actual flow, temperature, and combustion process in the freeboard region above the lime bed through heat and mass exchanges between the two parts.

The physics of the lime bed in a rotary lime kiln is complex. The figure below shows a typical cross-section of a rotary lime kiln and the movement of lime particles within the lime bed.

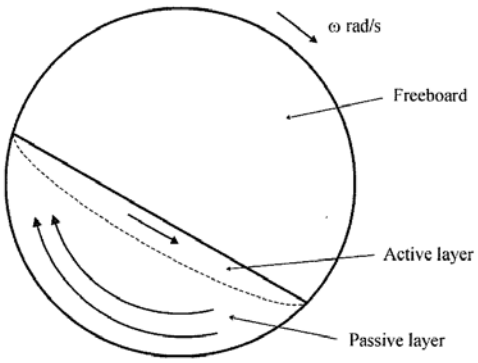

Figur 7. Typiskt tvärsnitt i roterande mesaugn

Figure 7. A typical cross-section of a rotary lime kiln [1]

As shown, the particles move concentrically with the wall of the kiln in the passive layer until they reach the surface of the bed, where they slide downwards in the active layer. Considering a single particle, this repeated process can cause the particle to move in the axial direction every time it moves down the active layer, as long as the rotary lime kiln is tilted in the axial direction. Several approaches for the modelling of the lime bed are possible. In this project, we have developed a lime bed model which is relatively simple and cost effective, i.e. a plug flow type of one-dimensional model for the lime bed. In nature, the one-dimensional model assumes that the perfect mixing of lime particles exist in the cross-section of the lime bed. This approach is acceptable since detailed description of the temperature and species in the cross-section of the lime bed is not available in this project. The possibility to further extend the modelling approach, to include for example a resolved mass and heat transfer in the cross section of the bed, exists. However, care must be taken to ensure physical accuracy and numerical stability of all modelling steps, and any extension to the modelling approach should be made in stepwise validated increments.

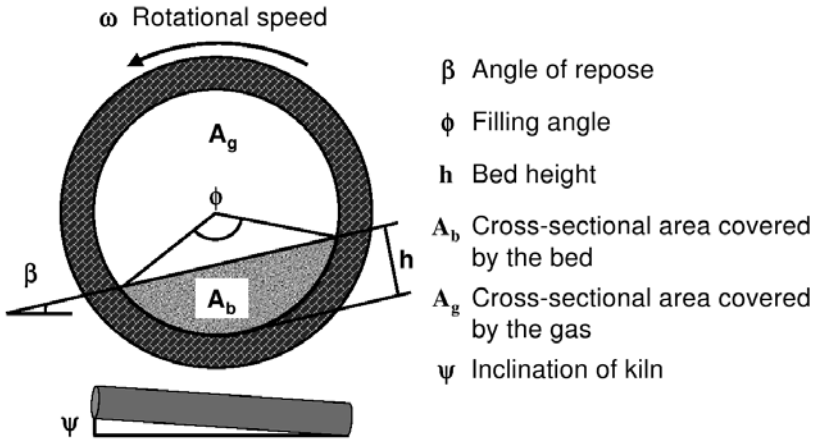

Figur 8. Geometridefinitioner för roterande mesaugn

Figure 8. Geometrical definitions for a rotary lime kiln

Figure 8 presents the geometrical definitions for a rotary lime kiln.

The cross-sectional area covered by the lime bed can be calculated by the equation:

$$A_b = \frac{D_i^2}{8}\left(\phi - \sin\phi\right)$$

The interface length between the freeboard gas and the lime bed in the cross-section of the lime kiln is given by the relation:

$$L_{g-b} = D_i \sin\frac{\phi}{2}$$

The contact perimeter between the wall and the lime bed in the cross-section of the lime kiln is calculated by

$$P_{w-b} = D_i \frac{\phi}{2}$$

Where D_i is the inner diameter of the kiln (m) and φ is the filling angle of the lime bed (radian).

Figure 9 shows the heat transfer in the cross-section of a rotary lime kiln.

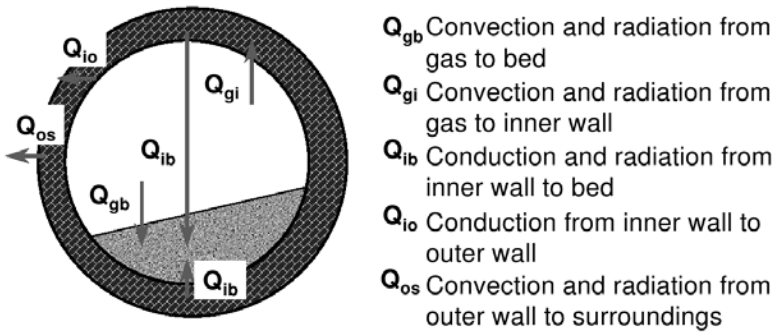

Figur 9. Värmeöverföring i roterande mesaugns tvärsnitt

Figure 9. Heat transfer in the cross-section of a rotary lime kiln

As shown in this figure, the Q_{gb}, Q_{ib} and Q_{gi} are actually computed by the freeboard hot flow model described previously. Q_{ib} is due to the heat conduction from the inner wall to the bed. This is commonly called heat regeneration. This part of the Q_{ib} (W/m) can be calculated by the equation:

$$Q_{ib} = hP_{w-b}\left(T_w - T_b\right)$$

Where h is the effective heat transfer coefficient (W/m^2), T_w and T_b are the local temperatures for the wall and the bed respectively. The h can be derived from the penetration theory [1] and is given by the relation:

$$h = \sqrt{\frac{8\omega\rho_b c_b k_b}{\beta}}$$

Where ρ_b is the density of the bed (kg/m^3), c_b is the specific heat capacity of the bed (J/kg-K) and k_b is the thermal conductivity of the bed (W/m-K). The ω is the rotational speed of the kiln (radian/s) and β the angle of repose (radian). The c_b and k_b are treated as constants which are taken as 1000 J/kg-K and 1.5 W/m-K respectively. The density of the bed, ρ_b, is the function of the bed geometry and the local mass flow rate of lime particles in the bed. The ρ_b can be calculated by the equation:

$$\rho_b = \frac{\dot{m}_b}{A_b v_b}$$

Where $\dot{m}_b$ is the local mass flow rate of lime particles in the bed (kg/s) and v_b is the averaged axial velocity of the lime particles (m/s).

The averaged axial velocity of the lime particles is proportional to the kiln inner diameter, D_i, the kiln rotational speed, ω, and the inclination of the kiln, ψ, and is related to the angle of repose, β, by the following equation [1]:

$$v_b = C_{vb}\frac{D_i}{2}\psi\omega\sin\beta$$

Where C_{vb} is an empirical constant, allowing adjustment of the lime residence time in the kiln, and has a value between 0.5 and 1.

The averaged residence time of the lime particles in the kiln can then be obtained by the following relation:

$$t_b = \frac{L_b}{v_b}$$

Where L_b is the axial length of the lime bed (m).

As described previously, the function of the lime bed model is to determine the heat and mass exchanges between the freeboard hot flow and the lime bed. In practice, this can be achieved by determining the profile of lime bed temperature and the mass and species sources for carbon-dioxide and water vapour at the cells adjacent to the lime bed surface along the kiln axial direction. In general the lime bed model developed in this work considers six variables, i.e. $T_b, \dot{m}_b, \dot{m}_{CaCO3}, \dot{m}_{CaO}, \dot{m}_{CO2}, \dot{m}_{H2O}$.. These variables are the functions of kiln axial coordinate and represent the local temperature of the lime bed and the local mass flow rates for the lime and its individual species: $CaCO_3$, CaO, CO_2 and H_2O respectively. Based on the mass and energy conservation in the lime bed, the plug-flow type of a one-dimensional lime bed model can be derived as described below:

(1) Drying of the lime bed when $\dot{m}_{H2O} > 0$ and $T_b = 100°C$

$$\frac{dT_b}{dx} = 0$$

$$\frac{d\dot{m}_b}{dx} = \frac{d\dot{m}_{H2O}}{dx} = -\frac{Q_{gb} + Q_{ib}}{\Delta H_{evap}}$$

$$\frac{d\dot{m}_{CaCO3}}{dx} = \frac{d\dot{m}_{CaO}}{dx} = \frac{d\dot{m}_{CO2}}{dx} = 0$$

(2) Calcination of the lime bed when $\dot{m}_{CaCO3} > 0$ and $T_b \geq 550°C$

$$\frac{d\left(\dot{m}_b c_b T_b\right)}{dx} = Q_{gb} + Q_{ib} - Q_{reac}$$

$$\frac{d\dot{m}_b}{dx} = -\frac{d\dot{m}_{CO2}}{dx} = 0.44\frac{d\dot{m}_{CaCO3}}{dx}$$

$$\frac{d\dot{m}_{CaO}}{dx} = -0.56\frac{d\dot{m}_{CaCO3}}{dx}$$

$$\frac{d\dot{m}_{CaCO3}}{dx} = -\frac{k\dot{m}_{CaCO3}}{v_b}$$

$$\frac{d\dot{m}_{H2O}}{dx} = 0$$

(3) Heating or cooling of the lime bed in any other conditions

$$\frac{dT_b}{dx} = \frac{Q_{gb} + Q_{ib}}{\dot{m}_b c_b}$$

$$\frac{d\dot{m}_b}{dx} = \frac{d\dot{m}_{CaCO3}}{dx} = \frac{d\dot{m}_{CaO}}{dx} = \frac{d\dot{m}_{CO2}}{dx} = \frac{d\dot{m}_{H2O}}{dx} = 0$$

Where ΔH_{evap} is the latent heat of water vaporization (J/kg) and k is the production rate of CaO (1/s). The reaction rate is kinetically controlled by temperature, which can be expressed in the following Arrhenius form:

$k = A\exp(-E/RT)$

Where A = 4.55×10^{31} – pre-exponential factor (1/s) and E = 7.81×10^{5} –activation energy (J/mole). The calcination reaction occurs in the temperature between 550°C and 950°C. The calcination heat is 3.17 MJ/kgCaO. Thus the Q_{reac} is calculated by the equation:

$$Q_{reac} = 3.17 \times 10^{6} \frac{0.56 k \dot{m}_{CaCO3}}{v_b}$$

With the known kiln geometrical data and operating conditions, the system of the ordinary differential equations presented above for the lime bed model can be solved for successive axial positions using any of a proper numerical technique. In this work the Runge-Kutta method has been used to integrate the lime bed model. Finally the coupling of the one-dimensional lime bed model with the three-dimensional freeboard hot flow model is achieved by means of the UDFs (User Defined Functions) provided in FLUENT code [10]. In this work, six user defined functions have been used to implement the lime bed model. In addition the UDFs developed in this work have been coded in such a way that they can be implemented for both serial and parallel computing configurations.

3.1.3 Rotating refractory wall model

The wall model utilizes the built-in models in FLUENT [10]. In FLUENT the wall boundaries can be either stationary or moving. The moving boundary condition can be used to specify the translational or rotational velocity of the wall. In this work the rotational speed of the lime kiln, ω is 1.6 (rpm) or 0.1676 (1/s). The thermal boundary condition at the kiln wall considers the external thermal radiation and convection losses to the surroundings and the thin-wall thermal resistances through the wall refractories. The thermal resistance of the refractories is $\Delta x/k_w$, where k_w is the effective thermal conductivity of the wall refractories and Δx is the total thickness of the wall. FLUENT will solve a 1D conduction equation to compute the thermal resistance offered by the wall refractories. For the composite refractory walls in a lime kiln, the effective thermal conductivity of the wall refractories, k_w, can be calculated by the relation:

$$\frac{\Delta x}{k_w} = \frac{\Delta x_1}{k_{w1}} + \frac{\Delta x_2}{k_{w2}} + \cdots$$

Where Δx_1, Δx_2, k_{w1}, k_{w2} are the thicknesses and thermal conductivities for the respective refractories. In this work, k_w is equal to 0.785W/m-K when $\Delta x_1 = 0.15$m, $k_{w1} = 1.7$W/m-K and $\Delta x_2 = 0.05$m, $k_{w2} = 0.3$W/m-K.

3.2 Operational data and additional furnace measurements

A measurement campaign at the Södra Cell Mönsterås lime kiln #2 was made in June 2009. The purpose of the campaign was two-fold: (i) collect suitable operational data that can be used as input to the CFD model and (ii) collect experimental data on gas composition, gas temperatures and lime bed temperatures that can be used to validate the CFD model. The measurement campaign lasted for three days during which the kiln was fired with a total of three different fuel mixtures: (A) 100% oil, (B) 70% oil / 30% sawdust, and (C) 50% oil / 50% sawdust (on energy basis).

3.2.1 Kiln operation data

In order to facilitate the analysis and comparison between the different fuel mixtures efforts were made to keep the kiln operation as stable as possible for a period of 12 hours for each of the three fuel mixtures. Operational data from the existing control system of the lime kiln was collected to be used directly or as input to calculations. Sampling of lime, lime mud and the solid biomass fuel was also made and sent for standard chemical analysis. The operational data and results from the chemical analysis were later used as input data to the CFD model.

Production rate and composition of reburned lime and lime mud

The production rate of reburned lime during the campaign was about 235 ton/day corresponding to 2.73 kg/s. The energy requirement per tonne of reburned lime was 6.6 GJ/t. Samples of both reburned lime and lime mud were taken during the campaign. See Table 2 and Table 3 for reburned lime and lime mud production rate (mass flow) and composition.

Tabell 2. Kalkproduktion och kalksammansättning

Table 2. Reburned lime production rate and composition

Parameter	Unit	Value
Production rate	kg/s (dry)	2.73
CaO	wt-% (dry)	91
$CaCO_3$	wt-% (dry)	2
Inert	wt-% (dry)	7
Sum	wt-% (dry)	100

Tabell 3. Massflöde av mesa och mesasammansättning

Table 3. Lime mud mass flow and lime mud composition

Parameter	Unit	Value
Lime mud massflow	kg/s (dry)	4,6
Density	kg/m^3	1180
Dry solids content	wt-%	77
CaO	wt-% (dry)	1
CaCO3	wt-% (dry)	95
Inert	wt-% (dry)	4
Sum	wt-% (dry)	100

Fuel

The power supplied to the burner was kept constant at about 18.2 MW_{th} during the whole campaign. The fuel mass flow and fuel composition, particle size distribution etc. of the fuel oil (#3) and sawdust (pulverised softwood) expressed as wt-% for specific particle sizes of 0.1, 0.35, 0.6, 0.86, 1.2 and 1.7, that was used during the campaign can be seen in Table 4.

Tabell 4. Bränsleparametrar under mätkampanjen

Table 4. Fuel mass flow and composition during the measurement campaign

Parameter	Unit	Fuel oil #3	Wood powder
Mass flow	kg/s (wet)	100% oil: 0.43 70/30 oil/bio: 0.3 50/50 oil/bio: 0.22	100% oil: 0 70/30 oil/bio: 0.30 50/50 oil/bio: 0.48
C	wt-% (dry)	86.4	50.6
H	wt-% (dry)	13.1	5.9
O	wt-% (dry)	0.38	42.9
S	wt-% (dry)	0.07	0.01
N	wt-% (dry)	0.05	0.04
Cl	wt-% (dry)		< 0.01
K	wt-% (dry)		0.05
Ash	wt-% (dry)	0	0.5
Sum	wt-% (dry)	100	100
Moisture	wt-%	0	4.2
Volatiles	wt-% (dry)		73.6
Fixed carbon	wt-% (dry)		25.9
LHV	MJ/kg (dry)	42.15	19.18
LHV	MJ/kg (wet)	42.15	18.27
HHV	MJ/kg (dry)	44.81	20.47

Diameters of wood powder (mm)	1.7	1.2	0.86	0.6	0.35	0.1
wt-%	0.7	0.4	2.9	10.5	31.7	53.8

The oil droplets size distribution is modelled as a Rosslin-Rammler distribution, with mean diameter of 0.05 mm [2]. Regarding the wood powder, the on-site measurements shows a higher value for moisture than later reported from operational personell. The implemented size distribution is slightly shifted, the particles beeing approximately 10 percent smaller, in the size range around 0.35-0.1 mm, while no particles smaller than 0.1 mm is modelled.

Combustion air

The transportation air and primary air is measured by the kiln control system and it is assumed to have a temperature of 27 ^{o}C. The secondary air flow, which is heated by the reburned lime in the product coolers, was estimated to have a temperature of 327 ^{o}C. The secondary air is not measured by the kiln control system. The amount of secondary air used in the CFD modelling is thus estimated from the measured oxygen concentration in the flue gas. See Table 5 for data on the combustion air.

Tabell 5. Förbränningsluftsflöde

Table 5. Combustion air flow

Parameter	Unit	50% oil/50% sawdust	70% oil/30% sawdust	100% oil
Primary air	Nm3/s	0.73	0.70	0.72
Transport air	Nm3/s	0.36	0.34	0.36
Secondary air (estimated)	Nm3/s	4.53	4.71	4.73

Lime kiln filling degree and bed angle

The lime kiln filling degree and bed angle was estimated by taking a series of photographs of the lime bed through a hatch that was positioned right below the burner. The bed angle and filling degree was then calculated by manual measurement in the photos that was made in black/white to enhance the contrast between the lime bed and the bright flame, see Figure 10. The angle of repose and depth of the bed or kiln filling degree is presented in Table 6.

Tabell 6. Resultat från beräkning av fyllnadsgrad och bäddvinkel för olika lastfall

Table 6. Estimations of the lime kiln filling degree and bed angle at different load

Parameter	Unit	Values			
Load	ton reburned lime per day	220	240	260	280
Angle of repose	Degrees	36	34	32	32
Filling degree	% of radius	18	22	21	23

Based on these measurements the average angle of repose was set to 35°, and the depth of the bed was set to 0.3 meters.

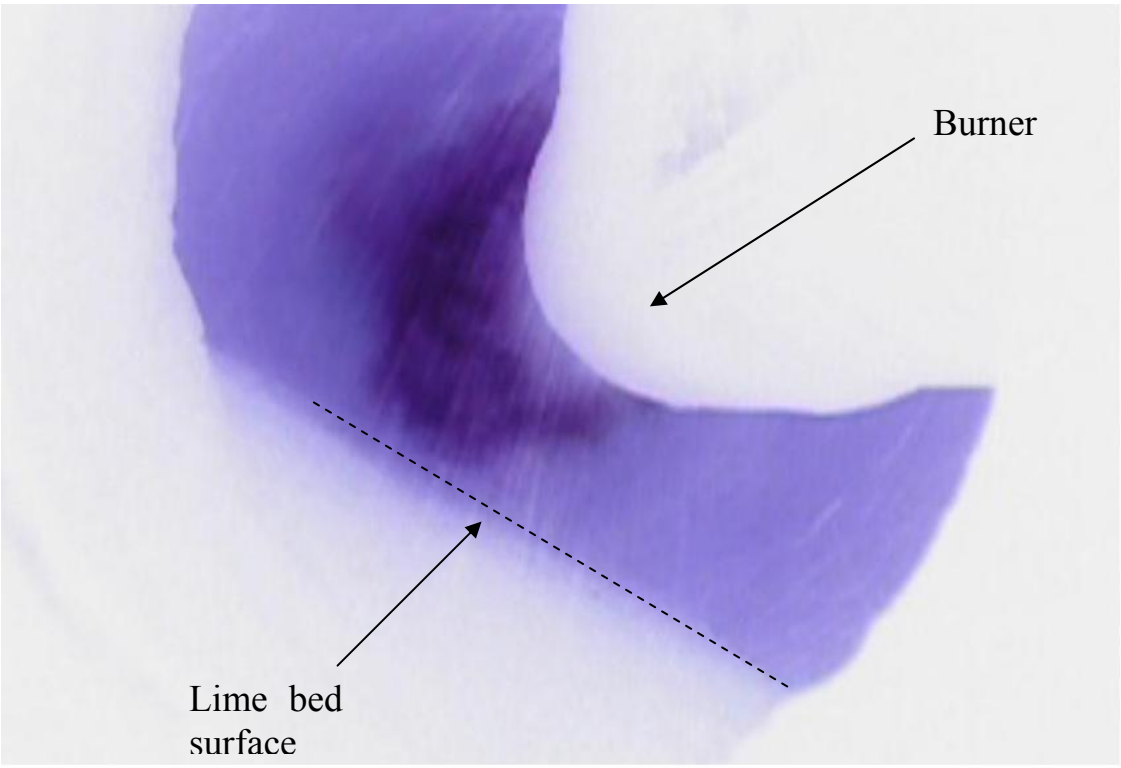

Figur 10. Exempel på ett av de svartvita fotografier som användes för att bestämma bäddens lutning och ugnens fyllnadsgrad

Figure 10. Example of a black and white photograph that was used to estimate the angle of repose and depth of the bed/filling degree of the kiln.

Temperatures and gas composition

Examples of operational data from the lime kiln control system are shown in Figure 11. From the figure it is evident that the reburning zone temperature (measured by a thermocouple positioned just below the burner) is affected by the choice of fuel. The average temperatures with the different fuel mixtures were 775 °C for 50% oil / 50% sawdust, 811 °C for 70% oil / 30% sawdust and 877 °C for 100% oil. It is clear that the temperature decreases as more sawdust is used in the fuel mix. The oxygen concentration, which is measured further downstream in the flue gas channel, ranges between 3 and 5 vol-% in average, displaying strong variation for every fuel mixture. The measured oxygen content is high, due to air leaking into the flue gas between the exit of the kiln and the position of the O_2 meter in the stack. Strong variations and very high concentrations in CO can be observed when 50% oil / 50% sawdust is fired. The maximum CO levels were over 10000 ppmv (for a better graphical presentation the values of CO have been divided by a factor 10). NOx concentration ranged between 80 – 120 ppmv with the higher values corresponding to the case when sawdust was used in the fuel mix.

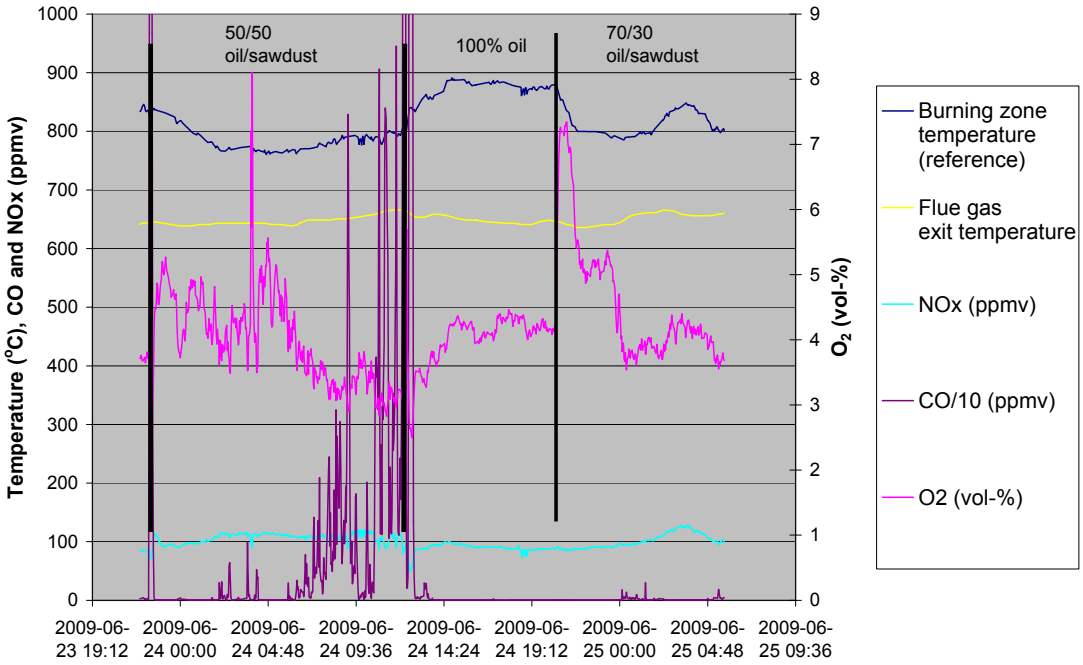

Figur 11. Driftdata från ugnens eget mätdatasystem; temperatur i brännzon, temperatur på utgående rökgas och syrekoncentration i utgående rökgaser (torr gas)

Figure 11. Operation data from the lime kiln control system: temperature in the reburning zone, exit temperature of the flue gas and oxygen concentration in the flue gas (dry gas)

3.2.2 Additional measurements of gas composition, gas temperature and lime bed temperature

Additional measurements of gas composition, gas temperatures and lime bed temperature were made to validate the final CFD model.

Gas composition and gas temperatures

In-situ gas composition measurements and gas temperatures were made possible by the use of a six meter long titanium probe. The probe is both used as a suction pyrometer and an extraction device for hot flue gas. Two different types of gas analysers were connected to the probe: one FTIR analyser which measured CO_2, H_2O, CO, NO, SO_2 and N_2O and the oxygen was measured using one paramagnetic O_2-analyser. The FTIR analyser was calibrated for CO2 concentrations up to 30 vol-%. The temperature was measured by a thermocouple at the tip of the probe. The thermocouple is shielded from radiation by a ceramic housing. See Figure 12 and Figure 13 for images of the probe itself and the measurement system that was used.



Figur 12. Den sex meter långa mätproben som användes för att extrahera rökgas för mätning av gassammansättning och gastemperatur (vänster bild). Mätprobens keramiska spets (höger bild)

Figure 12. The 6 meter long probe that was used to extract flue gas for measurement of flue gas composition and temperature (left). Close up the ceramic tip of the probe (right).



Figur 13. Analysutrustningen som användes för att mäta gassammansättning och gastemperatur

Figure 13. The gas analysing system that was used to measure gas composition and gas temperature

The probe measurements were done at one position in the cold end of the kiln (lime mud feed end) and two positions at the hot end of the kiln (burner end), see positions "1" and "2 and 3" respectively in Figure 14. The distance that the probe was inserted varied between 2.5 and 5.0 meters as the probe was traversed in the kiln. At the hot end, the practical insertion depth was 5 meters. At the cold end, the practical insertion depth was reduced to 2.5 meters due to the presence of moving carrier pins inside the kiln that could potentially cause mechanical damage to the ceramic tip of the probe.

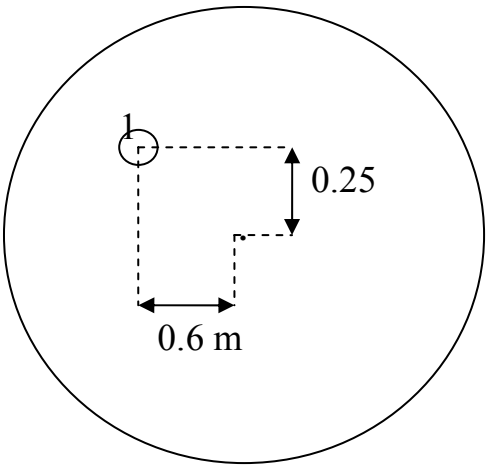

Cold end (lime mud feed end)

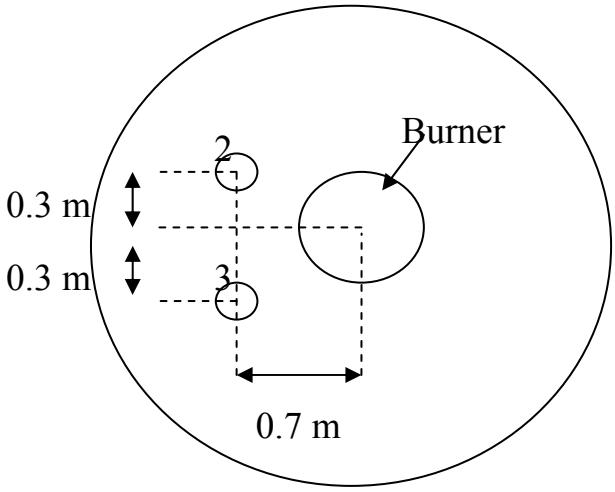

Hot end (reburned lime end)

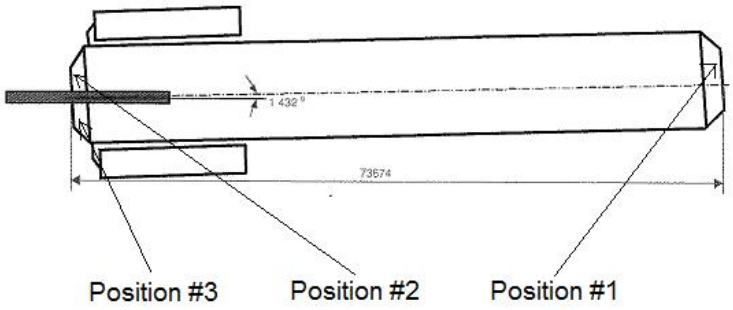

Figur 14. Positioner i den kalla (mesainmatningen) och varma (brännaren) ugnsgaveln där probmätningar på rökgastemperatur och rökgassammansättning gjordes.

Figure 14. Approximate position at the cold end (lime mud feed) and hot end (burner) of the lime kiln where point measurements of flue gas temperature and composition were made.

Lime bed temperature

The bed temperature was measured by a non-contact measurement method utilising an IR camera from FLIR systems (FLIR SC640), see Figure 15. A hatch in the kiln wall below the burner provided optical access to the lime bed. The camera was positioned about 4 m from the hatch, in a position that gave a clear view of the point were the reburned lime falls down into the lime product cooling system. Thus, the temperature measurement was done on the lime that was as far away from the flame radiation as possible without having left the kiln. Figure 16 shows an example of the IR image from the 100% oil-firing case. The lime bed temperature was taken as the average over 4-5 image sequences along the (blue) line that can be seen in figure. The temperature along the line was calculated using post-processing software from FLIR.



Figur 15. IR-kamera från FLIR, SC 640, som användes för att mäta kalkbäddstemperaturen

Figure 15. The FLIR thermocamera SC640 used to record image sequences from the lime bed

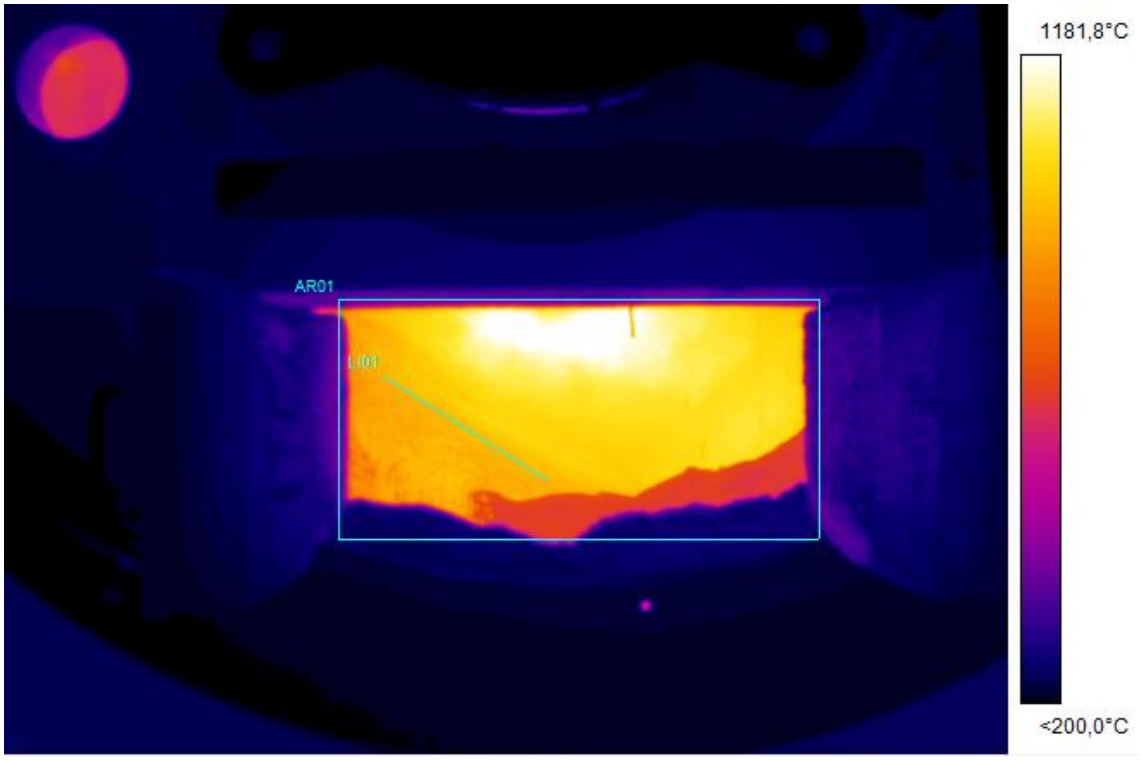

Figur 16. Exempelbild från bäddtemperaturmätningen, i detta fall när 100% olja användes. Den blå linjen markerar den position på bädden där temperaturen mättes.

Figure 16. Example of an IR image from the lime bed temperature measurements when 100% oil was fired. The blue line on the lime bed indicates where the temperature measurement was made.

3.2.3 Other measurements and observations during the campaign

During the second day of the campaign (afternoon 24th of June) the staff of Södra Cell Mönsterås reported that the lime product threshold had increased 0.1-0.2 m, possibly due to the initial steps in the formation of a ring. This observation was made as the gas and temperature measurement at the hot end was conducted, during the 100% oil firing case.

4 Results

4.1 CFD modelling results

Numerical simulations using the developed CFD model for rotary lime kilns are performed for the three selected kiln operations described previously. The results obtained from the CFD modelling are presented in order to compare the impacts on the kiln performance due to different firing conditions using three different fuel mixtures.

The following two sub-chapters presents the CFD simulation results from general and measurement comparison specific perspectives. A discussion of the CFD simulation results is given in chapter 5.

4.1.1 Comparison of kiln performances during different fuel firing conditions

Figures 17-18 present the comparisons of the predicted temperature contours of the kiln wall and the lime bed for the kiln operations fired with three different fuel mixtures (100%oil, 50%oil/50%sawdust, 70%oil/30%sawdust) respectively.

Figures 19-20 show the comparisons of the predicted contours of gas temperature in the central-vertical plane of the kiln (z=0, x<=20m) and in five cross-sections of the kiln (x=5m, 10m, 15m, 20m and 25m) for the firing conditions using the three different fuel mixtures respectively.

The comparisons of the predicted contours of oxygen concentration (mole fraction) in the central-vertical plane of the kiln (z=0, x<=20m) and in five cross-sections of the kiln (x=5m, 10m, 15m, 20m and 25m) for the firing conditions using the three different fuel mixtures are presented in Figures 21-22 respectively.

In the same manner, the comparison of the predicted contours for the combustion products: H_2O and CO_2 are shown in Figures 23-26 respectively.

Figure 27 presents the comparison of the predicted contours of the vaporized oil concentration (mole fraction) in the central-vertical plane of the kiln (z=0, x<=20m) for the kiln operations fired with the three different fuel mixtures.

The intermediate species CO is an important species used in combustion technology to indicate where the combustion reactions take place. Figures 28-29 show the comparisons of the predicted contours of CO concentration (mole fraction) in the central-vertical plane of the kiln (z=0, x<=20m) and in five cross-sections of the kiln (x=5m, 10m, 15m, 20m and 25m) for the kiln operations fired with the three different fuel mixtures respectively.

In combustion technology [9], the flame length may be estimated by the iso-surface of the CO concentration at which the mole fraction = 0.01. Figure 30 shows the comparison of the predicted iso-surfaces of the CO concentration at which the mole fraction = 0.01 for the firing conditions using the three different fuel mixtures.

The hot gas flow in the freeboard of a rotary lime kiln is fully three-dimensional. Figures 31 illustrates the comparison of the predicted velocity vectors near the burner in the central-vertical plane of the kiln and Figure 32 shows the comparison of the predicted velocity vectors in four cross-sections (x=10m, 15m, 20m and 25m) of the kiln for the kiln operations fired with the three different fuel mixtures.

The lime bed performance predicted by the one-dimensional lime bed model, i.e. the integration of the system of the ordinary differential equations described in Chapter 3.1.2 is presented in Figures 33-34. Figure 33 presents the comparison of the predicted average temperature profiles along the kiln axial direction for the lime bed and for the kiln inner wall when firing the three different fuel mixtures. The comparison of the predicted mass flow rate profiles along the kiln axial direction for the lime and the conversion of the individual species in the bed are shown in Figure 34.

The outlet temperature, the outlet concentrations of O_2, CO_2, H_2O, and the outlet flue gas flow in Nm^3/s are presented in Table 7. Figures 35-37 present cross sectional averages along the kiln for temperature, O_2, H_2O, CO and CO_2.

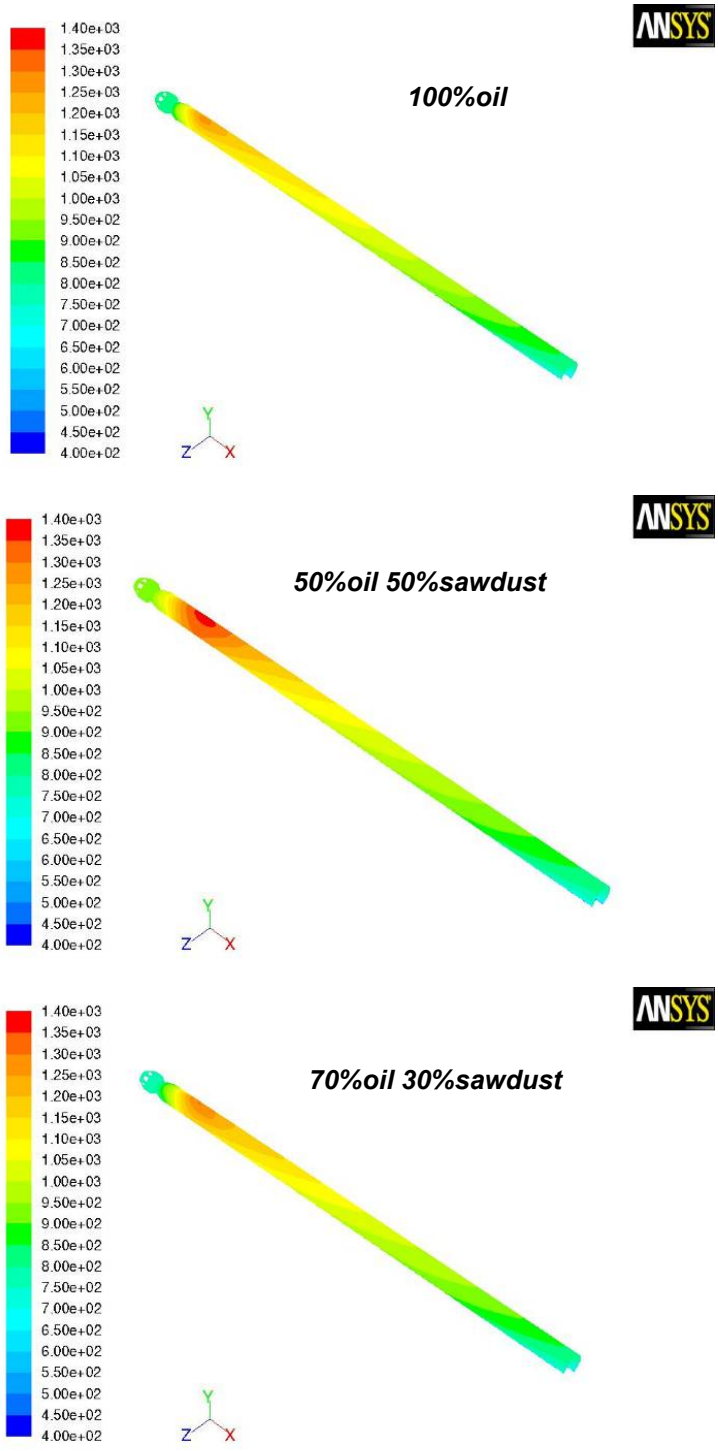

Figur 17. Konturplottar för jämförelse av väggtemperaturer (°C) på ugnens innerväggar för de tre bränsleblandningarna

Figure 17. Comparison of the predicted contours of kiln inner wall temperature (°C) for the three different fuel mixtures

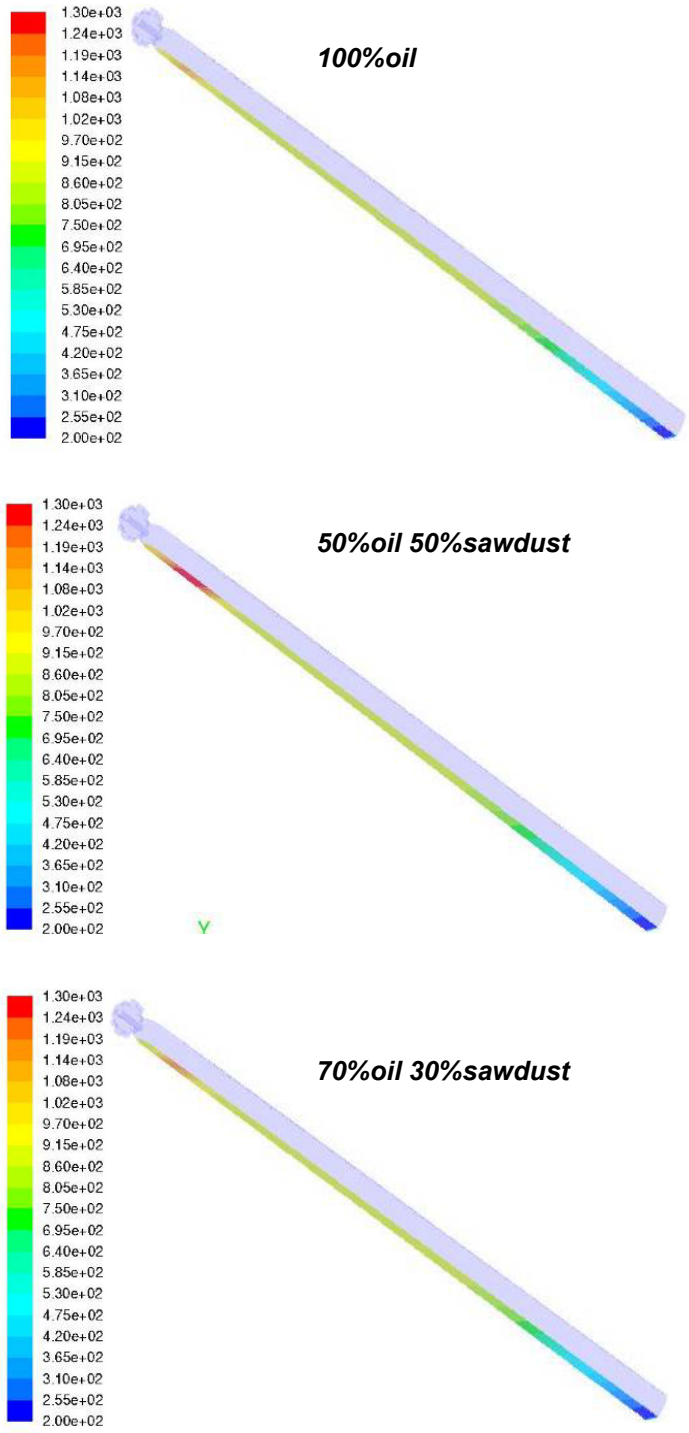

Figur 18. Konturplottar för jämförelse av mesatemperatur (°C) för de tre bränsleblandningarna

Figure 18. Comparison of the predicted contours of lime bed surface temperature (°C) for the three different fuel mixtures

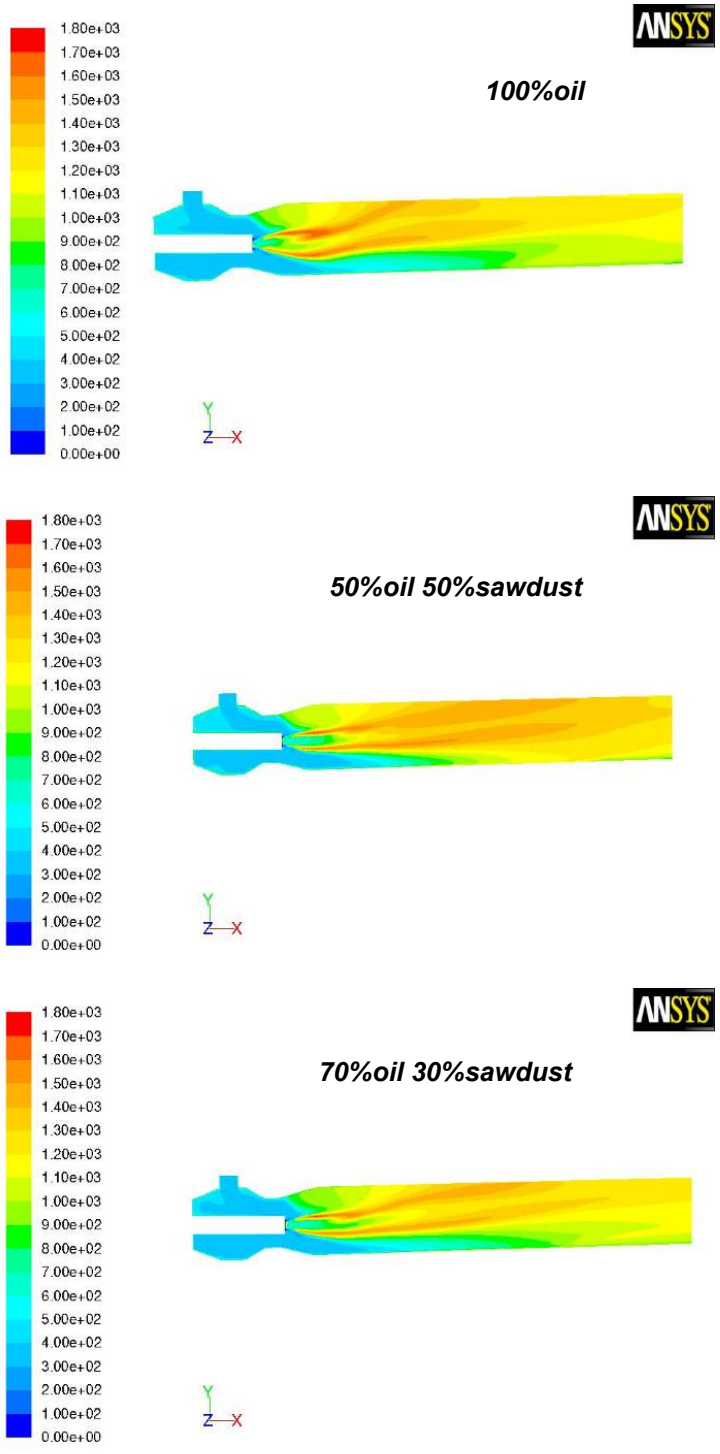

Figur 19. Konturplottar för jämförelse av gastemperaturer (°C) i central-vertikala plan (z=0 och x<=20m) för de tre bränsleblandningarna

Figure 19. Comparison of the predicted contours of gas temperature in the central-vertical plane (z=0 and x<=20m) of the kiln for the three different fuel mixtures

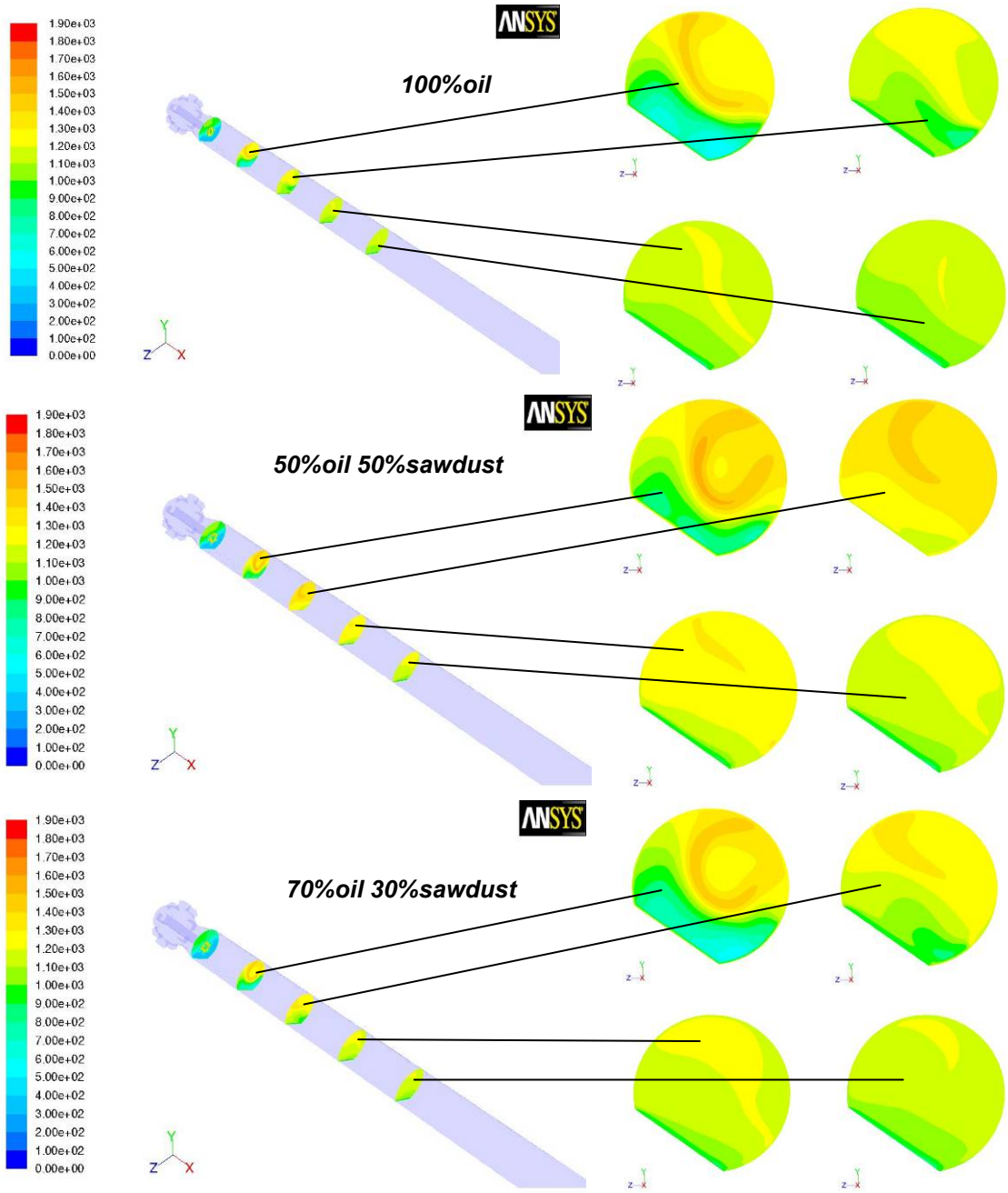

Figur 20. Konturplottar för jämförelse av gastemperaturer (°C) i fem tvärsnitt (x=5m, 10m, 15m, 20m, and 25m) för de tre bränsleblandningarna

Figure 20. Comparison of the predicted contours of gas temperature (°C) in five cross-sections of the kiln (x=5m, 10m, 15m, 20m, and 25m) for the three different fuel mixtures

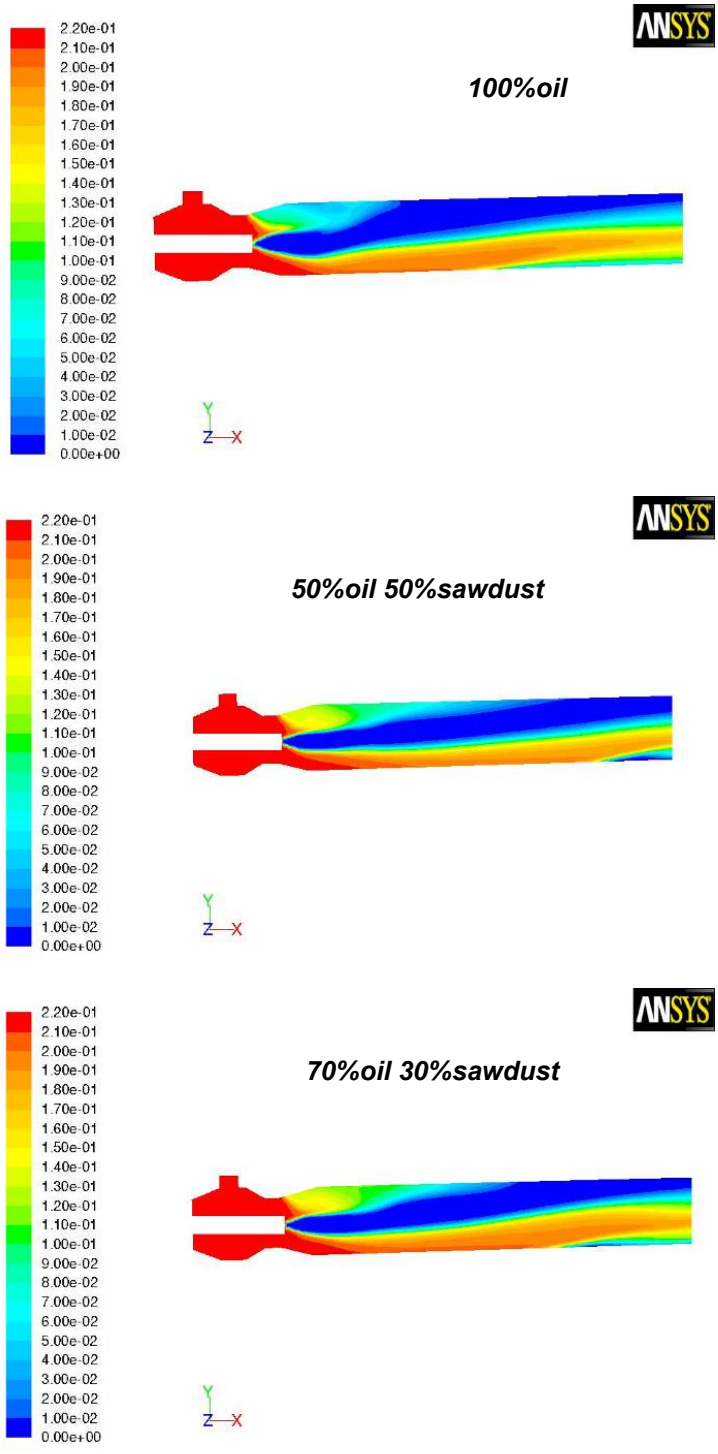

Figur 21. Konturplottar för jämförelse av syrekoncentrationer (molfraktioner) i central-vertikala plan (z=0 och x<=20m) för de tre bränsleblandningarna

Figure 21. Comparison of the predicted contours of oxygen concentration (mole fraction) in the central-vertical plane (z=0 and x<=20m) for the three different fuel mixtures

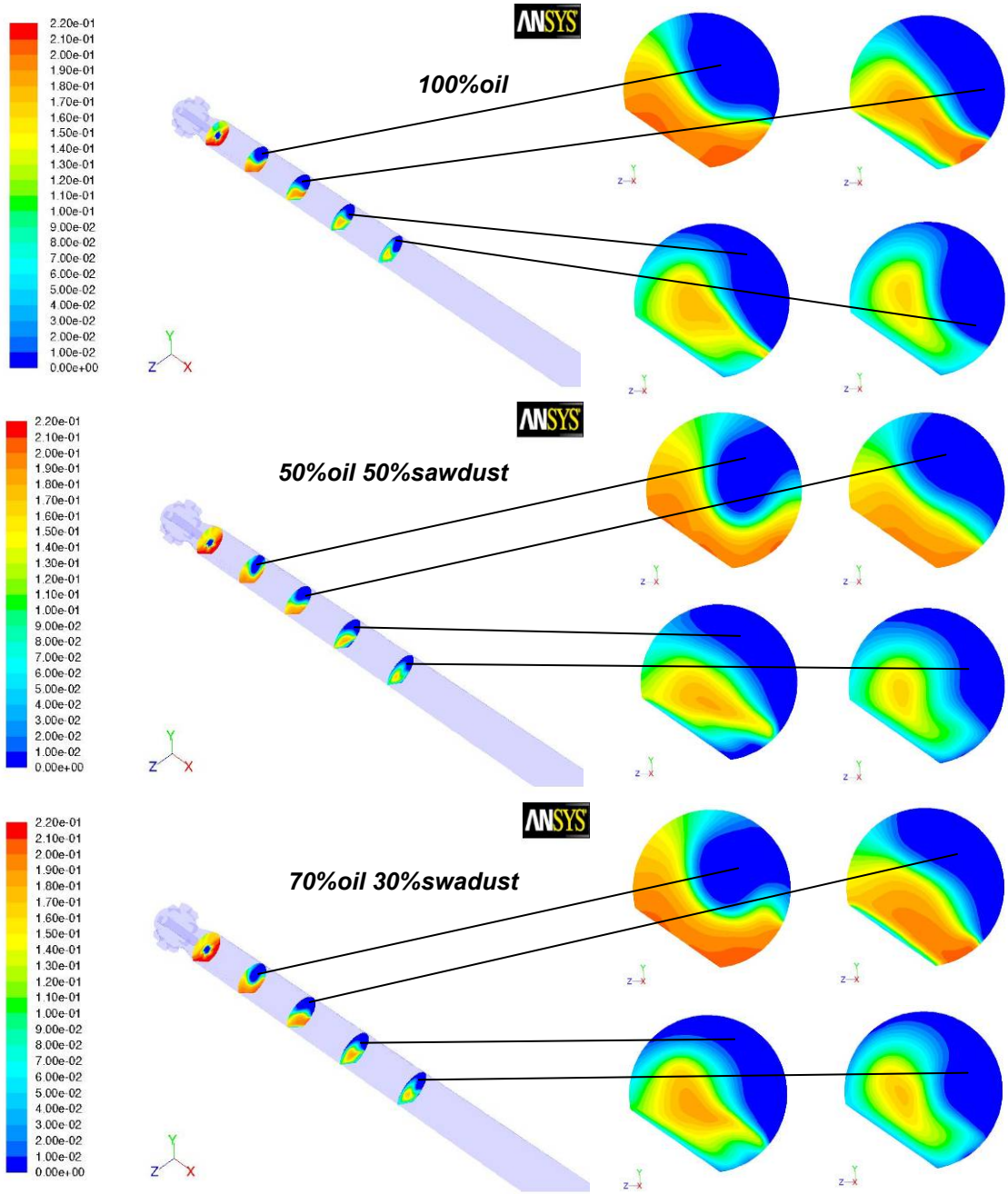

Figur 22. Konturplottar för jämförelse av syrekoncentration (molfraktioner) i fem tvärsnitt (x=5m, 10m, 15m, 20m, and 25m) för de tre bränsleblandningarna

Figure 22. Comparison of the predicted contours of oxygen concentration (mole fraction) in five cross-sections of the kiln (x=5m, 10m, 15m, 20m, and 25m) for the three different fuel mixture

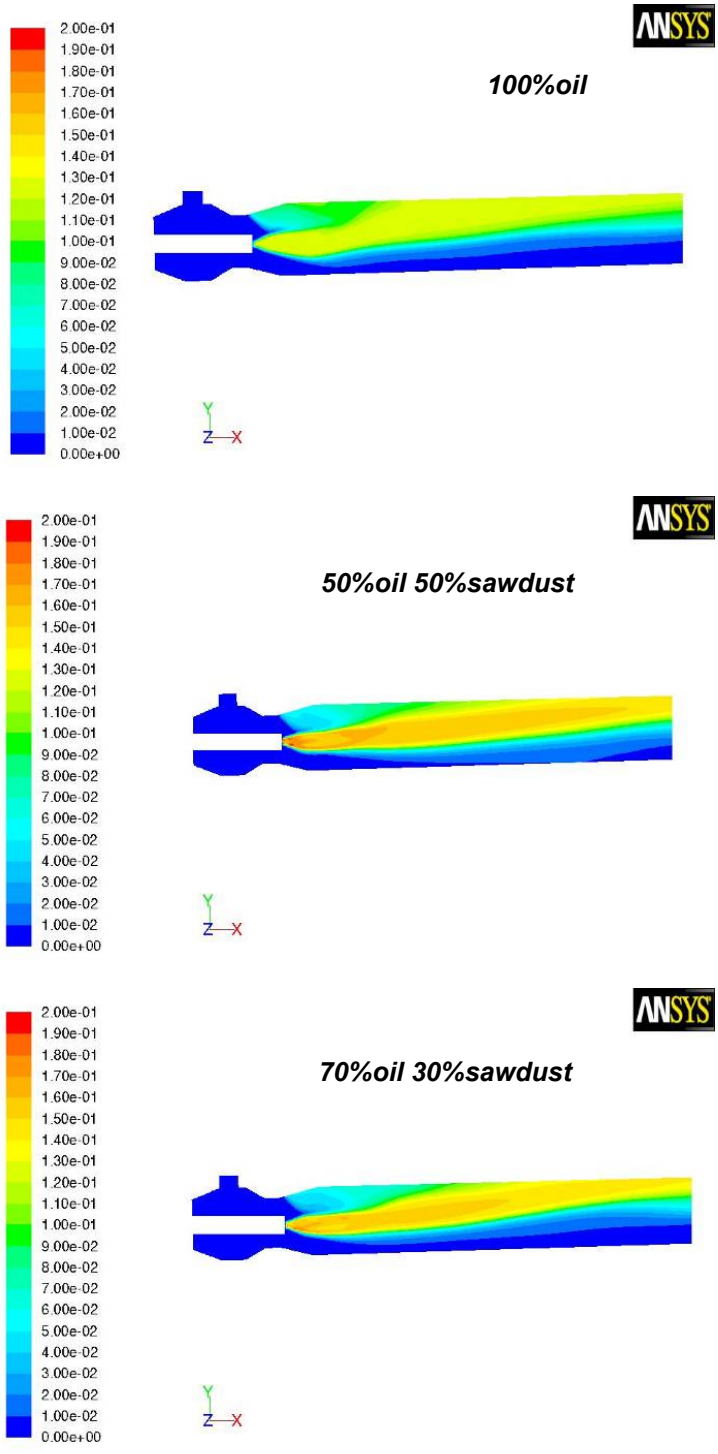

Figur 23. Konturplottar för jämförelse av H_2O koncentrationer (molfraktioner) i central-vertikala plan (z=0 och x<=20m) för de tre bränsleblandningarna

Figure 23. Comparison of the predicted contours of H_2O concentration (mole fraction) in the central-vertical plane (z=0 and x<=20m) for the three different fuel mixtures

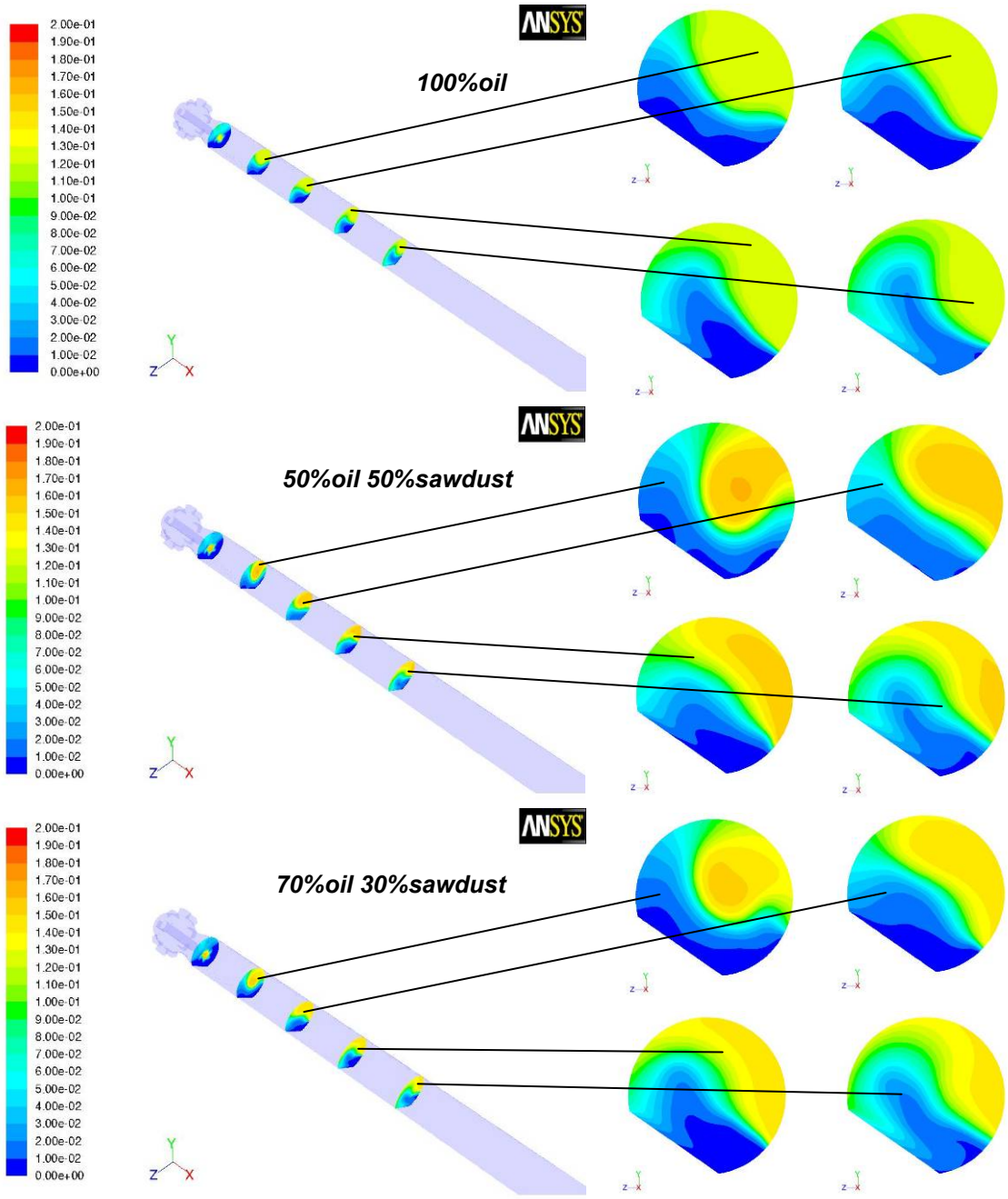

Figur 24. Konturplottar för jämförelse av H_2O koncentrationer (molfraktioner) i fem tvärsnitt (x=5m, 10m, 15m, 20m, and 25m) för de tre bränsleblandningarna

Figure 24. Comparison of the predicted contours of H_2O concentration (mole fraction) in five cross-sections of the kiln (x=5m, 10m, 15m, 20m, and 25m) for the three different fuel mixtures

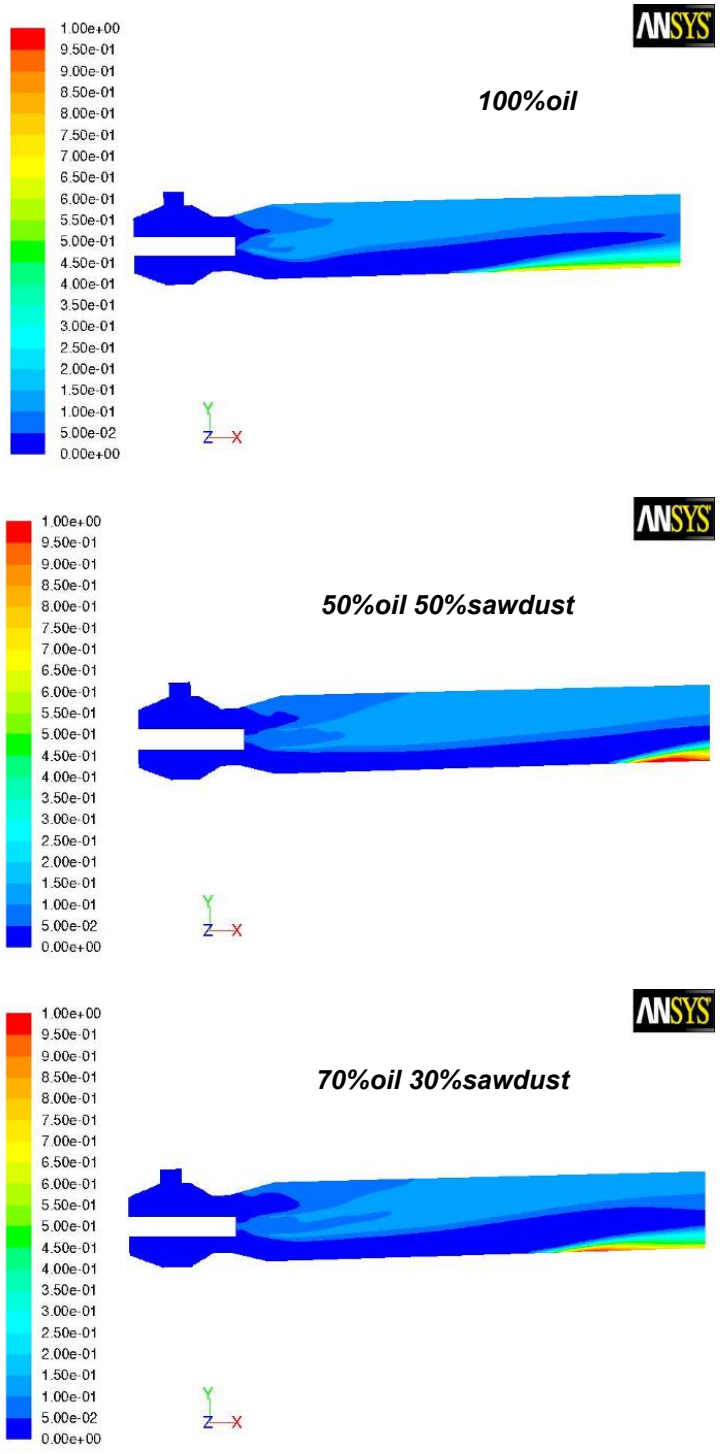

Figur 25. Konturplottar för jämförelse av CO_2 koncentrationer (molfraktioner) i central-vertikala plan (z=0 och x<=20m) för de tre bränsleblandningarna

Figure 25. Comparison of the predicted contours of CO_2 concentration (mole fraction) in the central-vertical plane (z=0 and x<=20m) for the three different fuel mixtures

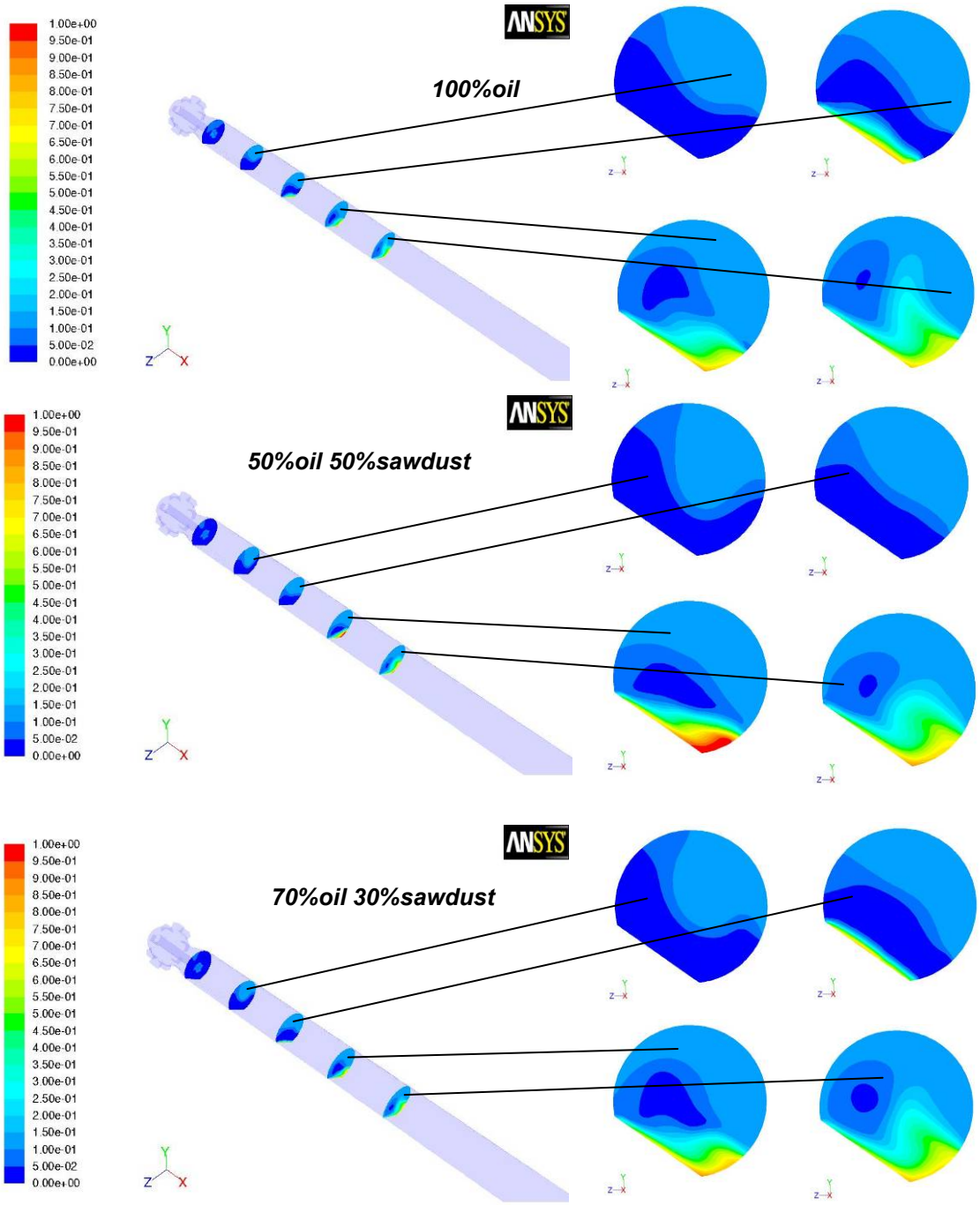

Figur 26. Konturplottar för jämförelse av CO_2 koncentrationer (molfraktioner) i fem tvärsnitt (x=5m, 10m, 15m, 20m, and 25m) för de tre bränsleblandningarna

Figure 26. Comparison of the predicted contours of CO_2 concentration (mole fraction) in five cross-sections of the kiln (x=5m, 10m, 15m, 20m, and 25m) for the three different fuel mixture

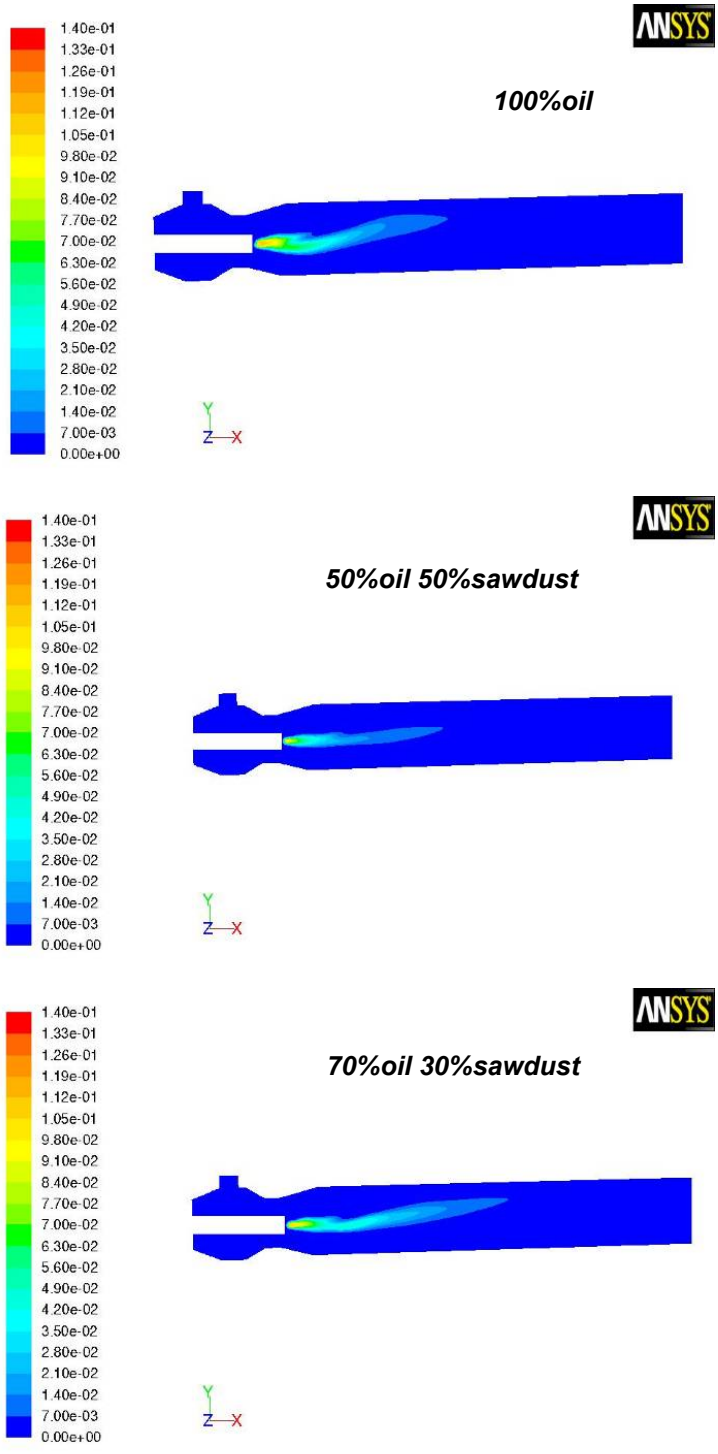

Figur 27. Konturplottar för jämförelse av koncentrationer av evaporiserad olja (molfraktioner) i central-vertikala plan (z=0 och x<=20m) för de tre bränsleblandningarna

Figure 27. Comparison of the predicted contours of oil vapour concentration (mole fraction) in the central-vertical plane (z=0 and x<=20m) for the three different fuel mixtures

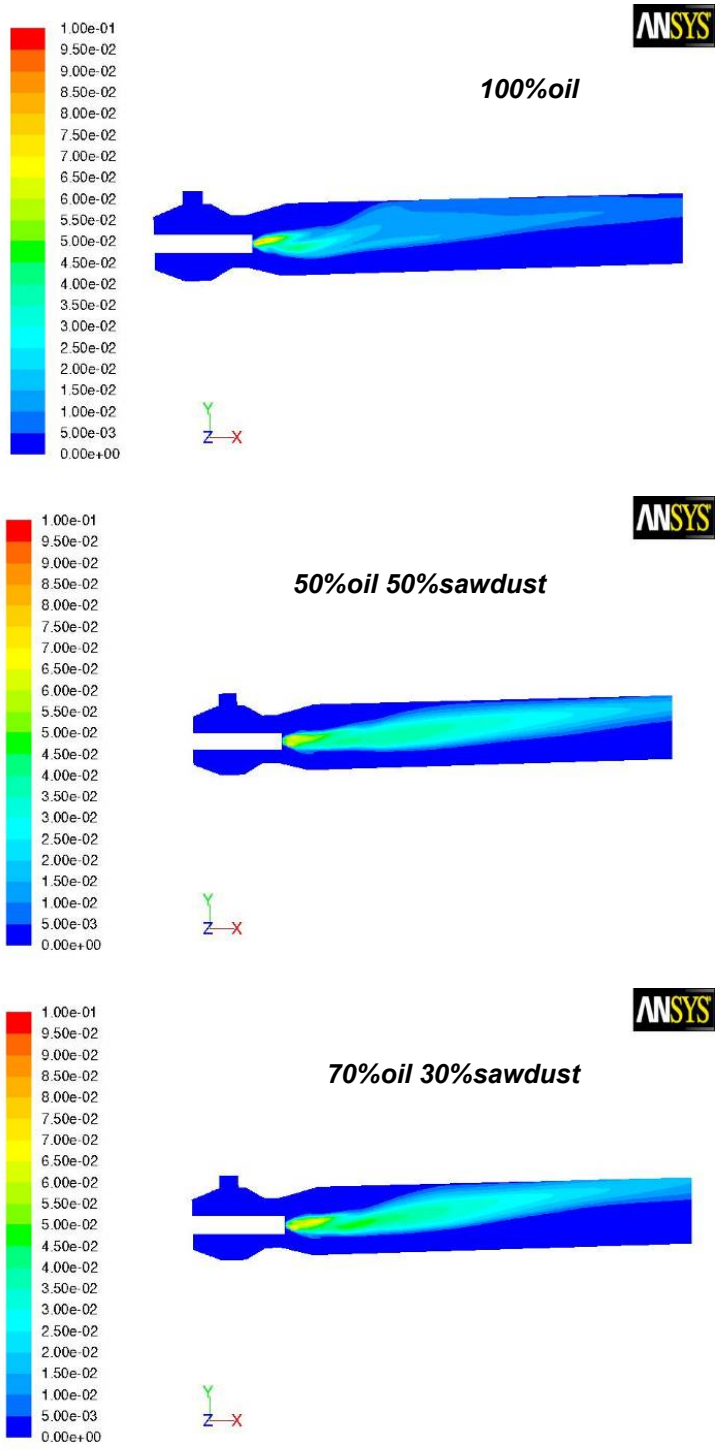

Figur 28. Konturplottar för jämförelse av CO koncentrationer (molfraktioner) i central-vertikala plan (z=0 och x<=20m) för de tre bränsleblandningarna

Figure 28. Comparison of the predicted contours of CO concentration (mole fraction) in the central-vertical plane (z=0 and x<=20m) for the three different fuel mixtures

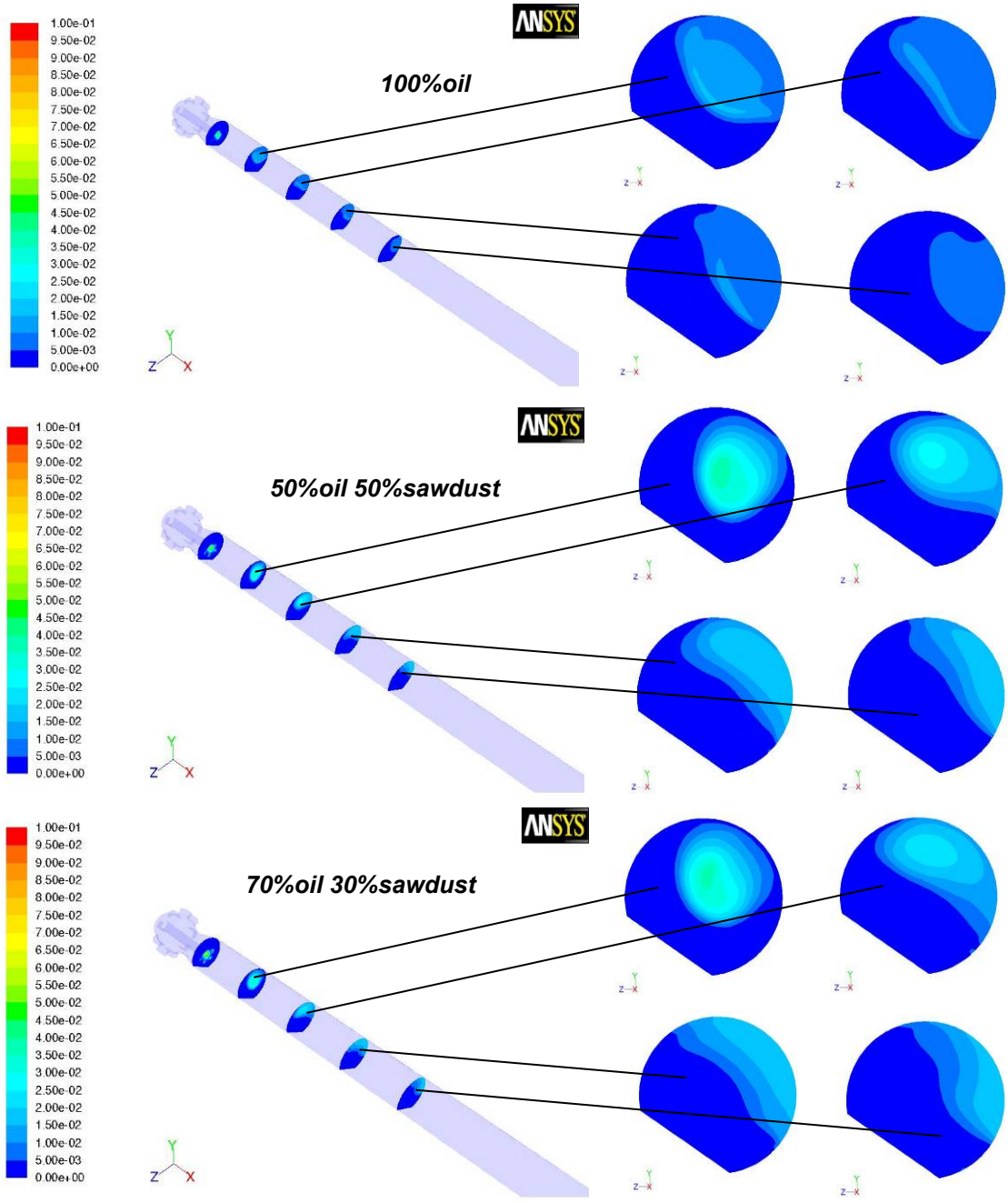

Figur 29. Konturplottar för jämförelse av CO koncentrationer (molfraktioner) i fem tvärsnitt (x=5m, 10m, 15m, 20m, and 25m) för de tre bränsleblandningarna

Figure 29. Comparison of the predicted contours of CO concentration (mole fraction) in five cross-sections of the kiln (x=5m, 10m, 15m, 20m, and 25m) for the three different fuel mixture

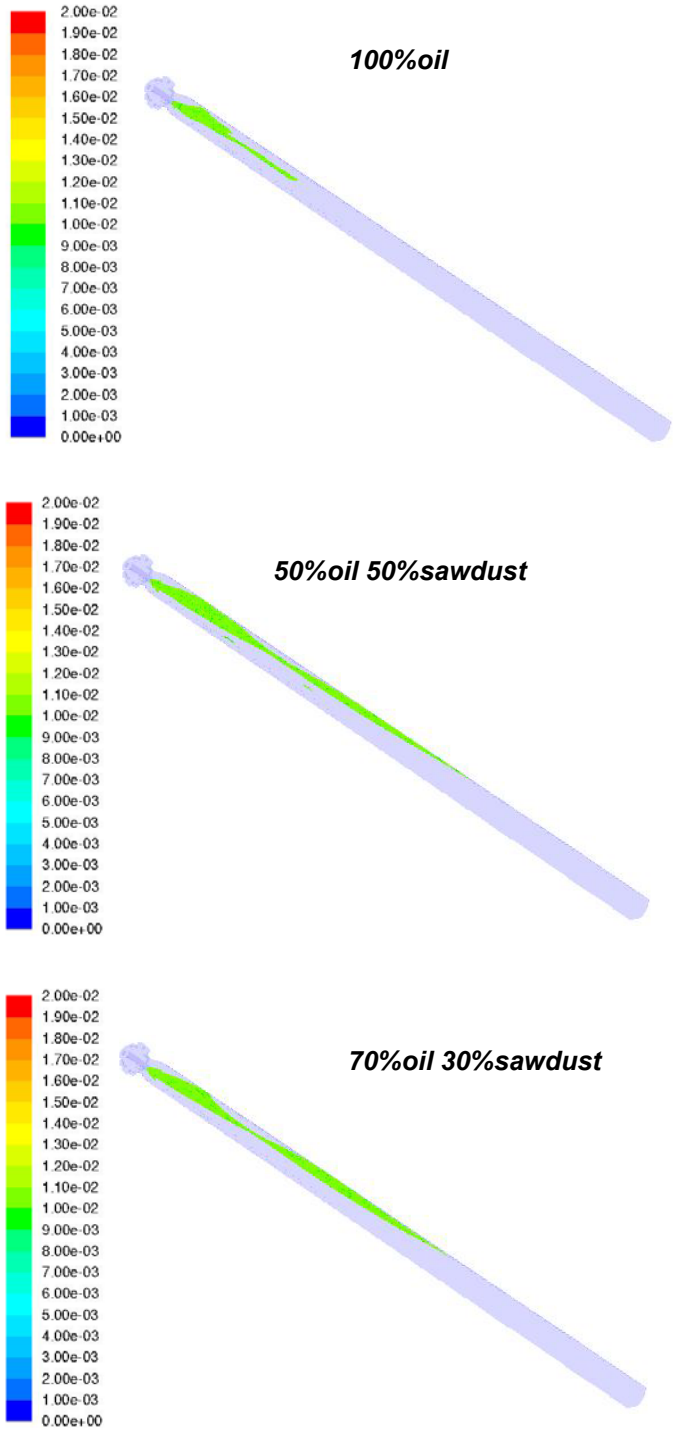

Figur 30. Iso-ytor för jämförelse av CO koncentrationer (molfraktion = 0.01) för de tre bränsle-blandningarna

Figure 30. Comparison of the predicted iso-surfaces of the CO concentration (mole fraction = 0.01) for the three different fuel mixtures

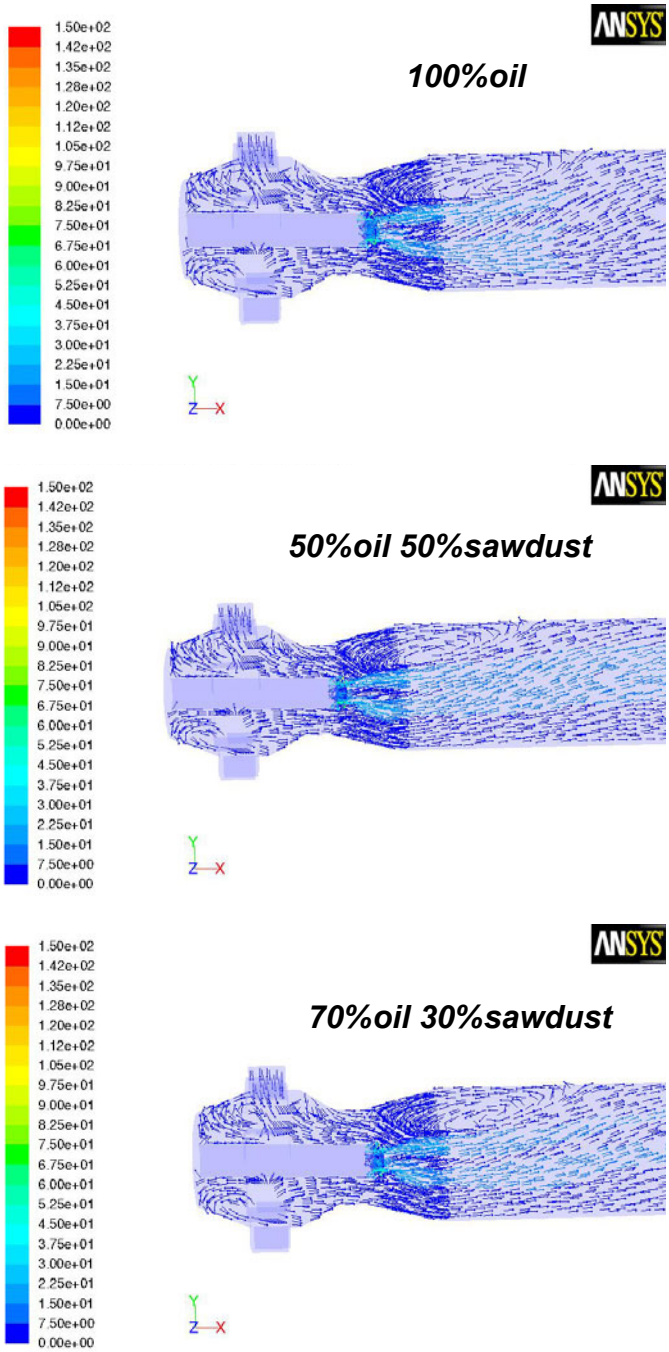

Figur 31. Vektorplottar för jämförelse av hastighetsvektorer [m/s] i central-vertikala plan (z=0) för de tre bränsleblandningarna

Figure 31. Comparison of the predicted velocity vectors [m/s] near the burner region in the central-vertical plane of the kiln for the three different fuel mixtures

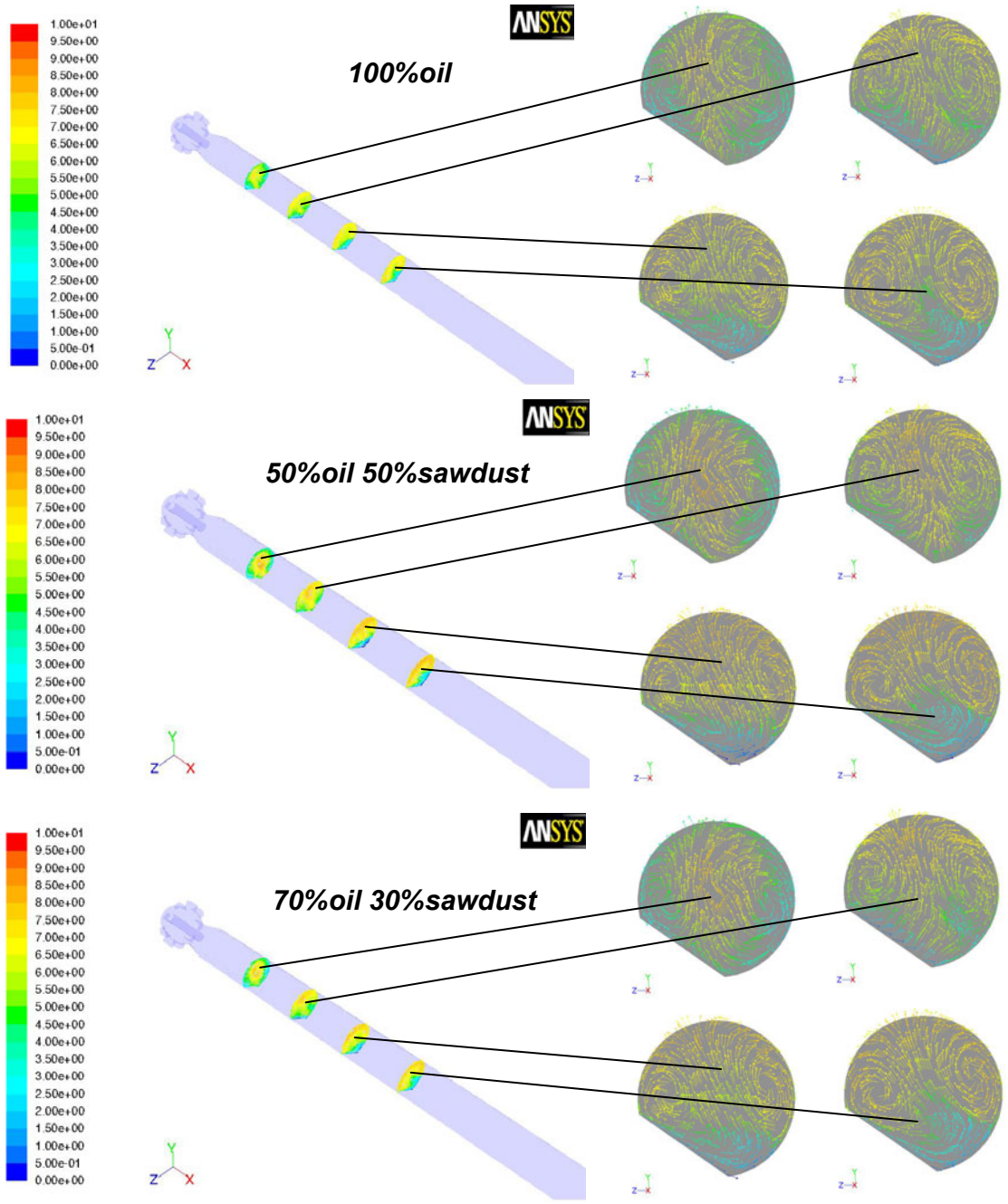

Figur 32. Vektorplottar för jämförelse av hastighetsmagnitud [m/s] (storlek och riktning) i fyra tvärsnitt (x= 10m, 15m, 20m, and 25m) för de tre bränsleblandningarna

Figure 32. Comparison of the predicted velocity magnitude vectors [m/s] in four cross-sections of the kiln (x=10m, 15m, 20m, and 25m) for the three different fuel mixtures

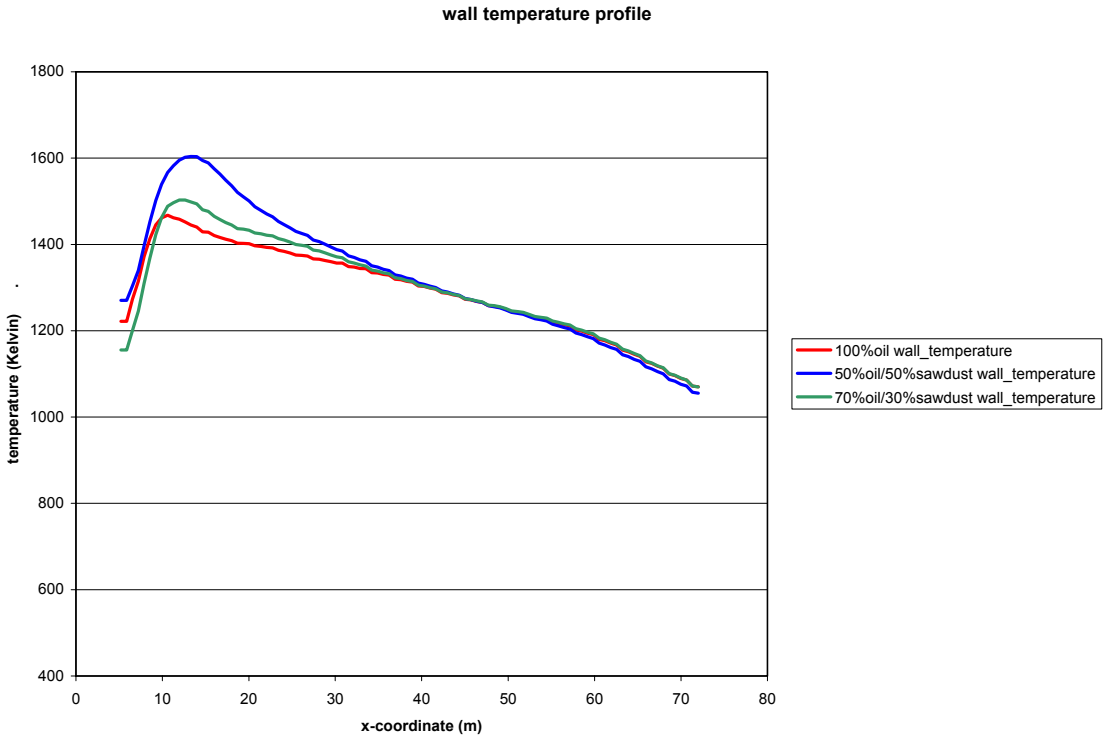

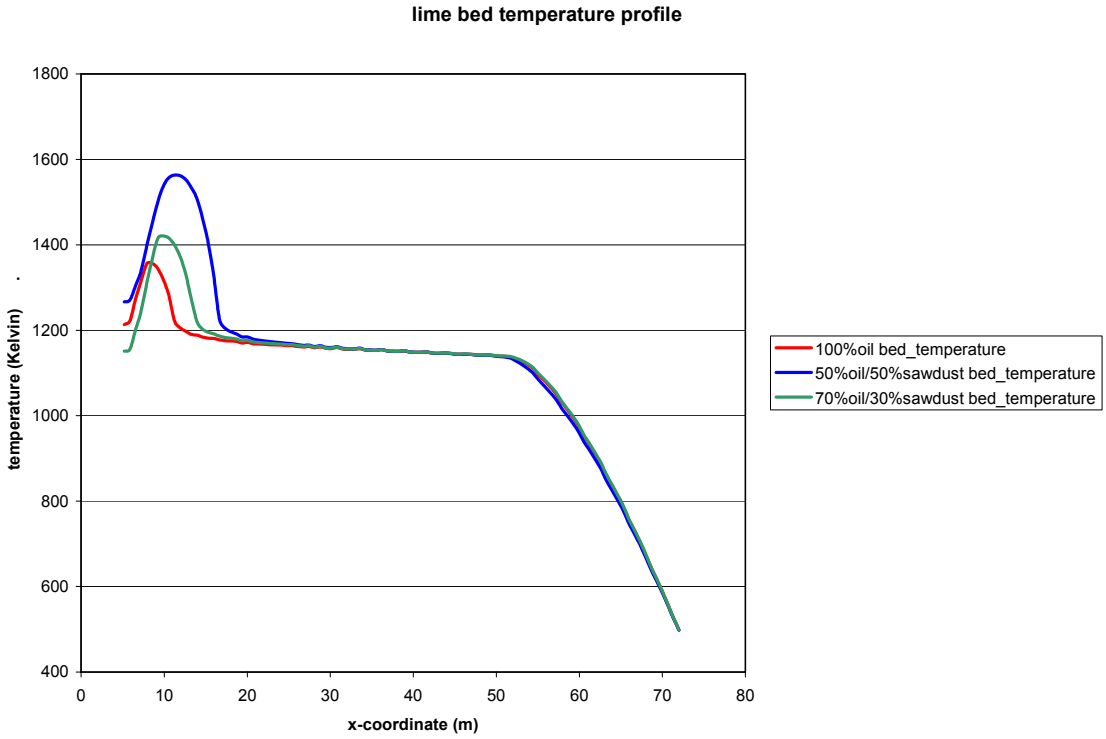

Figur 33. Jämförelse av medeltemperaturprofilerna i bädden samt vid ugnsväggens insida för de tre bränsleblandningarna

Figure 33. Comparison of the predicted average temperature profiles of the lime bed and kiln wall for the three different fuel mixtures

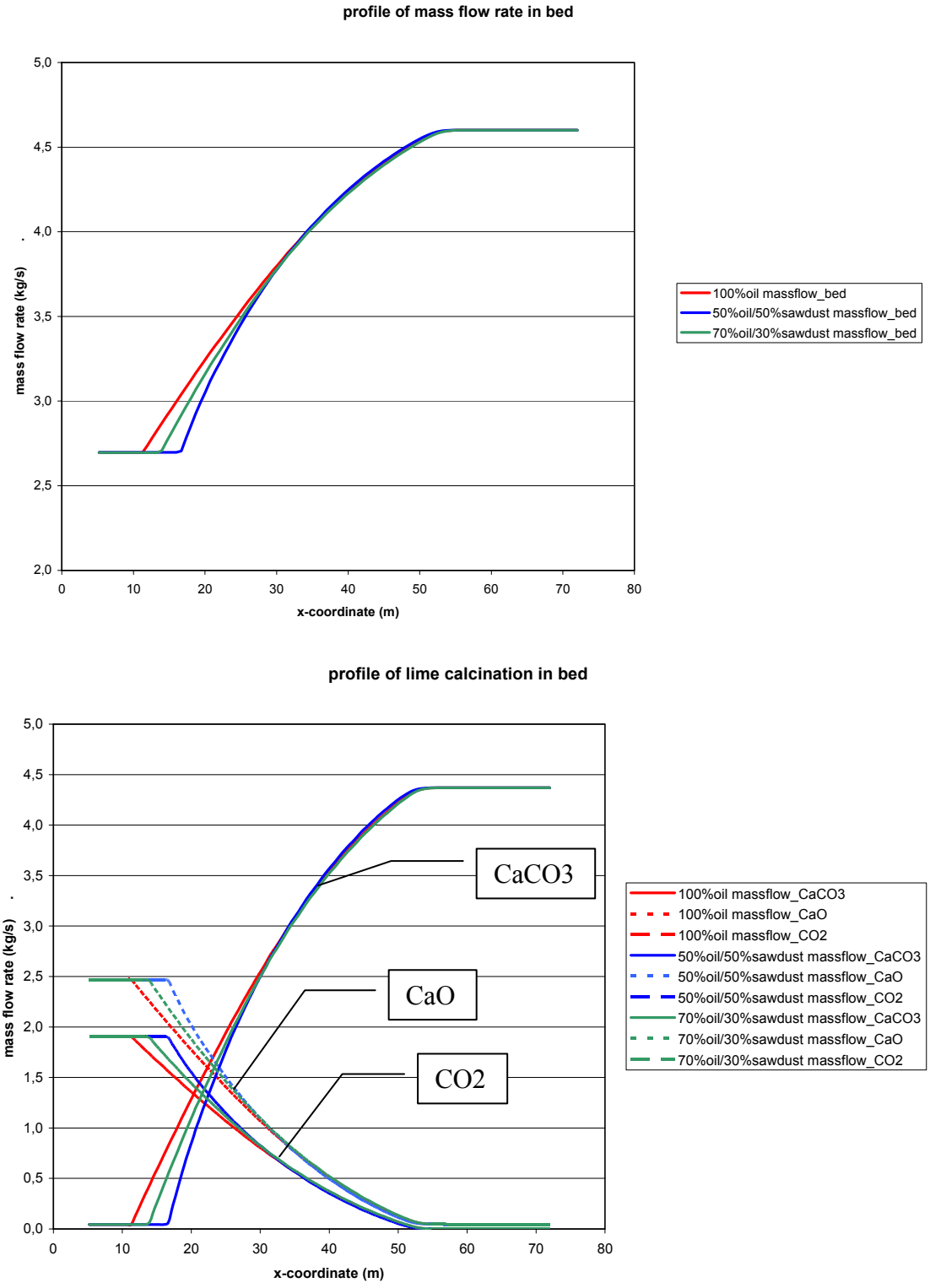

Figur 34. Jämförelse av massflödesförändringen för de tre olika bränsleblandningarna

Figure 34. Comparison of the predicted mass flow rate profiles for the three different fuel mixtures

Tabell 7. Beräknade gastemperaturer, gassammansättning och flöde vid ugnens utlopp

Table 7. Calculated flue gas temperature, composition and flow rate at the outlet

	100% oil	50% oil/50% sawdust	70% oil/30% sawdust
Temperature °C	801	787	801
O_2 vol.%	3.2	3.1	3.3
CO_2 vol.%	24.4	26	25.3
H_2O vol.%	8.7	9.1	8.9
Flow rate Nm^3/s	7.48	7.49	7.54

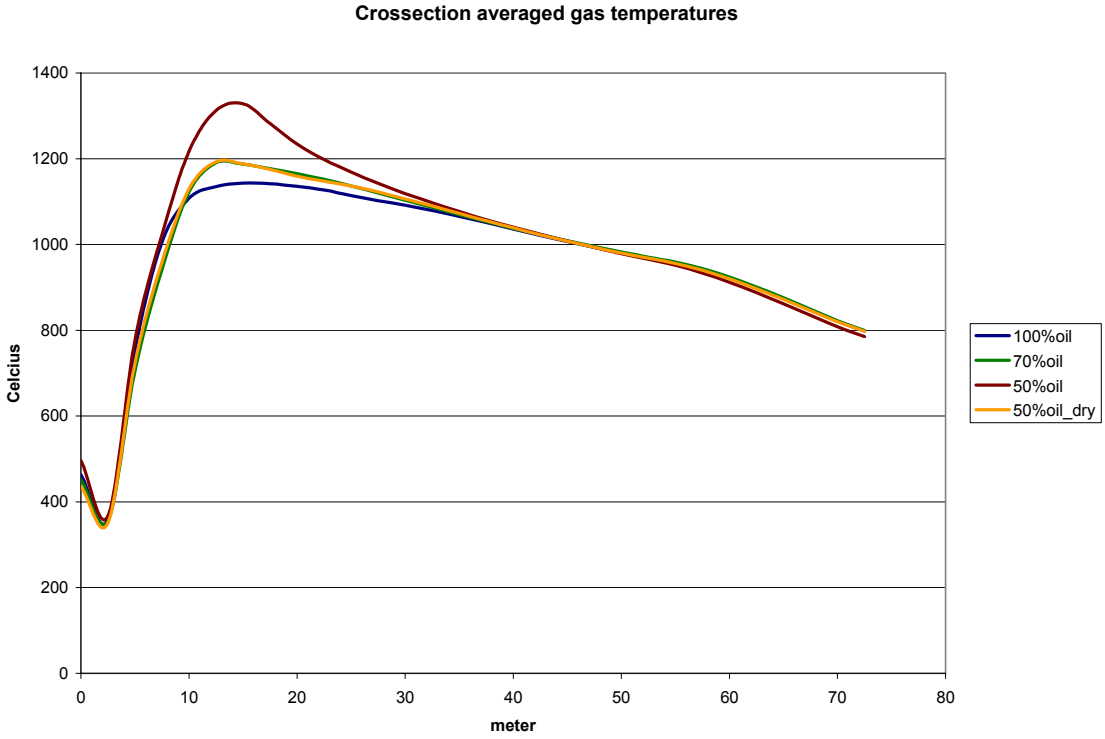

Figur 35. Jämförelse av medelgastemperatur i ugnens tvärsnitt för de tre olika bränsleblandningarna

Figure 35. Comparison of the predicted average gas temperature over the crossection of the kiln for the three different fuel mixtures

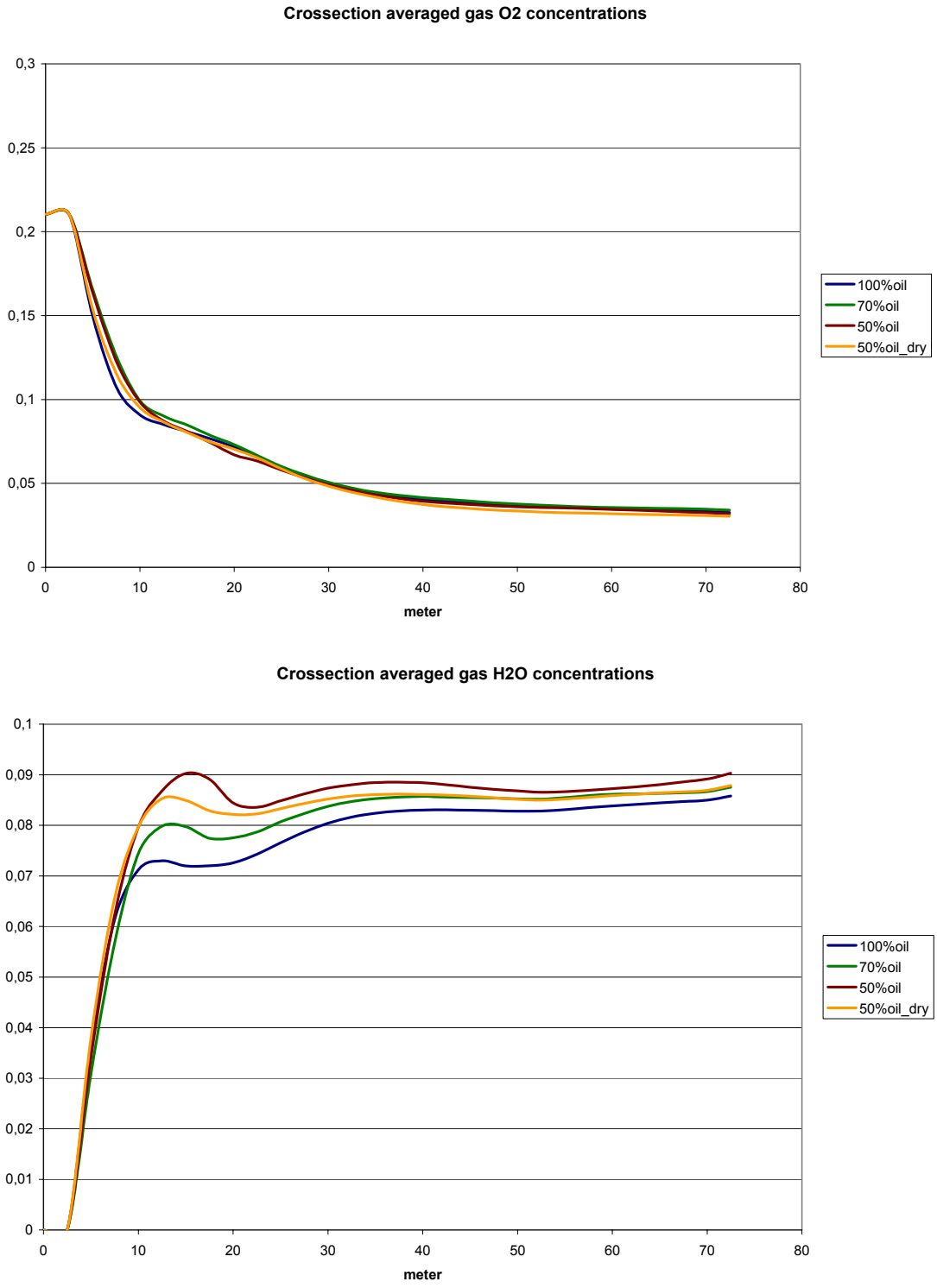

Figur 36. Jämförelse av medelconcentrationer (molfraktioner) av O_2 och H_2O i ugnens tvärsnitt för de tre olika bränsleblandningarna

Figure 36. Comparison of the predicted average concentrations (mole fractions) of O_2 and H_2O over the crossection of the kiln for the three different fuel mixtures I mixtures

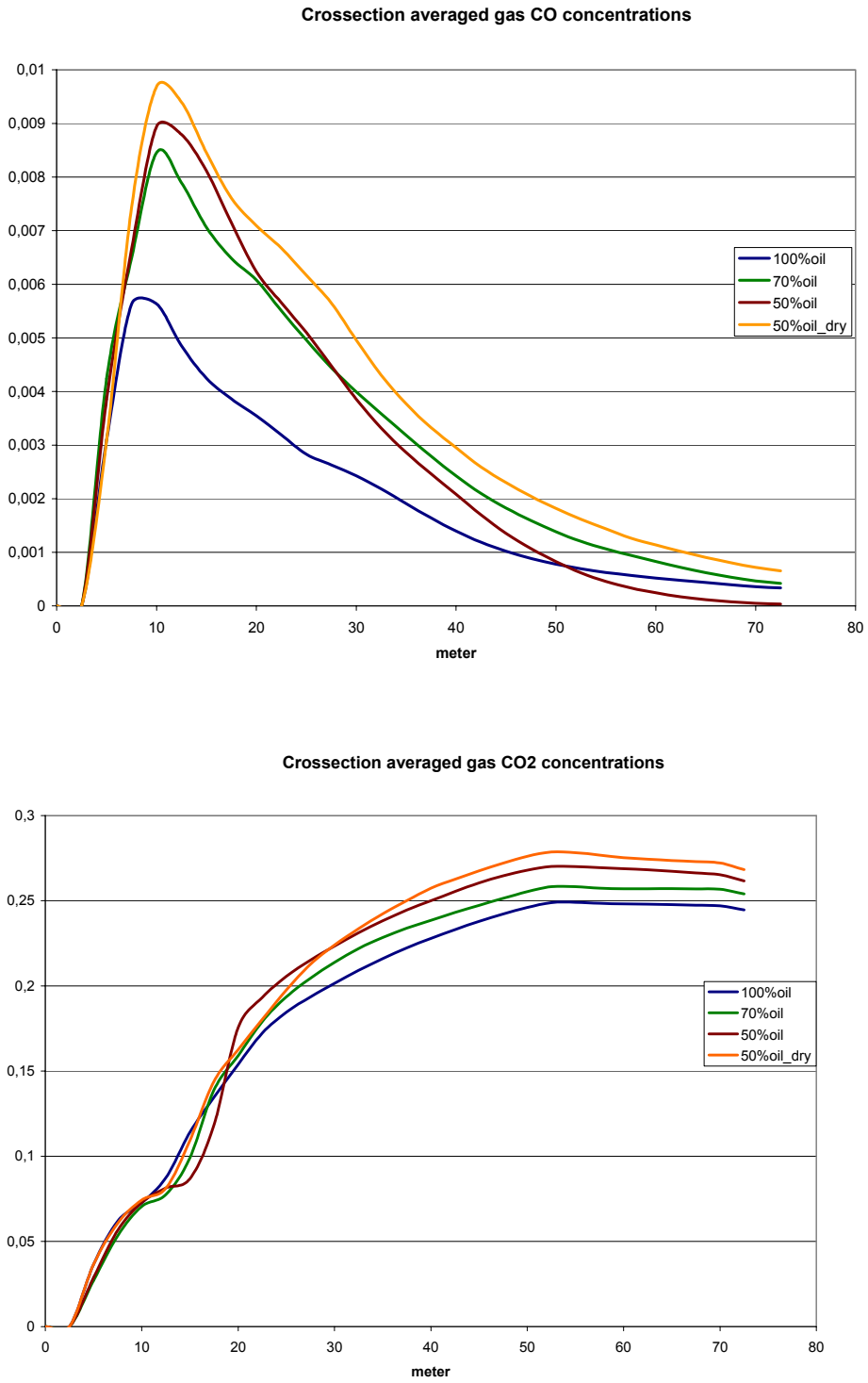

Figur 37. Jämförelse av medelconcentrationer (molfraktioner) av CO och CO_2 i ugnens tvärsnitt för de tre olika bränsleblandningarna

Figure 37. Comparison of the predicted average concentrations (mole fractions) of CO and CO_2 over the crossection of the kiln for the three different fuel mixtures

4.2 Results from the measurement campaign

4.2.1 Gas composition and gas temperatures at the hot end

Figure 38 - Figure 39 show the temperatures and gas composition at the hot end of the kiln for the cases 50% oil /50% sawdust and 100% oil, respectively. Position #2 is located about 0.3 m above the burner and position #3 is located approximately 0.3 m below the burner, see Figure 14.

In both cases, a clear trend is that the upper parts of the kiln are much warmer than the lower parts, at an insertion depth of 5 m into the kiln. In the 50% oil /50% sawdust case, Figure 39, at 5 meter into the kiln a distinct vertical temperature gradient can be seen (i.e. a line connecting positions #2 and #3). The temperature gradient translates into a temperature difference of up to 400 ^{o}C along a 0.6 meter vertical line (5 meter into the kiln). It is also clear that for the 100% oil case, Figure 38, the temperature gradient is still evident, although reduced to about 100 ^{o}C along a 0.6 meter vertical line.

A closer look at the absolute temperatures shows that the maximum peak temperature was recorded for the 50% oil /50% sawdust case at 974 ^{o}C (average over 10 minutes was 935 ^{o}C). The corresponding value for the 100% oil case was 938 ^{o}C (average over 10 minutes was 887 ^{o}C). Both of these recordings were made when the probe was moved to a position in the upper part of the kiln, and moved to the right closer to the burner. Expanding the analysis to other positions at an insertion depth of 5 meters reveals that the 50% oil / 50% sawdust case displays higher temperature at all these positions. This trend result is the opposite of that found in the data from the existing thermocouple (position just below the burner) where the 100% oil case showed about 100 ^{o}C higher temperature in average (see Figure 11).

A general trend in the gas composition, Figure 40 - Figure 41, is that the concentration of combustion products, e.g. CO_2, CO, and NO, is higher in the upper part of the kiln (position #2). A comparison between the fuel mixture and the CO_2 concentration in the upper part of the kiln shows that the levels range between 0.5 and 3.5 vol-%, and that the 50% oil /50% sawdust case in general has about 1 vol-% higher CO_2 concentration than the 100% oil case. The N_2Ooch SO_2 concentrations were close to zero and are not presented here.

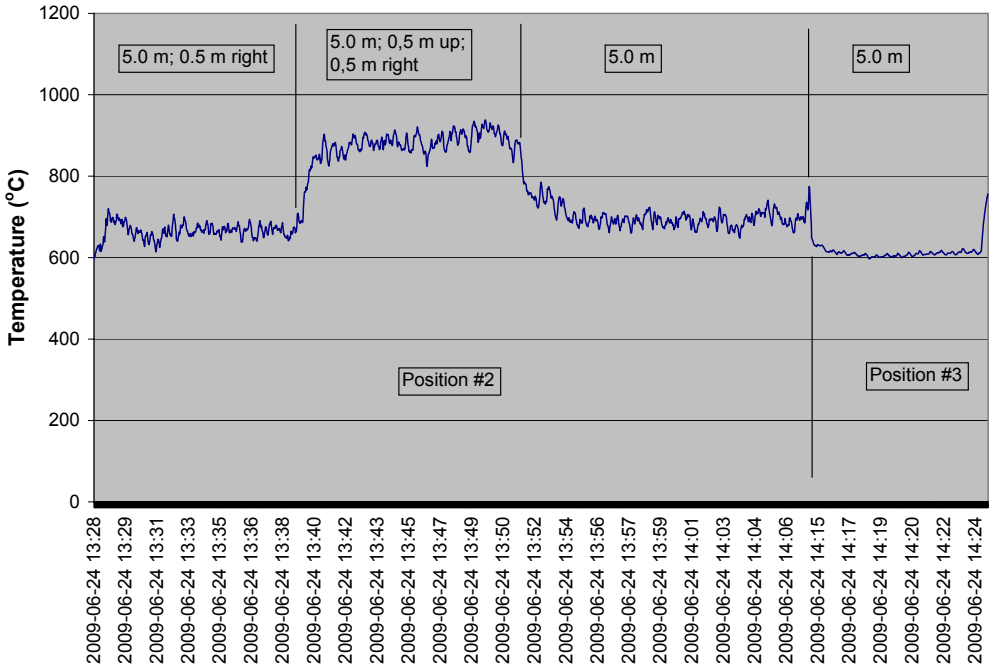

Figur 38. Rökgastemperatur vid varma gaveln för 100% olja

Figure 38. Flue gas temperature at the hot end for 100% oil

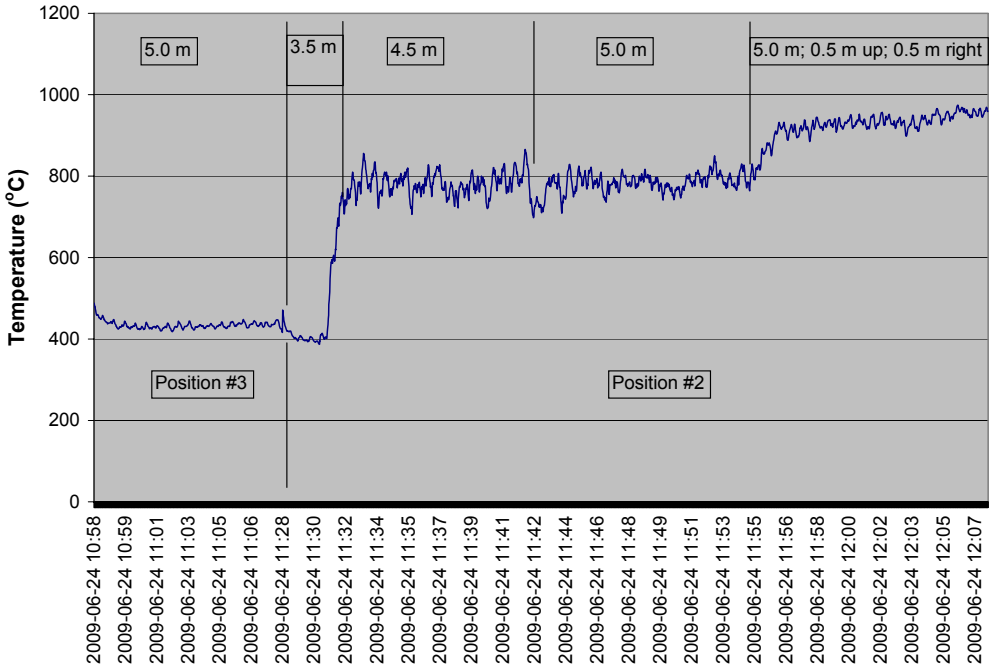

Figur 39. Rökgastemperatur vid varma gaveln för 50% olja / 50% sågspån

Figure 39. Flue gas temperature at the hot end for 50% oil / 50% sawdust

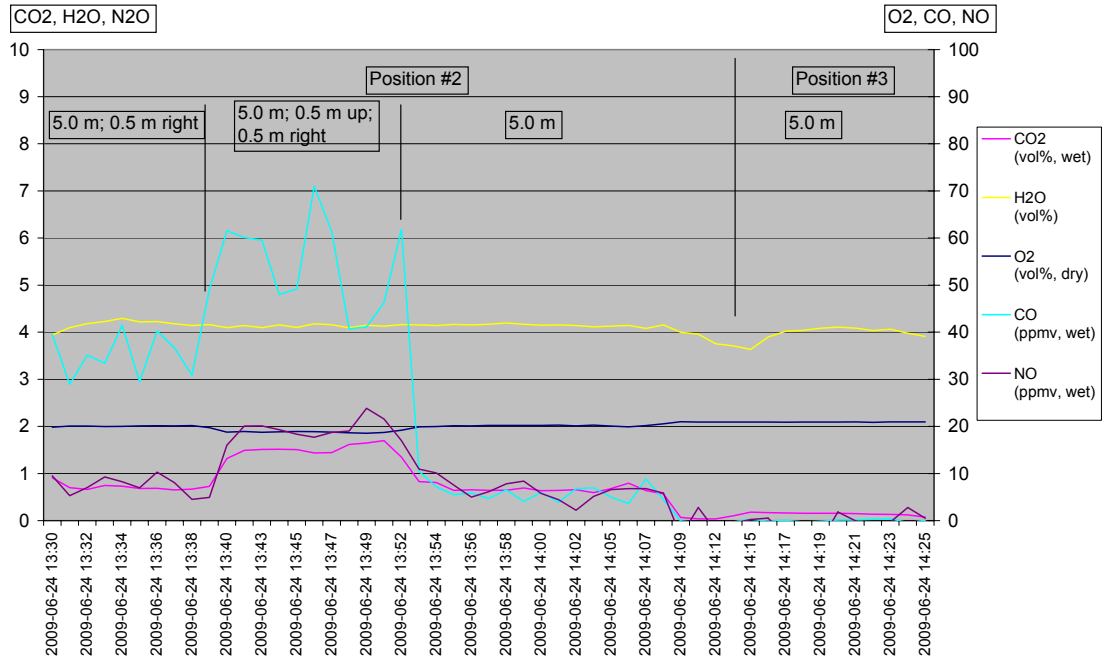

Figur 40. Rökgassammansättning vid varma gaveln för 100% olja

Figure 40. Flue gas composition at the hot end for 100% oil

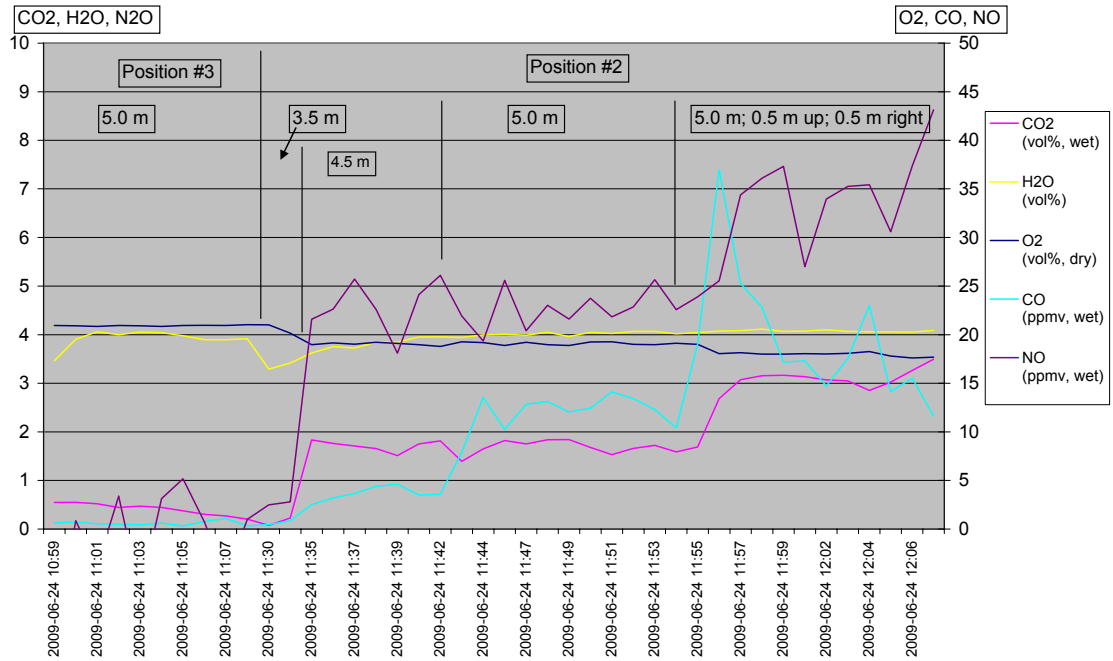

Figur 41. Rökgassammansättning vid varma gaveln för 50% olja / 50% sågspån

Figure 41. Flue gas composition at the hot end for 50% oil / 50% sawdust

4.2.2 Gas composition and gas temperatures at the cold end

Figure 42 - Figure 43 and Figure 44 - Figure 45 shows the temperatures and gas composition at the cold end of the kiln for the 100% oil and 50% oil /50% sawdust cases respectively. Position #2 and #3 corresponds to a position about 0.3 meter above the burner (position #2) and 0.3 m below the burner (position #3), see Figure 14.

In both cases, two clear results are that (i) the upper parts of the kiln are much warmer than the lower parts and (ii) the maximum temperature is just above 800 ^{o}C at an insertion depth of 2.5 meter into the kiln. At an insertion depth of 2.5 the temperature gradient is in the range of 140 – 150 ^{o}C along a vertical distance of 1 meter

Large differences in CO concentration can be observed between the two fuel mixtures. The 50% oil /50% sawdust case did occasionally reach close to 4800 ppm of CO at the cold end whereas the levels for 100% oil never went higher than some 30 ppm in CO. The O_2 concentration was very low for the 50% oil /50% sawdust case, between 0.1-0.2 vol-%, and this may explain the high CO concentrations. NO concentrations were slightly higher when sawdust was used. A comparison with the oxygen data recorded by the kiln control system shows (i) similar trends and (ii) that the control system values are about 3 vol-% units higher than the probe measurements indicated. A possible explanation to this is that leakage air has entered the flue gas channel between the kiln exit and the position of the oxygen sensor of the control system. The N_2O och SO_2 concentrations were close to zero and are not presented here.

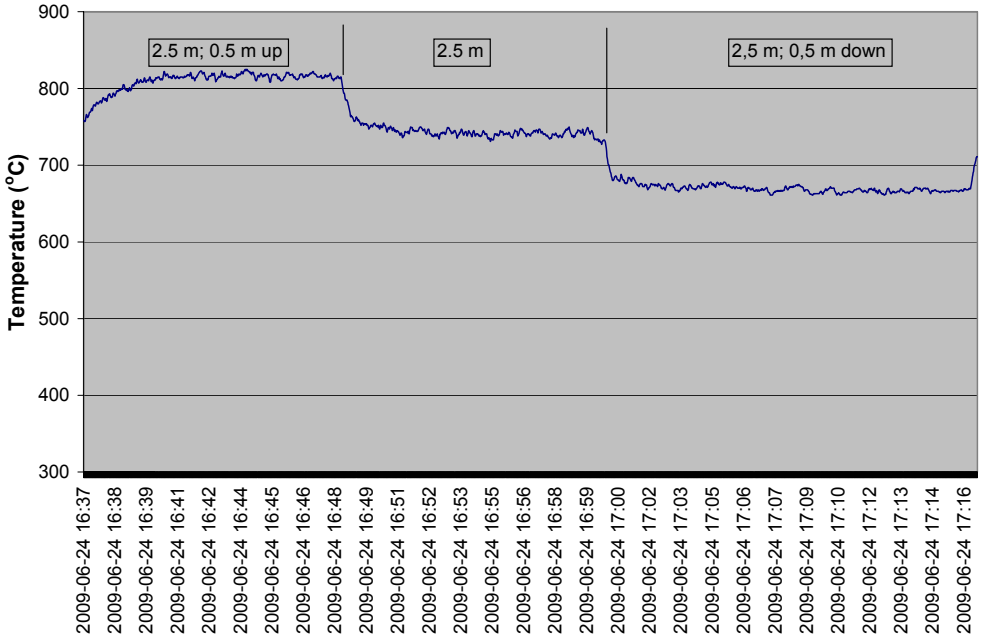

Figur 42. Rökgastemperatur vid kalla gaveln för 100% olja

Figure 42. Flue gas temperature at the cold end for 100% oil

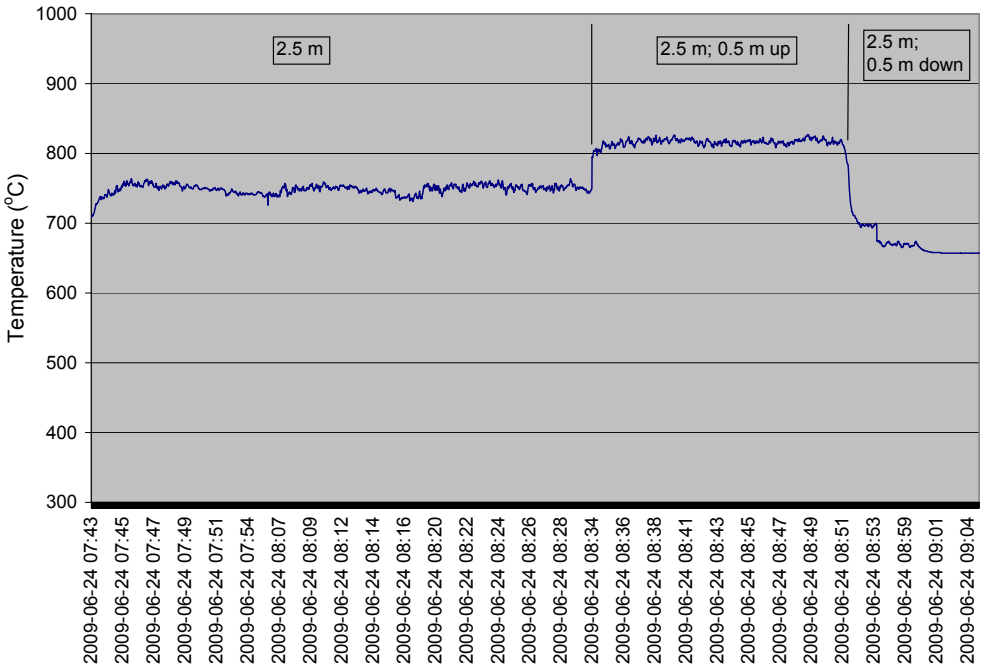

Figur 43. Rökgastemperatur vid kalla gaveln för 50% olja / 50% sågspån

Figure 43. Flue gas temperature at the cold end for 50% oil / 50% sawdust

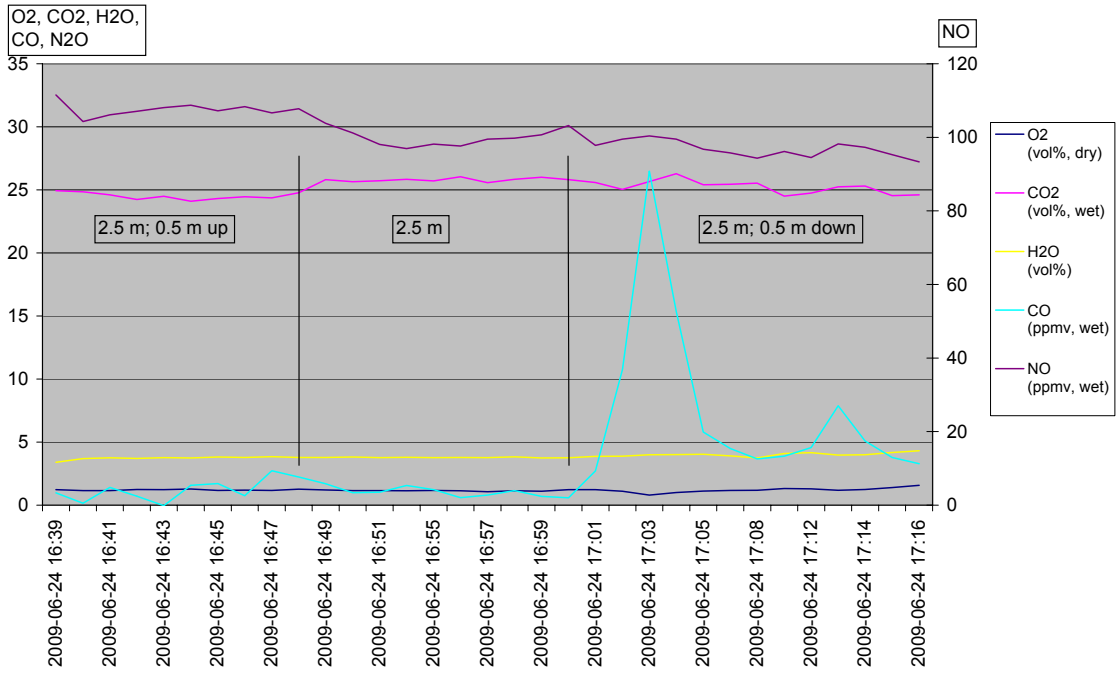

Figur 44. Rökgassammansättning vid kalla gaveln för 100% olja

Figure 44. Flue gas composition at the cold end for 100% oil

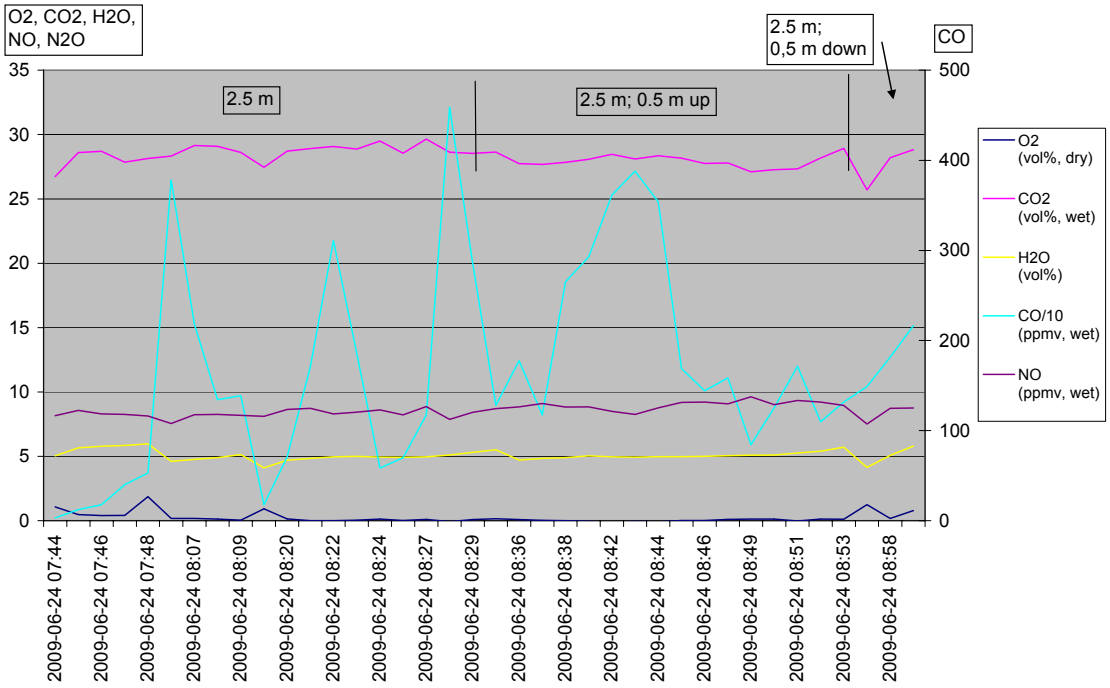

Figur 45. Rökgassammansättning vid kalla gaveln för 50% olja / 50% sågspån

Figure 45. Flue gas composition at the cold end for 50% oil / 50% sawdust

4.2.3 Lime bed temperature

The average lime bed temperatures measured by the IR camera for all fuel mixtures are shown in Table 8. The highest temperature was registered for the 100% oil case at 951 ^{o}C and the lowest temperature was measure for the 50% oil / 50% sawdust case at 843 ^{o}C. From the temperatures listed in the table, it becomes clear that the lime bed temperature decreases as the share of solid biomass in the fuel increases. The trend is similar in the temperature that was recorded by the existing thermocouple positioned just below the burner (reference temperature).

Tabell 8. Genomsnittlig bäddtemperatur för de olika att bränslemixarna

Table 8. Average lime bed temperatures for the different fuel mixtures

Fuel mix	Temperature (^{o}C)
100% oil	951
70% oil / 30% sawdust	930
50% oil / 50% sawdust	843

4.3 Evaluation of the simulations against the in-plant measurement data

The in-plant measurements are carried out at the Södra Cell Mönsterås mill by Innventia. Two measurement positions (Position #2 and Position #3) on the hot end (the burner side) and one measurement position (Position #1) on the cold end (the lime mud entrance side) were used to measure the gas temperature and species concentrations as described previously. The comparison between the measured data and the predicted values at these measurement points are presented in Figures 35-38. Furthermore, an average value over a cylindrical volume representing the estimated measurement precision (radius and length 0.15 meter) around the measurement points on the hot side is presented.

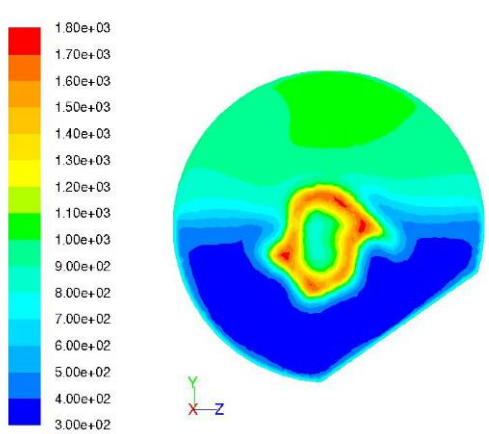

100% oil case, hot end:

	P#2	P#3
Calculated, point value	858°C	404°C
Calculated,vol. average	669 °C	366°C
Measured	691°C	611°C

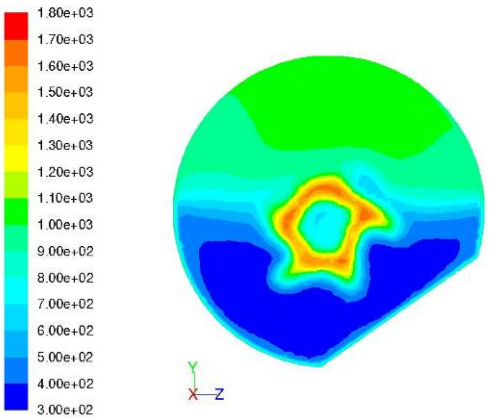

50%oil 50%sawdust case, hot end:

	P#2	P#3
Calculated, point value	905°C	389°C
Calculated,vol. average	746 °C	362°C
Measured	785°C	434°C

Figur 46. Konturplottar för jämförelse av gastemperaturer i mätplan vid ugnens varma sida (x=5m), samt jämförelse av beräknade och uppmätta värden i mätpunkterna: Position #2 och Position #3

Figure 46. Comparison of the predicted contours of gas temperature (°C) at the measurement plane (hot end, x=5m) and the comparisons between the calculated and measured values at the measurement points: Position #2 and Position #3

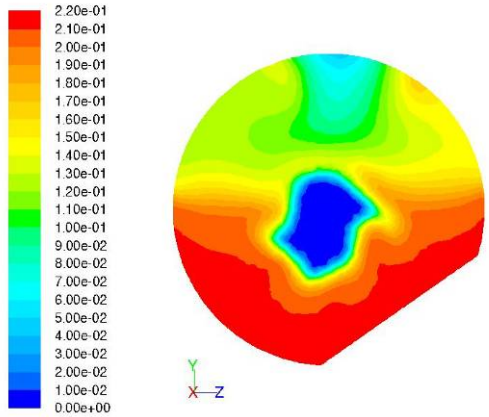

100%oil case, hot end:

	P#2	P#3
Calculated, point value	0.138	0.202
Calculated,vol. average	0.166	0.208
Measured	0.202	0.209

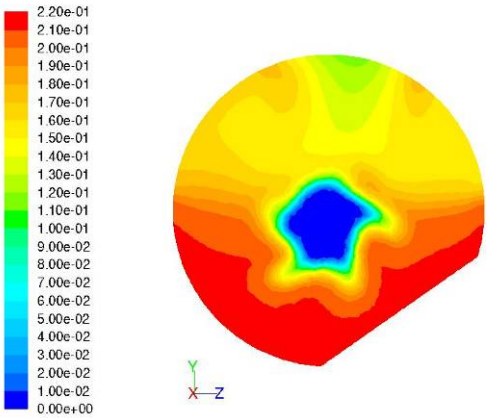

50%oil 50%sawdust case, hot end:

	P#2	P#3
Calculated, point value	0.165	0.208
Calculated,vol. average	0.179	0.209
Measured	0.191	0.21

Figur 47. Konturplottar för jämförelse av syrekoncentrationer (molfraktioner) i mätplan vid ugnens varma sida (x=5m), samt jämförelse av beräknade och uppmätta värden i mätpunkterna: Position #2 och Position #3

Figure 47. Comparison of the predicted contours of oxygen concentration (mole fraction) at the measurement plane (hot end, x=5m) and the comparisons between the calculated and measured values at the measurement points: Position #2 and Position #3

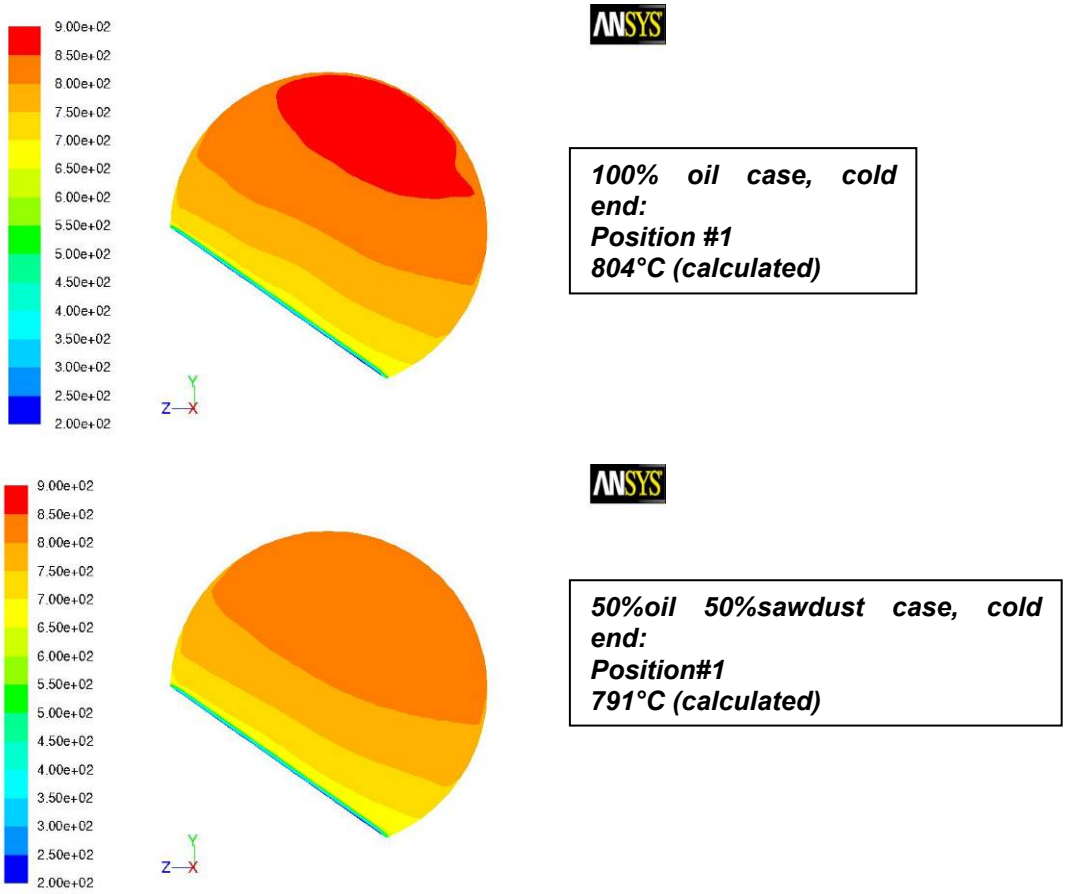

Figur 48. Konturplottar för jämförelse av gastemperaturer i mätplan på ugnens kalla sida (x=71.8m), samt jämförelse av beräknade och uppmätta värden i mätpunkterna: Position #1

Figure 48. Comparison of the predicted contours of gas temperature (°C) at the measurement plane (cold end, x=71.8m) and the comparisons between the calculated and the measured values at the measurement point: Position #1

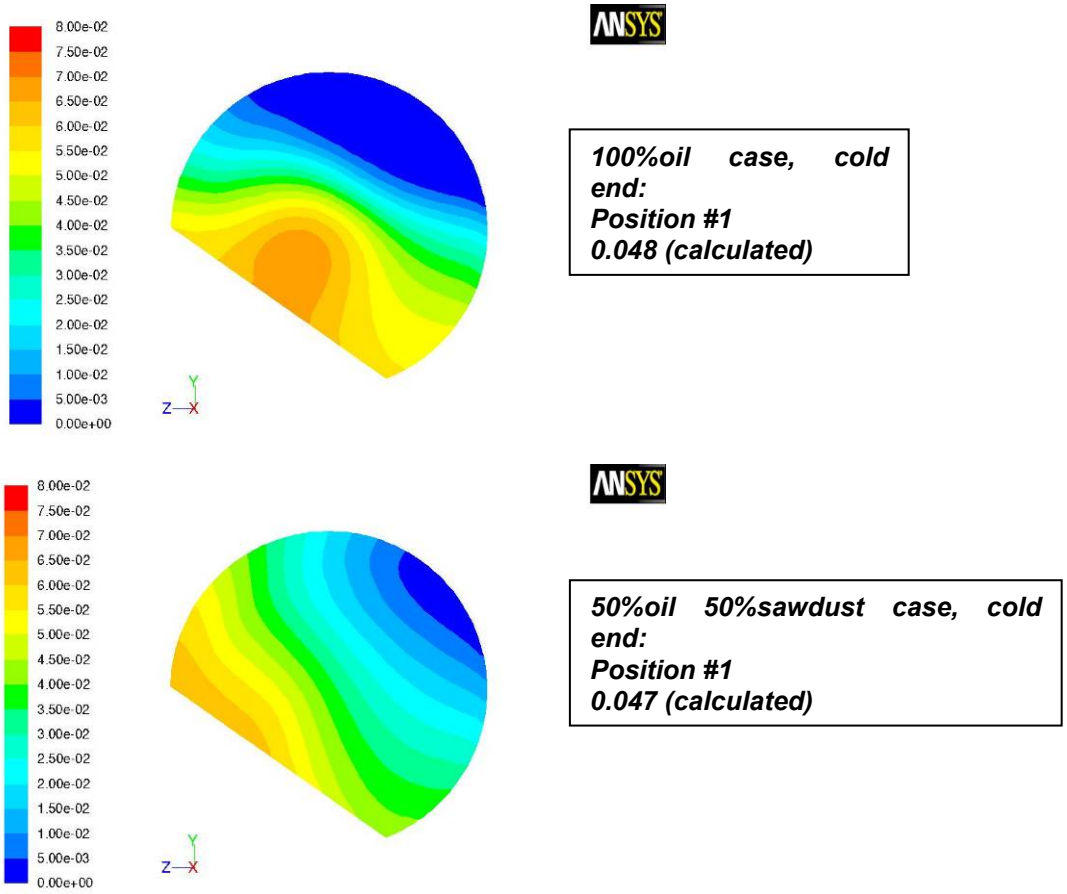

Figur 49. Konturplottar för jämförelse av syrekoncentrationer (molfraktioner) i mätplan vid ugnens kalla sida (x=71.8m), samt jämförelse av beräknade och uppmätta värden i mätpunkterna: Position #1

Figure 49. Comparison of the predicted contours of oxygen concentration (mole fraction) at the measurement plane (cold end, x=71.8m) and the comparisons between the calculated and the measured values at the measurement point: Position #1

5 Analysis of the results

Critical analysis and discussion of the numerical and measurement results and the affecting factors are presented as follows.

5.1 CFD MODELLING

The predicted gas temperature fields for the three different firing conditions are presented in Figures 19-20. As shown in these figures, the same trend as for the inner wall temperature is obtained for the gas temperature field as well. In the region from 35m to the fuel inlet (x < 40m), the gas temperature level is generally the hottest for the kiln operation fired with the fuel mixture: 50% oil/50% sawdust while the coolest for the kiln operation fired with 100% oil although the highest peak temperature in the near burner region can be found for the kiln operation fired with 100% oil. These results are in contradiction with results previously seen; however this trend exists both in the CFD simulation and in measurements. The kiln operation fired with the fuel mixture: 70% oil/30% sawdust has a gas temperature level in between. The higher gas temperature level in the freeboard of the lime kiln enhances the heat transfer to the lime bed and hence speeds up the lime calcination. The lime calcination rate is primarily controlled by the heat transfer rate from the hot gas flow to the lime bed.

As shown in Figures 17-18 and also the more quantitative information given in Figure 33, the three-dimensional CFD model for rotary lime kilns predicts that at the first 35m from the fuel inlet (x < 40m), the kiln operation fired with the fuel mixture: 50% oil/50% sawdust has the highest inner wall temperature level while the inner wall temperature level is the lowest for the kiln operation fired with 100% oil. The kiln operation fired with the fuel mixture: 70% oil/30% sawdust has an inner wall temperature level in between. After 35m from the fuel inlet (x > 40m), the inner wall temperature of the kiln becomes nearly identical for all the three firing conditions. The difference in the inner wall temperature is a consequence of the flame temperatures, and reflects the difference in the heat transfer rate to the lime bed. This leads to that the lime bed has the shortest time for calcination and reaches the highest sintering temperature level for the kiln operation fired with the fuel mixture: 50% oil/50% sawdust compared to the other two firing conditions. The lime bed is shown to have the longest time for calcination and reaches the lowest sintering temperature level for the kiln operation fired with 100% oil. The kiln operation fired with the fuel mixture: 70% oil/30% sawdust has a performance in between.

Figures 21-22 show the predicted oxygen concentration fields for the three different firing conditions. The oxygen concentration field has a close link with the actual flame. The general structure of the flame can be considered as a diffusion flame [9]. Inside the flame sheet the oxygen concentration is close to zero. As illustrated in these figures, the actual flame is not centralised in the freeboard of the lime kiln instead it is situated at

the upper-right corner in the cross-section of the lime kiln. The lift-up of the flame is obviously due to the buoyancy forces. In addition it can be noticed that the oxygen concentration field is affected by both the combustion process and the lime bed process in the kiln. The differences in the predicted oxygen concentration fields for the three firing conditions can be seen in these figures.

The predicted species concentration fields for the combustion products: H_2O and CO_2 are presented in Figures 23-26 for the three different firing conditions. As shown in Figures 23-24, the concentration of H_2O in the flame region is significantly higher for the co-firing of oil and sawdust than for the firing of 100% oil because significant moisture content exists for the sawdust which is 4.2% as given by the fuel analysis. Furthermore, it can be seen that the CO_2 concentration field is significantly affected by the lime bed process. As illustrated in Figures 25-26, the CO_2 released from the lime bed is more intensive for the kiln operation fired with the fuel mixture of 50% oil/50% sawdust compared to the other two firing conditions. This is due to the enhanced lime calcination in the bed.

Figure 27 presents the predicted oil vapour concentration field in the kiln for the three different firing conditions. The oil vapour is the gaseous product resulted from the vaporization of the oil droplets injected from the oil gun. As illustrated in this figure, the region with high oil vapour concentration becomes larger and more intensive for the kiln operation fired with 100% oil than for the co-firing oil and sawdust as expected from the practice. The comparison of relative size and intensity of the evaporated oil indicates that the flame is controlled by the gas-phase combustion rate rather than the vaporisation speed.

As described previously, the intermediate species CO is an important species used in combustion technology to indicate where the combustion reactions take place. Figures 28-29 present the predicted CO concentration fields for the three different firing conditions. As illustrated in these figures, the region with significant CO concentration is the largest and most attenuated for the kiln operation fired with the fuel mixture of 50% oil/50% sawdust. As CO is an intermediate step to a complete combustion, a larger volume with comparably high CO concentrations indicates slower burning process a longer flame length. The region with significant CO concentration is the smallest for the kiln operation fired with 100% oil, which indicates a shorter flame length and more rapid burning process as expected from the practice. The kiln operation fired with the fuel mixture of 70%oil/30%sawdust produces a result in between. Figure 30 presents the comparison of the predicted iso-surfaces of the CO concentration at which the mole fraction = 0.01 for the three firing conditions. The actual flame lengths can be estimated from the predicted iso-surfaces shown in this figure [9]. As illustrated, the flame length for co-firing oil and sawdust is roughly double the flame length for firing 100% oil.

The predicted gas flow fields in the freeboard of the lime kiln are presented in Figures 31-32 for the three different firing conditions. As shown in these figures, the predicted flow patterns for all the three firing conditions show strong similarities, although some differences in the velocity magnitudes can be noticed due to the differences in the gas temperature fields discussed previously. As illustrated in Figure 31, there is a

longitudinal recirculation zone near the burner in the upper part of the kiln. This recirculation zone circulates the hot gases from the hot region to the relatively cold region. Figure 32 shows the predicted velocity vectors in four cross-sections of the kiln for the three different firing conditions. As shown in this figure, significant secondary flow is created by the buoyancy forces from the relatively cold lime bed surface to the hot flame region.

The comparison of the predicted profiles of the mass flow rates for the lime, and the conversion of the individual species in the bed, is presented in Figure 34 for the three different firing conditions. As demonstrated, the lime bed model responses well to the freeboard hot flow model. As shown in this figure, the lime calcination proceeds most rapidly for the kiln operation fired with the fuel mixture: 50%oil/50%sawdust while it proceeds slowest for the kiln operation fired with the 100% oil. The kiln operation fired with the fuel mixture: 70% oil/30% sawdust has a result in between. As discussed previously, the lime calcination rate is primarily controlled by the heat transfer rate to the lime bed. The higher gas temperature level that results from the co-firing of oil and sawdust enhances the heat transfer to the lime bed and thus the calcination proceeds more rapidly, the sintering starts earlier with a resulting higher maximum temperature. The heating zone is however similar in all three cases. All cases have a complete combustion before the heating zone, and thus all energy from the fuel is released, and all cases have comparable heat transfer coefficients due to near bed velocities of the flue gas.

5.2 Kiln operation and measurement campaign

Lime kiln operation

It should be clear that there were some small differences in kiln operation during the measurement campaign. As an example, the sum of the transportation air (for the solid fuel) and the primary air was almost 5% lower for the 70% oil / 30% sawdust case compared to the two other cases The kiln load was also slightly lower for this fuel mixture. During the second day of the campaign (afternoon 24th of June) the staff of Södra Cell Mönsterås reported that the lime product threshold had increased 0.1-0.2 meters, possibly due to the initial steps in the formation of a ring. This observation was made as the gas and temperature measurement at the hot end of the 100% oil firing case was conducted. These differences should be taken into account when interpreting the results.

Flue gas and temperature measurements

Due to the rather high concentration of dust in lime kilns, the performance of gas and temperature sampling methods based on extraction techniques should not be seen as straightforward. There is always a risk that the dust will cause plugging of the channels in the extraction probe. Although some problems with plugging did occur in this project, it should be clear that the techniques that were used did perform well during shorter periods of time e.g. some 20 minutes or so, and that this was enough to get good

and reliable data on the process. As always when making measurements with long probes in warm and turbulent environments, the location of the probe tip can only be seen as an approximate position, because (i) the probe will bend under its own weight, and (ii) the probe will fluctuate due to turbulence in the kiln. Thus, the position of the tip of the probe should be seen as approximate and we estimate that its position is subject to uncertainties around 0.15 m. This underscores that the results from the gas and temperature measurement should be seen as average values originating from a volume surrounding the probe tip and not as point measurements with millimetre precision. In this project, this translates into the following statements:

(i) The measurements do capture average values and trends in both gas composition and temperature in a sufficiently good way

(ii) A strong (vertical) gas composition and temperature gradient is present at the hot end and at an insertion depth of 5 meters, i.e. close to the tip of the burner.

(iii) The temperature gradient (hot end) seems to be more pronounced for the 50% oil / 50% sawdust case, displaying several hundred degrees difference along a vertical line of about 0.6 meters.

(iv) The 50% oil / 50% sawdust case displays higher temperatures at all positions with an insertion depth of 5 meters. This trend result is unexpected and also contrary to that found in the data from the existing thermocouple (position just below the burner), where the 100% oil case showed about 100 ^{o}C higher temperature on average (see Figure 11). A possible explanation to this is the uncertainty in the position of the probe tip, however, it does seem unlikely that the probe was positioned further in and/or higher up in the kiln each time it was moved (some 5 times per measurement). The gas concentration gradient along the same vertical line/distance (hot end) also seemed to be more pronounced for the 50% oil / 50% sawdust case. The CO_2 concentration in the upper part of the kiln was up to 3.2 vol-% which was about 2.5 vol-% units higher than that at the lower part of the kiln.

(v) The O2 concentrations measured at the kiln exit was much lower than the value recorded by the existing sensor positioned further downstream the flue gas channel. A possible explanation to this is that leakage air has entered the flue gas channel between the kiln exit and the position of the oxygen sensor of the control system.

(vi) A comparison between the probe data and kiln control system data on CO and NOx/NO show that the trends are similar but not the absolute values. The latter is especially true for CO. A possible explanation to this is that the probe measurements were made during a period of ~30 minutes and it may have been the case that this time period did not coincide with the period of really high CO concentration.

(vii) At the cold end, i.e. lime mud feed end, a clear vertical temperature gradient displaying differences between 140-150 ^{o}C at a vertical distance of about 1 meter.

(viii) The measurement error of a general suction pyrometer is normally considered to be maximum 5%, which in this project translates into a maximum absolute error of about 40-50 ^{o}C. The temperature gradients

observed were in the range of 100 to 400 ^{o}C, which means that the observed major trends in temperature should be seen as significant.

Based on the results from the probe measurements, especially at the hot end of the kiln, it would have been very interesting to see what would have happened if the probe had been 1-2 meters longer, i.e. if the maximum insertion depth would have been 6 or 7 meters. This would have opened up the possibility to get more details of the strong gradients that was present in the region close to the burner tip. However, it should also be clear that there is a maximum working temperature of the suction pyrometer, and that this temperature may be exceeded if the probe is positioned too close to the flame itself. Having said that, the maximum practical insertion depth is probably not that much longer than the 5 meters that was used in this project.

IR camera measurements

Prior to using an IR camera as a thermometer for measurement of the lime bed surface temperature, several aspects need to be considered. First, the camera needs to be adapted to measurements of high temperatures > 1200 ^{o}C. Secondly, a clear field of view of the lime bed is needed, and the third aspect to consider is that the flame should preferably not be seen in the images. The camera that was used in the project was indeed adapted to high temperatures (up to 1500 ^{o}C). However, due to the geometry of the working space below the burner (in the burner building), a clear field of view of the lime bed some 10 meters into the kiln, i.e. below the flame, was not possible if the requirement of a "non-flame containing" image was to be obeyed. As it was desirable to reach as far into the kiln as possible with the IR image, preferably some 5-10 meters further into the kiln, a compromise in which a small part of flame was allowed in the thermo image. It is estimated that that the optical focus of the IR camera was close to the position where the reburned lime falls down into the product coolers, i.e. estimated to some 2-3 meter into the kiln (that is, half way between the burner tip and the duct to the product coolers). This position is not far from the point where the secondary air enters the kiln. As the air enters the kiln at a temperature slightly above 300 ^{o}C, it may have had a cooling effect in the lime bed implying that measured temperatures are lower than that of the lime bed close to the burner tip. The trends that were seen from the IR measurement are similar to those recorded by the existing thermocouple positioned just below the burner (reference temperature).

5.3 Evaluation of simulation data against in-plant measurement data

Evaluation of the numerical simulations against the in-plant measurement data has been presented previously. In general, the predicted results from the CFD modelling agree reasonably well with the measured data. However, less good agreement is shown at one position for temperature and oxygen at the hot side for the 100% oil case, as well at one position for oxygen at the cold side of the 50%oil/50%sawdust case. One explanation to the differences can be found in the uncertainties in measurement probe positions, as discussed in chapter 5.2. The simulation results are quite sensitive to the exact position, as they are theoretical point values. Furthermore, on the hot side the measurement points are situated very close to the flame, and thus in an area with strong gradients. Due to the strong gradients at the hot side, no comparison has been explicitly made for the combustion species CO_2 and H_2O. The comparison of these values on the hot side would primarily give info regarding the momentary location of the flame front. On the cold side these values would primarily reflect the sum of all balances of chemical constituents entered in the kiln, as all reactions are completed at this measurement point.

From the CFD modelling, we expect that the gas temperature in the upper part of the kiln is higher than in the lower part of the kiln. The oxygen concentration in the upper part of the kiln is lower than the in the lower part of the kiln because a flow recirculation zone exists in the upper part of the kiln close to the burner. As demonstrated, the measurement results show exactly the same trends. The comparisons between the calculated and measured values at the measurement points are given in Figures 46-49. As shown in these figures, the predicted values agree reasonably well with the measurement. In addition it is quite clear that at the hot end the measured gas temperature level for the co-firing 50% oil and 50% sawdust is higher than for the firing 100% oil. This in-plant measured result is consistent with the result obtained from the CFD modelling, which implies that the gas temperature level in the flame region is higher for the kiln operation fired with 50% oil/50% sawdust than for the case fired with 100% oil.

This result that has been proven by both the in-plant measurement and the CFD modelling seems in contradiction to some previous industrial experience in which the gas temperature level in the flame region would be expected to be higher when firing 100% oil. One explanation to this may be found in the moisture content of the sawdust, where the fuel analysis performed at the measurement campaign showed water content of close to 4 percent, which is higher than values normally seen. High water content will strongly increase the emitted radiation from the flame region, and thus also increase wall and bed temperatures. However, in order to try and clarify this uncertainty, a sensitivity study for the CFD modelling is carried out by simulating the kiln operation fired with the fuel mixture: 50% oil/50% dry sawdust. Figure 50 presents the comparison of the predicted contours of gas temperature in the central-vertical plane of the kiln ($z = 0$, $x <= 20$m) for the three firing conditions using the fuel mixtures: 100% oil, 50% oil/50% sawdust, and 50% oil/50% dry sawdust. The comparison of the predicted contours of H_2O concentration in the central-vertical plane of the kiln ($z = 0$,

x <= 20m) for the three firing conditions is presented in Figure 51. Figure 52 shows the comparison of the predicted lime bed performances for the three firing conditions. As indicated in these figures, the kiln operation fired with 50% oil/50% **dry** sawdust produces significant lower gas temperature in the flame region than the kiln operation fired with 50% oil/50% sawdust. It is clear that the H_2O concentration in the flame region plays an important role in the heat transfer (primarily in the radiation heat transfer) as predicted by the CFD modelling. Higher H_2O concentration in the flame region leads to higher gas temperature levels as well as higher wall temperatures, and thus enhances the heat transfer to the lime bed. Table 9 below summarizes the comparison between measurements and CFD-simulation.

Tabell 9. Summering av jämförelse mellan mätning och CFD-simulering

Table 9. Summary of comparison between measurements and CFD-simulation

	MEASUREMENTS	CFD-SIMULATIONS
HOT SIDE		
Local temperatures near burner	Warmer for 50% oil than for 100% oil Warmer above burner than below burner	Warmer for 50% oil than for 100% oil Warmer above burner than below burner
Local combustion species concentration near burner	Higher concentrations above burner than below	Higher concentrations above burner than below
Temperature gradients	Approximately 100 – 400 degrees over 0.6 meter vertical	Approximately 200 – 450 degrees in 0.5 meter spherical volume
Lime bed temperatures (1)	Lower for 50% oil than for 100% oil	**Wet biomass:** Higher for 50% oil than for 100% oil **Dry biomass:** Lower for 50% oil than for 100% oil
Flame length	n/a	Approximately twice as long for 50% oil compared to 100% oil
COLD SIDE		
Temperature gradients	Approximately 140 – 150 degrees over 1 meter vertical	Approximately 100 – 150 degrees over 1 meter vertical.

(1) Note that measurements are taken approximately 3 meters downstream the simulation results, and significant temperature decrease should be expected in this region.

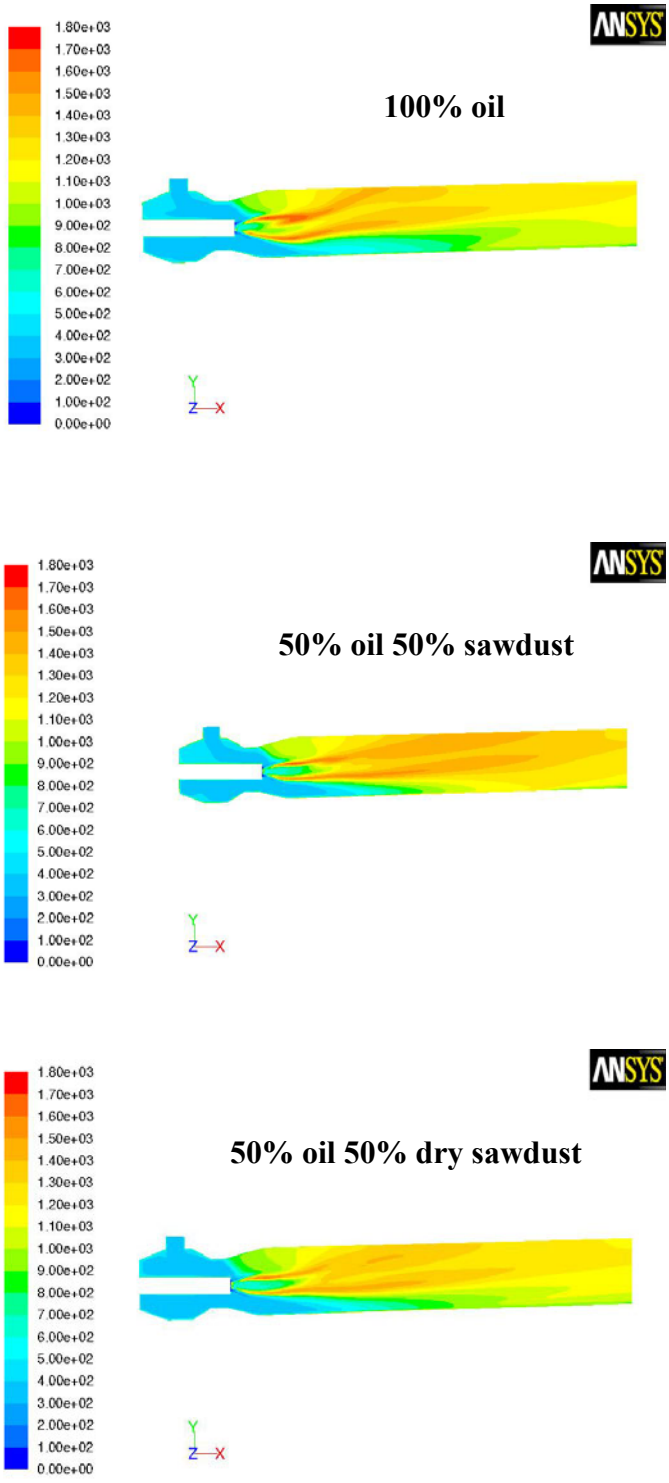

Figur 50. Konturplottar för jämförelse av gastemperaturer i ett central-vertikalt plan i ugnen (z=0m, x<=20m) för tre bränsleblandningar varav 2 med olika fukthalt.

Figure 50. Comparison of the predicted contours of gas temperature in the central-vertical plane of kiln (z=0,x<=20m) for three different firing conditions, where 2 differ in

moisture.

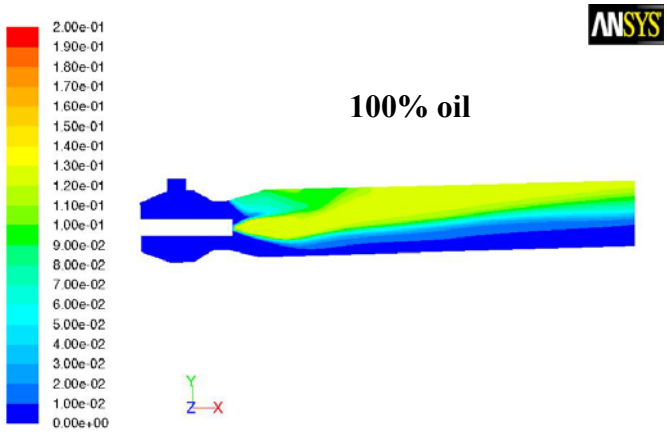
2.00e-01
1.90e-01
1.80e-01
1.70e-01
1.60e-01
1.50e-01
1.40e-01
1.30e-01
1.20e-01
1.10e-01
1.00e-01
9.00e-02
8.00e-02
7.00e-02
6.00e-02
5.00e-02
4.00e-02
3.00e-02
2.00e-02
1.00e-02
0.00e+00
ANSYS
100% oil
Y
Z
X

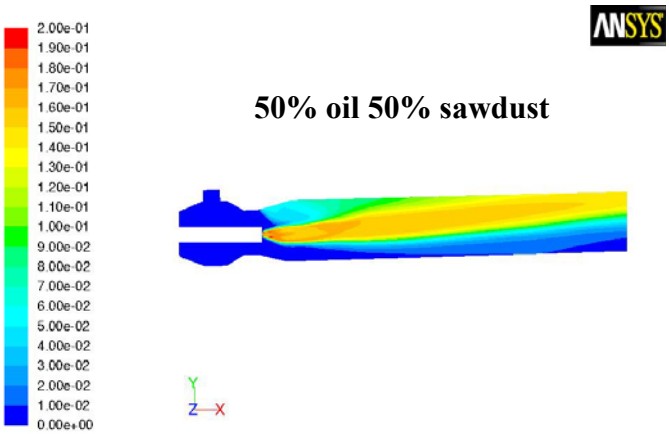
2.00e-01
1.90e-01
1.80e-01
1.70e-01
1.60e-01
1.50e-01
1.40e-01
1.30e-01
1.20e-01
1.10e-01
1.00e-01
9.00e-02
8.00e-02
7.00e-02
6.00e-02
5.00e-02
4.00e-02
3.00e-02
2.00e-02
1.00e-02
0.00e+00
ANSYS
50% oil 50% sawdust
Y
Z
X

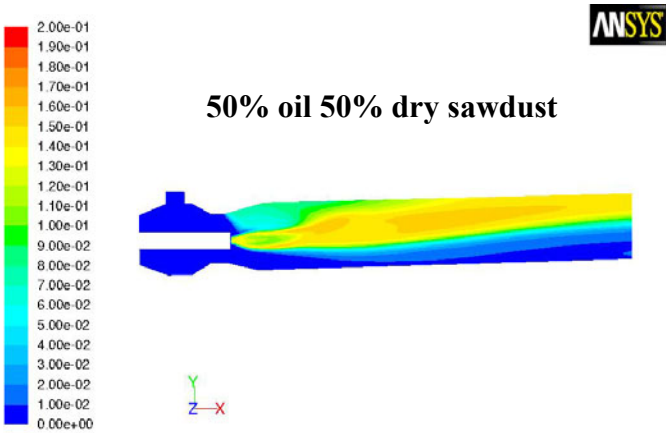
2.00e-01
1.90e-01
1.80e-01
1.70e-01
1.60e-01
1.50e-01
1.40e-01
1.30e-01
1.20e-01
1.10e-01
1.00e-01
9.00e-02
8.00e-02
7.00e-02
6.00e-02
5.00e-02
4.00e-02
3.00e-02
2.00e-02
1.00e-02
0.00e+00
ANSYS
50% oil 50% dry sawdust
Y
Z
X

Figur 51. Konturplottar för jämförelse av H_2O koncentrationer (molfraktioner) i ett central-vertikalt plan i ugnen (z=0m, x<=20m) för tre bränsleblandningar

Figure 51. Comparison of the predicted contours of H_2O concentration in the central-vertical plane of the kiln (z=0, x<=20m) for the three different firing conditions

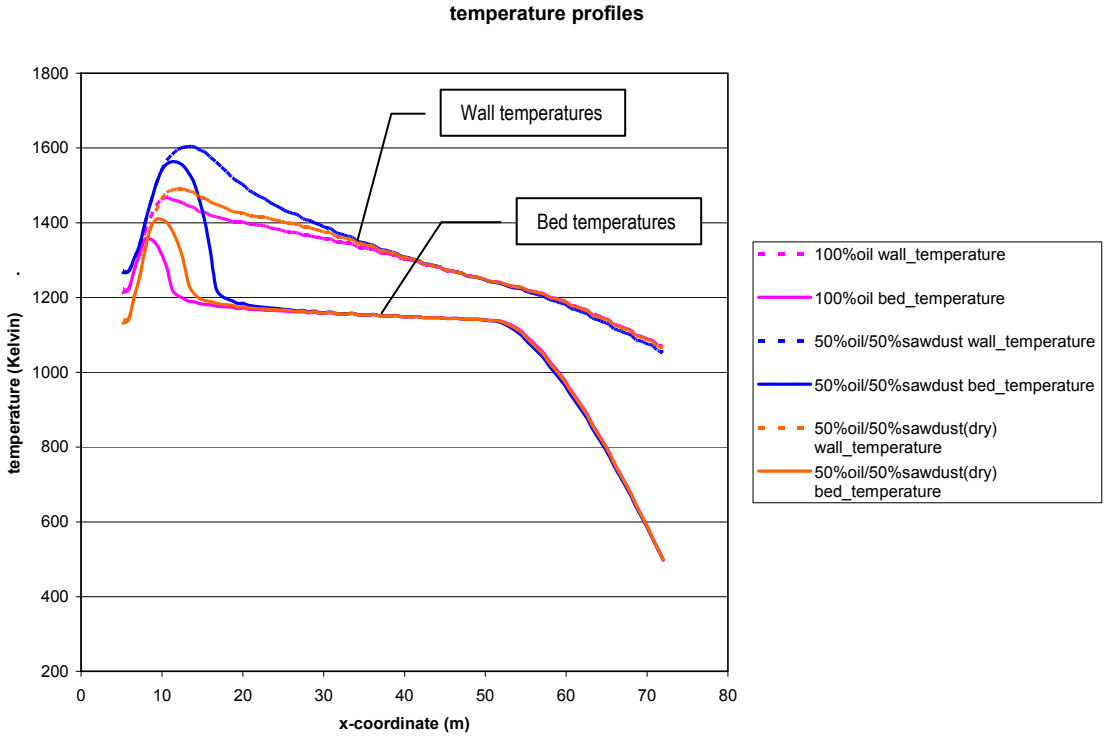

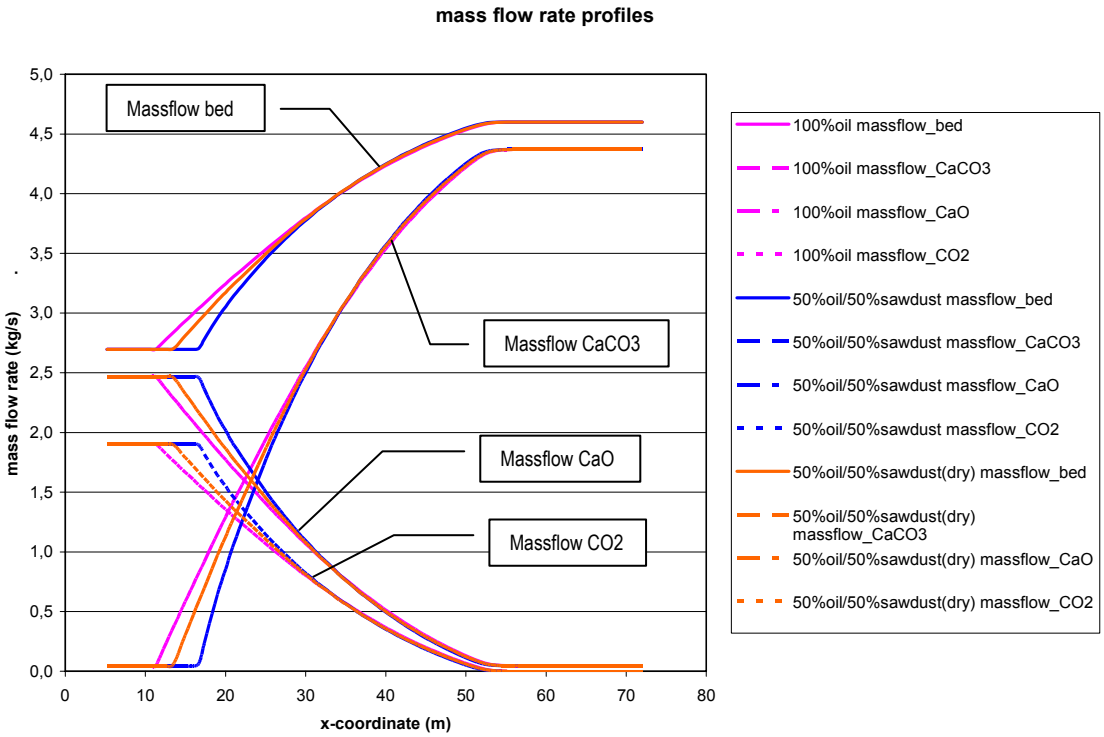

Figur 52. Jämförelse av mesabäddens beteende för de tre olika bränslekonfigurationerna

Figure 52. Comparison of the predicted lime bed performances for the three different firing conditions

6 Conclusions

The developed three-dimensional CFD model for rotary lime kilns generally demonstrates that

(i) The developed CFD model can be used as a powerful tool to study the detailed flame characteristics and burner design parameters for a rotary lime kiln and to examine the impacts on the kiln performance due to varied kiln operation parameters and firing conditions.

(ii) The evaluation of the developed CFD model against the in-plant measurements shows that the predicted results from the CFD modelling agree reasonably well with the in-plant measured data.

(iii) The result obtained from both the CFD modelling and the in-plant measurements shows that the predicted gas temperature level in the flame region for the kiln operation fired with 50% oil/50% sawdust is higher than that for the kiln operation fired with 100% oil. This result is in contradiction to some previous industrial experience in which the gas temperature level would expect to be higher when firing 100% oil. Additional sensitivity analysis shows that the gas temperature level in the flame region has a close link with the H_2O concentration. The moisture content in the sawdust leads to significant higher gas temperature level and thus enhanced heat transfer to the lime bed as predicted by the CFD model.

(iv) The results obtained from the CFD modelling indicate that the co-firing oil and sawdust results in a longer flame length and relatively slow burning process which has both negative and positive effects. The negative effects are that the relative slow burning process may create a difficulty in kiln operation regarding the problem with flame ignition and instability and also the possible problem with excessive unburned combustibles in the flue gas. The positive effect is that the longer flame length generally improves the heat transfer to the lime bed and thus results in a shorter calcination time for the lime bed process.

Furthermore, it has been demonstrated that gas and gas and temperature sampling methods based on extraction techniques can be used in a high dust environment such as a lime kiln. Although some problems with plugging did occur in this project, it should be clear that the techniques that were used did perform well during shorter periods of time e.g. some 20 minutes or so, and that this was enough to get good and reliable data on the process.

The results from the gas and temperature measurement should be seen as average values originating from a volume surrounding the probe tip and not as point measurements with millimetre precision. In this project, it has been shown that distinct vertical gas concentration and temperature gradients are present around the tip of the burners, resulting in a temperature difference of several hundred degrees along a vertical distance of about 0.6 meters.

The measurement of the lime bed surface temperature by the use of an IR camera has been demonstrated. The focal point of the IR image was limited to 2-3 meters into the kiln, implying that the recorded temperature may be lower than the surface temperature just below the burner flame which is positioned some 5-10 meters further into the kiln. The resulting trends from the IR measurements are similar to the temperature that was recorded by the existing thermocouple positioned just below the burner (reference temperature). The bed temperature measurements are not easily comparable with the CFD-simulation results, as the temperature gradient in this area is strong and the measurements were made outside the simulated part of the bed.

7 Recommendations and applications

The use of the developed three-dimensional CFD model for simulation of rotary lime kilns is recommended as a tool to address issues primarily regarding;

(i) Kiln efficiency
(ii) Burner characteristics and burner design/operation
(iii) Refractory life
(iv) Flame stability and stable process operation
(v) Flame shape, length and general characteristics
(vi) Flue gas flow at kiln outlet (limits capacity)
(vii) Emissions formation (primarily NO_x, but also SO_2 and H_2S)
(viii) Emissions aftertreatment (for example UREA injections for NO_x)

Some specific examples when the above mentioned situations arise are;

a. change of fuels (for example oil to biofuel)
b. change of burner design
c. capacity comparisons and optimisations for different fuels
d. combustion disturbances, flame blow-off, flame instabilities
e. Evaluations of refractory wall thermal loads and resistance

8 Suggestions for continued research

Possible necessary continued research efforts that have been identified are shown here. These efforts should also be placed in their research context, by making fitting references to the description of the research area in chapter 1b

.

Areas where the developed numerical CFD-model has limitations, and where added value by further research and improvement is possible, and its purposes are:

(i) **Process Capacity and Lime Quality;** Increase the understanding of the sintering process, primarily regarding the sintering onset point and maximum temperature, as well as the regions for heat up, and calcinationand to further extend the possibilities to address capacity effects from for example a fuel change.

(ii) **Refractory Life;** Improved and coupled prediction of the local thermal loads on refractory walls by adding the heat regeneration due to the lime bed process and three-dimensional heat conductions along and across the refractory walls.

(iii) **Lime bed flow;** More detailed prediction of the lime bed heat- and mass transport in kiln cross-section would.

(iv) **Fuel and NO_x modelling;** The characteristics of solid biofuels (for example bark powder and sawdust) used for modelling in CFD, is an area where improved understanding and further validation for each fuel would add accuracy in all aspects of modelling. For NO_x modelling all capabilities exists, however little practical on-site validation have been made

Process Capacity and Lime Quality

In order to take full advantage of the modelling capabilities and its possibilities to predict process capacity changes and lime quality, a better understanding and validation of the distribution and characteristics of the sintering, calcination, heat-up and drying zones would be desirable. As the sintering effects the lime quality, it is of primary interest from a capacity and quality aspect to validate the predictions for sintering onset, sintering temperatures and total sintering durations.

Refractory life

By improving the present model and implementing an accurate and validated approach to simulate the heat transfer along and across the rotating refractory walls, changes to refractory wall temperatures would be easily accessible. This would provide a possibility to evaluate the thermal loads on the kiln walls, with a local temperature resolution down to approximately $1dm^2$, arising from a combustion and/or process change. An accurate prediction of the resolved temperatures would ensure that the kiln refractory wall resists the arising temperatures and heat loads, and thereby kiln failure can be predicted and avoided. Adding this possibility would extend the use of the simulation method to work also as a tool to tuning burner and process setup with regard to impacts on refractory walls. Furthermore, it would allow for a extended and more correctly resolved heat transfer between the kiln walls and the lime bed.

Lime bed flow

By adding a resolved heat and mass transfer in the cross section of the lime bed, the predictions for process capacity, refractory wall thermal loads and lime bed chemistry would be improved. New information would be made available regarding the interaction of calcination chemistry with the mass- and heat transfer within the bed. Access to this detailed information could serve as an important component when choosing how to improve the kiln performance and provide the insight of the calcination process such as ring built-up and related lime bed phenomena.

9 Literature references

[1] Boateng, Akwasi A.; “Rotary Kilns – Transport Phenomena and Transport Processes”, Butterworth-Heinemann, Linacre House, Jordan Hill, Oxford OX2 8DP, UK, 2008.

[2] Kristoffer Svedin, Christofer Ivarsson, Richard Lundborg; ”Lime Kiln Modeling – CFD & One-dimensional simulations”, Värmeforsk Service AB, 101 53 Stockholm, February 2008.

[3] Georgalllis, M., Nowak, P., Salcudean, M., and Gartshore, I. S., “Modelling the Rotary Lime Kiln”, Can. J. Chem. Eng. 83:212-223 (2005)

[4] Perron, J. and Bui, R.T., “Rotary Cylinders: Transverse Bed Motion Prediction by Rheological Analysis”, Can. J. Chem. Eng. 70:223-231 (1992)

[5] Tscheng, S.H. and Watkinson, A.P., “Convective heat transfer in rotary kilns”, Can. J. Chem. Eng. 57:433-443 (1979)

[6] Boateng, A.A. and Barr, P.V., “A thermal model for the rotary kiln including heat transfer within the bed”, Int. J. Heat Mass Transfer 39(10):2131-2147 (1996)

[7] Bui, R.T., Simard, G., Charette, A., Kocaefe, Y., Perron, J., “Mathematical Modelling of the Rotary Coke Calcning Kiln”, Can. J. Chem. Eng. 73:534-544 (1995)

[8] Guruz, H.K. and Bac, N., “Mathematical modelling of rotary cement kilns by the zone method”, Can. J. Chem. Eng. 59:54-548 (1981)

[9] Turns, Stephen R., “An introduction to combustion, concepts and applications”, Second edition, McGraw-Hill Higher Education, 2002.

[10] FLUENT 6.3 Manuals, Fluent Inc. November 13, 2006.

Värmeforsk är ett organ för industrisamverkan inom värmeteknisk forskning och utveckling. Forskningsprogrammet är tillämpningsinriktat och fokuseras på energi- och processindustrins behov och problem.

Bakom Värmeforsk står följande huvudmän:

- Elforsk
- Svenska Fjärrvärmeföreningen
- Skogsindustrin
- Övrig industri

VÄRMEFORSK SAMARBETAR MED STATENS ENERGIMYNDIGHET



VÄRMEFORSK SERVICE AB
101 53 Stockholm
Tel 08-677 25 80
Fax 08-677 25 35
www.varmeforsk.se

Beställning av trycksaker
Fax 08-677 25 35